# NATIONAL ADVISORY COMMITTEE FOR AERONAUTICS

TECHNICAL NOTE

No. 1593

## EFFECTS OF NACELLE POSITION ON WING-NACELLE INTERFERENCE

By Charles H. McLellan and John I. Cangelosi

Langley Memorial Aeronautical Laboratory
Langley Field, Va.




Washington
June 1948

NATIONAL ADVISORY COMMITTEE FOR AERONAUTICS

TECHNICAL NOTE NO. 1593

# EFFECTS OF NACELLE POSITION ON WING-NACELLE INTERFERENCE

By Charles H. McLellan and John I. Cangelosi

## SUMMARY

The interference effects between an airfoil of high critical speed with no sweepback and a nacelle of high critical speed mounted in various positions with respect to the wing were investigated. A modified NACA fuselage form 111 was used in conjunction with a modified NACA 65-210 airfoil section. The main objective of this investigation was to obtain a wing-nacelle combination which has the force break occurring at a Mach number as high as for the wing alone. This objective was realized throughout the Mach number range of the tests (up to 0.7) for angles of attack up to and including $2.5^{\circ}$ with only a small loss in lift at a given angle of attack.

A low nacelle position with the nose of the nacelle 0.66 chord ahead of the wing leading edge, with the upper surface of the wing tangent to the top nacelle line, and with the nacelle center line parallel to the wing chord gives a reasonable compromise between loss of lift and late drag rise. Raising the nacelle from the low nacelle position decreased the Mach number at which severe drag rises occurred. Moving the nacelle forward from this low position had little effect on the drag but increased the loss in lift. The presence of the nacelle in the most rearward position increased the lift slightly. This combination, however, had the greatest drag rise of the low position nacelles at $5^{\circ}$ angle of attack.

The problem of obtaining a wing-nacelle combination which has good high-speed characteristics is greatly simplified by the use of components which by themselves have good high-speed characteristics.

## INTRODUCTION

The ever increasing speed of airplanes has created a great need for detailed information concerning the interference effects at high speeds between wings and nacelles and for the development of wing-nacelle combinations which have the force break occurring at a Mach number as high as for the wing alone. The interference effects between an airfoil of high critical speed with no sweepback and a nacelle of high critical speed mounted in various positions with respect to the

wing were therefore investigated at the Langley 16-foot high-speed tunnel.

There are several effects resulting from wing-nacelle interference. The presence of the nacelle tends to increase the velocities over the wing, which results in a reduction in the wing critical Mach number. This reduction is of considerable importance because the wing normally has a critical speed lower than that of a well designed nacelle. The effect of the wing on the nacelle is to increase the velocities and consequently reduce the critical speed of the nacelle. This effect is not likely to be important inasmuch as the critical speed of the nacelle alone can easily be made considerably greater than that of the wing alone. A very large influence would be required from the wing to reduce the critical speed of the nacelle below that of the wing. Another important interference effect is that of the nacelle on the lift. A change of lift in the vicinity of the nacelle, in general, results in an increase in induced drag for a given lift because of a poorer span load distribution. For locally reduced lift, a greater section lift coefficient is required over the remainder of the wing than is required for the undisturbed wing. This change causes a reduction in the critical Mach number of the wing. At low angles of attack on a wing such as the one used in the present investigation, this reduction is of secondary importance because the rate of change of critical Mach number with lift coefficient is small. At higher angles of attack where the rate of change of critical Mach number with angle of attack is large, however, this reduction may be of considerable importance.

Inasmuch as the main objective of this investigation was to obtain a wing-nacelle combination with the force break occurring at a speed as high as for the wing alone, it seemed reasonable to start with components having good high-speed characteristics. A modified NACA fuselage form 111 with a fineness ratio of 6 and a wing having a modified NACA 65-210 airfoil section were therefore used.

## SYMBOLS

$C_L$ wing lift coefficient based on wing area

$C_D$ wing drag coefficient based on wing area

$c_n$ section normal-force coefficient based on wing chord

$\Delta C_D$ nacelle incremental drag coefficient based on maximum nacelle frontal area

$\Delta C_L$ nacelle incremental lift coefficient based on an area equal to wing chord times maximum nacelle width

$c$ wing chord

| | |
|---|---|
| $x$ | distance from leading edge of wing or from nose of nacelle along major axis |
| $V$ | free-stream velocity |
| $a$ | free-stream velocity of sound |
| $M$ | free-stream Mach number $(V/a)$ |
| $M_{cr}$ | critical Mach number |
| $P$ | pressure coefficient $\left(\frac{\text{Local static pressure - Free-stream static pressure}}{\text{Free-stream dynamic pressure}}\right)$ |
| $P_{cr}$ | critical pressure coefficient |
| $R$ | Reynolds number based on a wing chord of 44 inches |
| $\alpha$ | angle of attack of wing chord line, degrees |

## DESCRIPTION OF MODEL

The model was mounted in the Langley 16-foot high-speed tunnel as shown in figure 1. The wing, which was constructed of wood built around a steel spar, completely spanned the tunnel. During the construction of the model it became apparent that the wooden trailing edge was too flexible; therefore, 2.22 percent of the original chord was removed from the trailing edge. The airfoil ordinates given in table I are based on the original chord, whereas all other calculations are based on the actual chord of the wing (44 in.). The airfoil section is, therefore, referred to as a modified NACA 65-210 section for which the modification is simply the removal of 1 inch at the trailing edge of a wing which originally had a chord of 45 inches.

In order to reduce to a minimum the aerodynamic effects of wing-surface changes, strips of carborundum grains were added to the upper and lower surfaces of the wing at the 21-percent-chord station to fix boundary-layer transition at this station. No carborundum strips were used on the nacelle.

A modified NACA fuselage form 111 was selected for the nacelle in this investigation because of its relatively flat pressure distribution and its high critical speed. A fineness ratio of 6 and a length of 2.66 wing chords were used. These proportions approximate those used in current designs of high-speed airplanes. The modified NACA form 111 is described in reference 1; however, the ordinate at the 20-percent-chord station was changed in the present tests to improve the fairing. The

ordinates of the nacelle are given in table II. The nacelle was constructed so that it could be mounted on the wing in the positions shown in figure 2. For positions B, C, D, $C_{-2.5}$, and $C_{2.5}$ the nacelle was mounted with the upper surfaces of the nacelle and wing tangent at some point. In the high nacelle configuration, position $C_4$, the lower surfaces of the wing and nacelle were tangent.

A three-view drawing of the model with the nacelle in position C is shown as figure 3 and the same model configuration is shown mounted in the tunnel in figures 4 to 6. The sides of the nacelle under most of the wing were vertical from the center of the body to the wing as shown in figures 3 and 4. Near the leading and trailing edges these straight sides were altered to allow the fillets shown in figures 3, 5, and 6 to be formed. The fillets shown for position C were typical for all positions except positions $C_3$ and A. Position $C_3$, which was a centrally located position, had no fillets. Position A is shown in figures 7 and 8. The front fillet was essentially the same as for position C; however, since the trailing edge was considerably above the nacelle surface, a different rear fairing was required. The vertical sides of the nacelle were, therefore, extended to the rear of the nacelle as shown in figure 8.

In an attempt to reduce local pressure peaks a series of modifications was made to the part of the leading edge of the wing adjacent to the nacelle. These alterations were made by replacing a removable part of the wing leading edge (fig. 3) with blocks having the sections shown in figure 9 at orifice station 1. The sections of the blocks outboard of this station were determined by fairing with a straight line to the normal leading-edge section at a station $31\frac{1}{2}$ inches from the wing center line. The leading-edge modifications were tested only with nacelle position C.

Pressure orifices located on both the nacelle and wing are shown in figure 3. These orifices were used on all configurations. An additional row of orifices was installed 60° from the top of the nacelle for position $C_3$. In position $C_4$ the row of orifices normally 60° from the bottom shifted to 60° from the top on the opposite side because the nacelle was inverted to obtain this position. Four additional rows of orifices were installed between the orifices on the wing and those on the top center of the nacelle for a few of the tests of position C.

Four rows of orifices were used on the wing to show the large interference effects which were anticipated near the nacelle. A close spacing of the rows near the nacelle was selected inasmuch as the interference effects were expected to diminish rapidly with distance from the nacelle.

## METHODS

For each configuration, tests were made to determine (1) the effect of Mach number on the forces and pressures, (2) the variation of critical Mach number with angle of attack, and (3) the maximum lift characteristics of the configurations. The tests to determine the effect of Mach number were made at constant angles of attack with the tunnel speed varying from a Mach number of 0.15 to 0.70 (maximum speed obtainable in tunnel). The tests to determine maximum lift characteristics were made at a Mach number of 0.2. The corresponding range of Reynolds number based on the 44-inch chord is from $3.8 \times 10^6$ to $13.6 \times 10^6$. Figure 10 shows the average variation during the tests of the Reynolds number with Mach number.

Critical Mach numbers of the various parts of the model were estimated by extrapolating, by the use of a method derived by G. Temple and J. Yarwood in a British paper of limited distribution, pressures measured at a Mach number of 0.4. Critical Mach numbers were also obtained by using the high-speed pressure coefficients. These results are presented as tailed symbols to distinguish them from the values extrapolated from low Mach numbers.

Various coefficients used in the tests were obtained as follows: Incremental lift coefficients due to the presence of the nacelle have been based on an area equal to the maximum nacelle width times the wing chord since this area is independent of the wing span. The incremental drag coefficients due to the presence of the nacelle have been based on the nacelle frontal area. The normal-force coefficients over the wing were obtained from integration of pressure distributions. Equivalent wing normal-force coefficients were obtained at the center line of the nacelle from an integration of the pressures over the center of the upper and lower surfaces of the nacelle, which had been corrected for the difference between the nacelle length and wing chord.

The wing alone and the wing with the nacelle in position C are considered reference conditions. The results are therefore frequently presented in more than one figure. For the purpose of simplification, the test points are included only the first time the curves are presented.

The investigation was composed of two series of tests. Slight differences were found between the results of the first series of tests and the results of some of the repeat tests of the second series. In order to reduce the effect of these small differences to a minimum, comparisons are made as far as possible between tests of the same series.

## RESULTS

### Wing Alone

Results of tests of the wing alone are presented in figures 11 to 16 to provide a reference condition for this investigation. Two series of tests were made; most of the original wing-alone tests were repeated in the second series of tests. Figure 11 shows that the pressures from the two series were in good agreement. When the pressure peak at the nose of the airfoil was sharp, the actual value of the peak was not reproduced exactly, as is shown in figure 12 at an angle of attack of $2.5^\circ$; however, the agreement obtained is believed to be as good as can be expected under these conditions. A reasonably good agreement was obtained between the two series for the critical Mach number curves, as is shown in figure 13. The stall was slightly less abrupt in the second series than in the first series of tests, as can be seen in figure 14. The agreement between the other force data of the two runs was reasonably good (figs. 14 and 15). Figure 16 shows the variation of the section normal-force coefficients with spanwise location. Little variation was found in spanwise distribution between the two series of tests.

### Pressure Contours on Wing and Nacelle

Throughout the discussions of interference effects of the nacelle, position C will be considered as the reference position since it is included in all the nacelle position variations and because it is believed to be the position preferred by most airplane manufacturers.

The pressure contours on the upper surface of the wing and nacelle are shown in figure 17 for nacelle position C. This figure shows that the regions of high negative pressure are limited to the area of the wing adjacent to the nacelle. At $0^\circ$ angle of attack on which the peak negative pressure coefficient is near the center of the wing chord, the influence of the high negative pressures extend over a considerable width of the nacelle. The peak negative pressure is essentially the same at the center of the nacelle as over the undisturbed wing. Since, however, the peak negative pressure coefficient of the wing shifts to the leading edge as the angle of attack is increased and since the nacelle and fillets cover up the high curvature of the leading edge, the high peak negative pressure coefficient would not be expected to extend over the nacelle and fillets. This condition is confirmed by the test results shown in figure 17. The presence of the nacelle, however, increases the peak on the wing adjacent to the nacelle. The influence of the nacelle over the center of the wing is small at all angles of attack. Local pressure peaks occur at the leading edge of the wing near the nacelle. These pressure peaks, however, are very localized and at $0^\circ$ angle of attack are of approximately the same magnitude as the pressures over the center of the wing but at higher angles

of attack are much greater than those at any other place on the wing. It can therefore be seen that the important interference effects to be considered are those of the nacelle on the wing.

## Influence of Wing on Nacelle

The pressure-coefficient distributions over the nacelle for only two typical nacelle positions are presented (figs. 18 to 21), inasmuch as the effect of the wing on the nacelle is not a critical factor in the selection of the nacelle position. Figures 18 and 19 show that for position $C_3$ the most negative pressures were measured by a row of orifices 60° from the top of the nacelle. This row of orifices is very near the juncture of the nacelle with the upper surface of the wing. For 0° angle of attack the nacelle peak pressure coefficient is the same as that of the wing alone, whereas at 2.5° angle of attack it is approximately one-half as great as that of the wing. In position C (figs. 20 and 21) the peak pressure over the top center of the nacelle was less with respect to the wing pressure than for position $C_3$. The pressures were, however, measured over the center of the nacelle in this case. The variation of the pressures over the upper surface for position C has already been presented in figure 17. The variation of the critical Mach number with vertical, horizontal, and angular positions (fig. 22) shows that the critical speed of the nacelle in all but one position is above the critical speed of the wing alone. A localized area with a critical speed slightly lower than that for the wing alone was observed for the configuration with the nacelle in the high position, position $C_4$, at an angle of attack of 0°. This localized area was on the side of the nacelle close to the upper surface of the wing. The pressure coefficients could therefore be expected to approach those on the wing adjacent to the nacelle. Since the critical speeds of the nacelle in various positions were normally greater than those of the wing alone, the nacelle critical speed need not, in general, be considered in the selection of the nacelle position.

## Influence of Nacelle on Wing

Pressure distributions over wing.- The pressure distributions over the wing with the nacelle in the various positions tested are shown in figures 23 to 29 for a Mach number of 0.4 and angles of attack of 0° and 2.5°. Figures 23 and 24 show pressure distributions over the wing for the various vertical nacelle positions. At 0° angle of attack the peak negative pressure coefficients over most of the chord adjacent to the nacelle increased considerably as the height of the nacelle increased with respect to the wing. The influence of the nacelle decreased rapidly with distance from the nacelle. It should be noted that for the high nacelle position (position $C_4$) at 0° angle of attack a pressure

peak formed on the lower surface of the leading edge rather than on the upper surface. At an angle of attack of 2.5° the pressures were essentially the same for all nacelle positions in the vertical variation, with the exception of the high position $C_4$. In this position, the pressure peak disappeared from the leading edge near the nacelle. Over the rest of the chord adjacent to the nacelle, the negative pressures were considerably increased.

Figures 25 and 26 show the effect on the wing pressures of varying the nacelle position horizontally. The influence of the nacelle in these positions is confined largely to the leading and trailing edges at 0° angle of attack. The pressure peak, however, occurs over the midchord of the wing at 0° angle of attack. At an angle of attack of 2.5°, the effect of nacelle position is small over the entire chord.

The angular variation of the nacelle position influenced only the pressures over the leading edge. Therefore the pressure distributions are presented in figures 27 to 29 for only the leading edge of the airfoil.

Critical Mach number of wing.- Figures 30 to 32 show the variation of critical Mach number of the wing with angle of attack for the various nacelle positions tested. In general, the main effect of the presence of the nacelle was to reduce the range of angle of attack for high critical Mach numbers near the nacelle. The mid, semilow, and low nacelle positions (positions $C_3$, $C_2$, and C, respectively) in the vertical variation of the nacelle position reduce the critical Mach number at the positive angles of attack, whereas the high nacelle position $C_4$ decreases it at the negative angles of attack. The high position also reduces the peak value of critical Mach number more than do the other positions. At angles of attack above 2° the wing critical Mach number with the nacelle in the high position is essentially the same as that for the wing alone. Shifting the nacelle forward increases the wing critical Mach number at the positive angles of attack at the expense of the critical Mach numbers at negative angles. The importance of this shift in range of critical Mach number depends largely on the type of airplane.

Decreasing the nacelle incidence by 2.5° (position $C_{-2.5°}$) has a slight beneficial effect on the critical Mach number at angles of attack above 0°. Increasing the angle of incidence by 2.5° (from position C to position $C_{2.5°}$) reduces the critical Mach number at the positive angles of attack at most of the stations. At high angles of attack the critical Mach number measured at station 1 is greater than that at other stations. This variation is apparently due to local separation at the juncture of the leading edge and the nacelle.

Nacelle lift and drag.- Figure 33 shows that at 0° angle of attack the nacelle in the midposition $C_3$ has a slight positive lift. Lowering

the nacelle considerably reduces the nacelle lift increment due to the increase in the velocities on the underside of the wing. The nacelle in the high position $C_4$ contributes appreciable lift which, unlike that measured for the other positions, increases appreciably with Mach number. At 2.5° angle of attack, however, the lift increments become more positive with increasing Mach number. At a Mach number of about 0.7 the nacelle lift increment for the nacelle in position C is zero. At an angle of attack of 5° the lift increments are slightly more positive than for the lower angles.

At 0° angle of attack, the nacelle in the midposition $C_3$ has the lowest drag and the nacelle in the high position $C_4$ has the highest drag. Up to the maximum Mach number of the test, the effects of compressibility are small at 0° angle of attack except for the high position $C_4$. At 2.5° the low-speed drag at all the nacelle positions but position $C_4$ are essentially equal. The nacelle in position $C_4$ produces nearly twice as much drag increment as the nacelle in the other vertical positions. All the configurations with the exception of position C show a sudden drag rise below a Mach number of 0.675. The nacelle in the low position C does not show any appreciable drag rise up to a maximum test Mach number of 0.7. The drag increment for the nacelle in the low position C is considerably less than that for the nacelle in the semilow position $C_2$ or the midposition $C_3$ at high Mach numbers for an angle of attack of 5°. The high nacelle position was not tested at this angle of attack.

In general, the results of the tests of the horizontal variation of nacelle position show that moving the nacelle forward increases the loss in lift due to the nacelle (fig. 34). At high angles of attack the high-speed drag is greater for the most rearward nacelle position D.

The results from the angular variation tests (fig. 35) show that the lift is greatest for the nacelle having the positive angle of incidence, that is, position $C_{2.5°}$. The drag at 2.5° angle of attack, on the other hand, is considerably less for the nacelle having the negative angle of incidence, position $C_{-2.5°}$, and consequently the lowest lift. At high Mach numbers for an angle of attack of 2.5°, however, the nacelle at both positive and negative angles of incidence had an earlier drag rise than at zero angle of incidence.

Section normal-force coefficient.- The spanwise distribution of the lift is shown in figures 36 to 38. The section normal-force coefficient at low angles of attack decreases at the side of the nacelle (station 1) for the low vertical nacelle positions (fig. 36), whereas there is an appreciable increase for the high nacelle position. The loss in lift

near the low nacelle results from the acceleration of the air past the lower part of the wing, whereas for the high nacelle position $C_4$ the air is accelerated over the upper surface because of the presence of the nacelle.

In all variations of the horizontal position (positions A, B, C, and D) the presence of the nacelle reduced the section normal-force coefficients adjacent to the nacelle. (See fig. 37.) This result is to be expected because only low nacelle positions were included. Changes in the nacelle angle of incidence (fig. 38) had little effect on the wing section normal-force coefficients.

Maximum lift characteristics.- The influence of the nacelle position on the low-speed maximum lift characteristics of the wing is shown in figures 39 to 41. The results showed a loss of maximum lift for all wing-nacelle configurations with respect to the wing alone. It should be noted, however, that two wing-alone lift curves are presented. These curves, which represent results from two series of tests, have been compared in figure 14. Positions $C_4$ and D (figs. 39 and 40) show the least effect on maximum lift characteristics. The maximum loss in lift is encountered with the nacelle in position C. The maximum lift of this configuration is about 12 percent less than for the wing alone.

## Leading-Edge Modifications

In view of the fact that most detrimental effects of the nacelle - particularly the critical Mach number effects - arise from the high peak pressures occurring for nearly all configurations over the leading edge of the wing adjacent to the nacelle, an attempt was made to alleviate these peak pressures by modification of the leading edge.

Leading-edge pressure distribution.- Inasmuch as the pressures near the midchord were not seriously affected by the leading-edge alterations, only the wing leading-edge pressures are presented. At $0^\circ$ angle of attack shifting the leading edge forward and slightly downward from its normal position to leading-edge sections 2 and 3 reduces the pressure peak adjacent to the nacelle (station 1) with no appreciable effect on the pressures on the underside of the leading edge at this station (figs. 42(a) and (b)). Pressure peaks occurring on the underside of the leading edge at the next two stations, however, indicate that at this angle of attack, leading-edge alterations should not extend far outboard.

At a negative angle of attack the peak pressures on the lower surface are in general increased (fig. 42(c)). The pressures over the upper surface are not shown since they are not critical.

Figure 42(d) shows that at an angle of attack of 2.5° the most forward position of the leading edge (section 3) reduces the increment of peak pressure due to the presence of the nacelle to half that occurring on the normal leading edge. As can be seen in figure 43, drooping the leading edge (sections 4 and 5) has no great influence on the pressures over the upper surface at $\alpha = 0°$, whereas the pressures over the lower surface are adversely affected. The peaks are considerably reduced adjacent to the nacelle at 2.5° angle of attack, but the widening of the peaks which accompanied this reduction may actually have as great a detrimental effect as the original peak.

Leading-edge section 6, which combined a large forward extension and a large droop (fig. 44), shows a large negative peak on the lower surface at $\alpha = 0°$ and -1.5° without any improvement in the upper-surface distribution. At an angle of attack of 2.5° this section shows the greatest improvement of any tested.

Critical Mach number.- The critical Mach number curves for the leading-edge modifications (fig. 45) show that, in general, the modifications gave a slight improvement in the critical Mach number at the positive angles of attack at the expense of a considerably greater reduction in critical Mach number at the negative angles of attack. Section 6 gave the greatest improvement at the positive angles of attack - at the expense, however, of greatly reducing the critical Mach number at angles of attack below about 0.5°.

Lift and drag characteristics.- The leading-edge modifications have little effect on the lift or drag characteristics of the nacelle (figs. 46 to 48). Leading-edge section 6 is shown in figure 45(c) to delay the critical Mach number at an angle of attack of 2.5°. Despite this delay in critical Mach number, the drag (fig. 46(b)) showed a tendency to break very suddenly at a Mach number of about 0.65 as compared with the drag of the normal leading edge, which showed no sudden breaks up to the maximum test Mach number of 0.675 for this configuration.

Maximum lift characteristics.- The maximum lift coefficient of the wing-nacelle combination is slightly improved by the use of leading-edge section 3 (fig. 49(a)); leading-edge section 2 has very little effect. The maximum lift characteristics are greatly improved by the use of the modifications in which the leading edges have been drooped (fig. 49(b)). The improvements in maximum lift coefficient are approximately proportional to the amount of droop, with the leading-edge section 5 having approximately the same maximum lift characteristics as the wing alone for the same series of tests. Figure 49(c) shows that section 6 has approximately the same maximum lift coefficient but a more abrupt stall than the wing alone.

## DISCUSSION

The main objective of this investigation was to obtain a wing-nacelle combination having the force break occurring at a Mach number as high as for the wing alone. This objective was realized for the nacelle in position C up to the maximum Mach number of the tests for angles of attack up to and including 2.5° with only a slight loss in lift (figs. 15 and 33). At 5° angle of attack the drag breaks of the nacelle for positions A and B (fig. 34) were at a higher Mach number than for the wing alone (fig. 15); however, these configurations had the largest losses in lift.

The actual selection of the best nacelle position is complicated and depends to some extent on the airplane proportion, speed, and purpose. It is not necessarily best, in general, to select the nacelle position having the highest critical Mach number, since the critical Mach numbers over small areas were not found to be indicative of the Mach number at which severe drag rise occurs. Although position C had the lowest local critical Mach number, the drag break occurred at a higher Mach number for this configuration than for most of the other configurations. The other configurations which had late drag rises had more serious losses in lift. Position C, therefore, appears to be a reasonable compromise for the range of Mach number covered in this investigation. It is not considered safe to attempt any extrapolation of the results to higher Mach numbers since the critical Mach numbers were not indicative of the drag break in the range of the tests.

The low nacelle (position C) had much better drag characteristics than the other nacelles in the vertical variation; however, this position reduced the lift, particularly at low speeds. Only the low nacelles (positions A, B, C, and D) did not have a severe drag rise at a Mach number of 0.68 or less at an angle of attack of 2.5°.

Moving the nacelle forward and rearward had little influence on the drag characteristics for angles of attack of 2.5° and below. The lift losses were about twice as great for the configuration with the nacelle in the most forward position as for the configuration with the nose of the nacelle 0.66 chord ahead of the wing leading edge (position C). The nacelle located with its nose 0.35 chord ahead of the wing leading edge (position D) actually contributed lift; however, for this nacelle position the drag rise at $\alpha = 5°$ was greater than for any of the other low nacelle positions and might be expected to occur at a lower Mach number at $\alpha = 2.5°$ than for the nacelle in position C. (Data were not obtained above a Mach number of 0.65 for this configuration.)

In general, changing the angular relation between the wing and nacelle from position C does not appear advisable inasmuch as the test results show an abrupt rise in drag occurring at a lower Mach number for

the positions where the nacelle had either a positive or negative incidence than for position C. At lower angles of attack it appears feasible that a slight gain in lift may be obtained with no appreciable influence of drag when the nacelle is given a higher angle of attack than the wing.

The problem of obtaining a nacelle position which has good high-speed characteristics was greatly simplified in this investigation by the use of components which by themselves have good high-speed characteristics. This simplification has been emphasized by the fact that the differences between many of the positions were found to be small and hard to evaluate. The importance of selecting a nacelle having a high critical speed (well above that of the wing) is emphasized.

## CONCLUSIONS

The results of the investigation for the Mach number range of the tests (Mach numbers up to about 0.7) of the interference effects between an airfoil of high critical speed with no sweepback and a nacelle of high critical speed mounted in various positions with respect to the wing indicated the following conclusions:

1. The problem of obtaining a wing-nacelle combination which has good high-speed characteristics is greatly simplified by the adoption of components which by themselves have good high-speed characteristics. The importance of selecting a nacelle having a high critical speed (well above that of the wing) is emphasized.

2. The low nacelle position with the nose of the nacelle 0.66 chord ahead of the wing leading edge, with the upper surface of the wing tangent to the top nacelle line, and with the nacelle center line parallel to the wing chord line gives a reasonable compromise between loss of lift and late drag rise. No drag rise occurred in the Mach number range of the tests at angles of attack of 2.5° or less for this configuration; and the loss in lift, particularly at high speeds, was small.

3. The vertical variation of nacelle position showed that the Mach number at which severe drag rises occurred decreased with increasing height of the nacelle. Severe drag rises occurred below a Mach number of 0.68 on all but the low nacelle positions at an angle of attack of 2.5°.

4. Moving the nacelle forward from the low position with the nacelle nose 0.66 chord ahead of the wing leading edge had little effect

on the drag but increased the loss in lift. The presence of the nacelle in the most rearward position increased the lift slightly. The nacelle in this position, however, had the greatest drag rise of the low position nacelles at 5° angle of attack.

5. In general, giving the nacelle either positive or negative incidence reduced the Mach number at which the drag rise occurred.

6. The local high negative peak pressures which occurred on the upper surface of the wing fillets for the low nacelle positions could be removed at positive angles by drooping the leading edge of the wing adjacent to the nacelle; however, the removal of these peaks had no noticeable effect on the lift and drag characteristics and usually caused peaks on the under surface at small negative angles of attack.

Langley Memorial Aeronautical Laboratory
National Advisory Committee for Aeronautics
Langley Field, Va., November 4, 1947

REFERENCE

1. Becker, John V.: Wind-Tunnel Tests of Air Inlet and Outlet Openings on a Streamline Body. NACA ACR, Nov. 1940.

TABLE I

NACA 65-210 AIRFOIL ORDINATES

[Stations and ordinates given in percent of airfoil chord]

| Upper surface | | Lower surface | |
|---|---|---|---|
| Station | Ordinate | Station | Ordinate |
| 0 | 0 | 0 | 0 |
| .435 | .819 | .565 | - .719 |
| .678 | .999 | .822 | - .859 |
| 1.169 | 1.273 | 1.331 | -1.059 |
| 2.408 | 1.757 | 2.592 | -1.385 |
| 4.898 | 2.491 | 5.102 | -1.859 |
| 7.394 | 3.069 | 7.606 | -2.221 |
| 9.894 | 3.555 | 10.106 | -2.521 |
| 14.899 | 4.338 | 15.101 | -2.992 |
| 19.909 | 4.938 | 20.091 | -3.346 |
| 24.921 | 5.397 | 25.079 | -3.607 |
| 29.936 | 5.732 | 30.064 | -3.788 |
| 34.951 | 5.954 | 35.049 | -3.894 |
| 39.968 | 6.067 | 40.032 | -3.925 |
| 44.984 | 6.058 | 45.016 | -3.868 |
| 50.000 | 5.915 | 50.000 | -3.709 |
| 55.014 | 5.625 | 54.986 | -3.435 |
| 60.027 | 5.217 | 59.973 | -3.075 |
| 65.036 | 4.712 | 64.964 | -2.652 |
| 70.043 | 4.128 | 69.957 | -2.184 |
| 75.045 | 3.479 | 74.955 | -1.689 |
| 80.044 | 2.783 | 79.956 | -1.191 |
| 85.038 | 2.057 | 84.962 | - .711 |
| 90.028 | 1.327 | 89.972 | - .293 |
| 95.014 | .622 | 94.986 | .010 |
| [a]100.000 | 0 | [a]100.000 | 0 |

L. E. radius: 0.687
Slope of radius through L. E.: 0.084

[a]2.22 percent of the chord was removed at the trailing edge for this investigation.

TABLE II

NACELLE ORDINATES

[Stations and radii in percent of nacelle length]

| Station | Radius | Station | Radius |
|---|---|---|---|
| 0 | 0 | | |
| 1.25 | 1.583 | 50.00 | 8.217 |
| 2.50 | 2.392 | 55.00 | 7.933 |
| 5.00 | 3.592 | 60.00 | 7.483 |
| 7.50 | 4.467 | 65.00 | 6.833 |
| 10.00 | 5.167 | 70.00 | 6.033 |
| 15.00 | 6.183 | 75.00 | 5.100 |
| 20.00 | 6.925 | 80.00 | 4.092 |
| 25.00 | 7.483 | 85.00 | 3.092 |
| 30.00 | 7.900 | 90.00 | 2.075 |
| 35.00 | 8.183 | 95.00 | 1.033 |
| 40.00 | 8.333 | 97.50 | .520 |
| 45.00 | 8.333 | 100.00 | 0 |

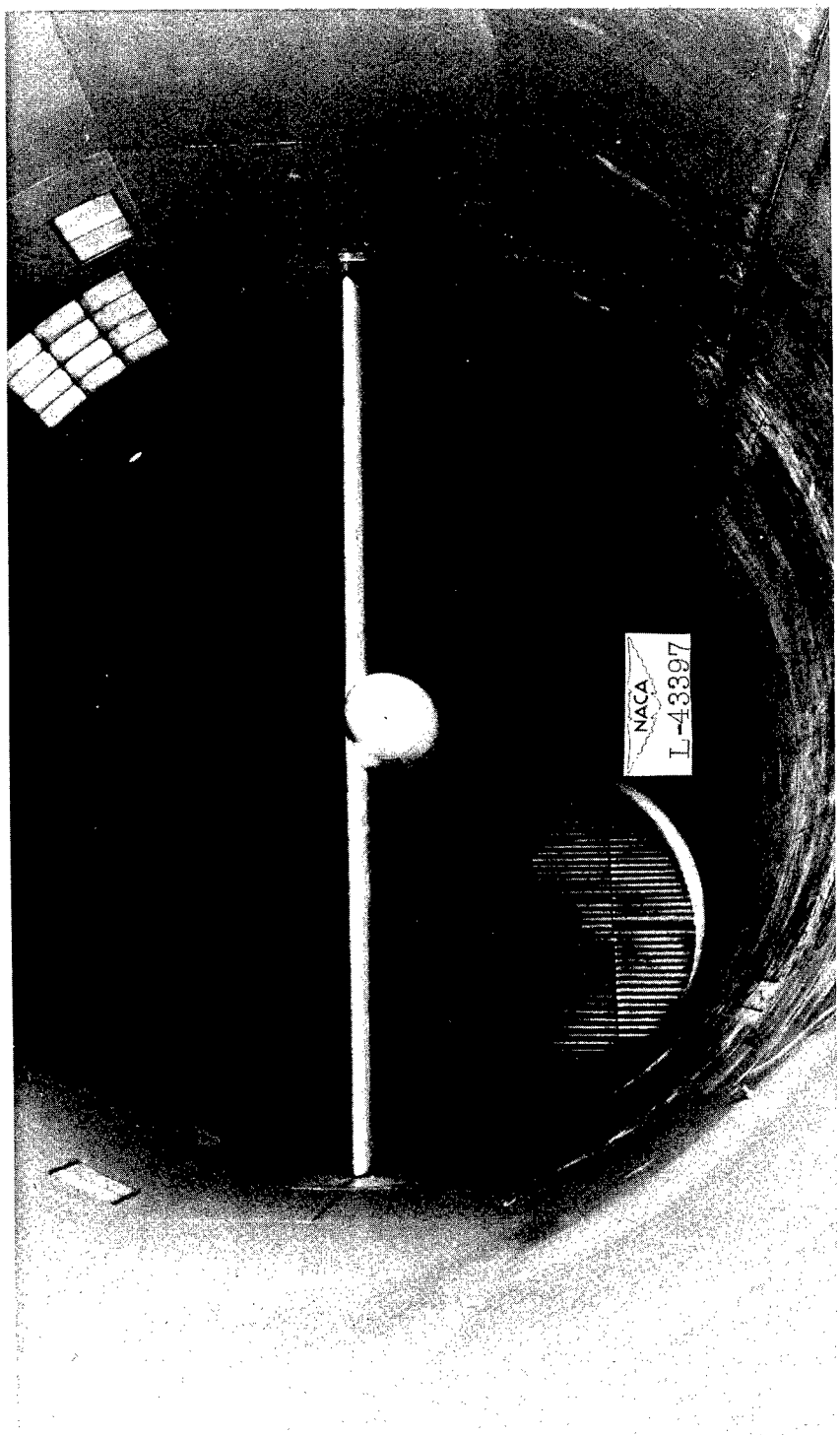


Figure 1.- Model mounted in Langley 16-foot high-speed tunnel.

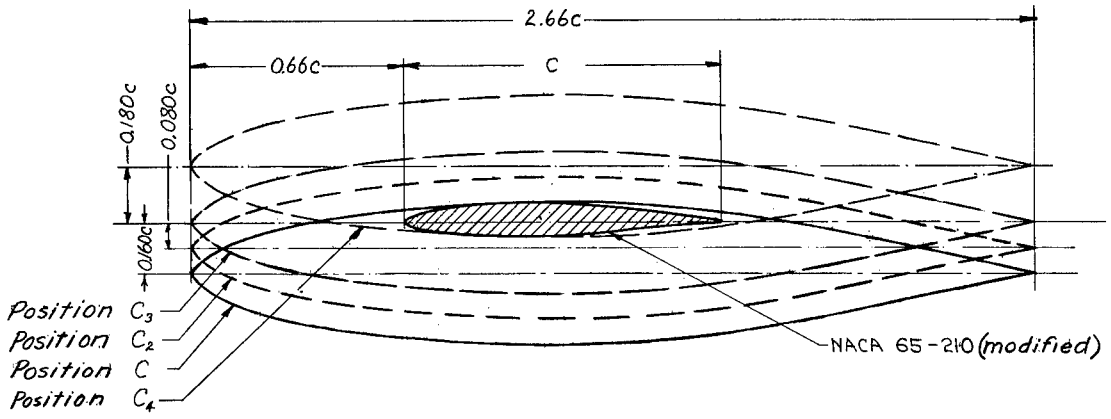


(a) Vertical variations of nacelle positions.

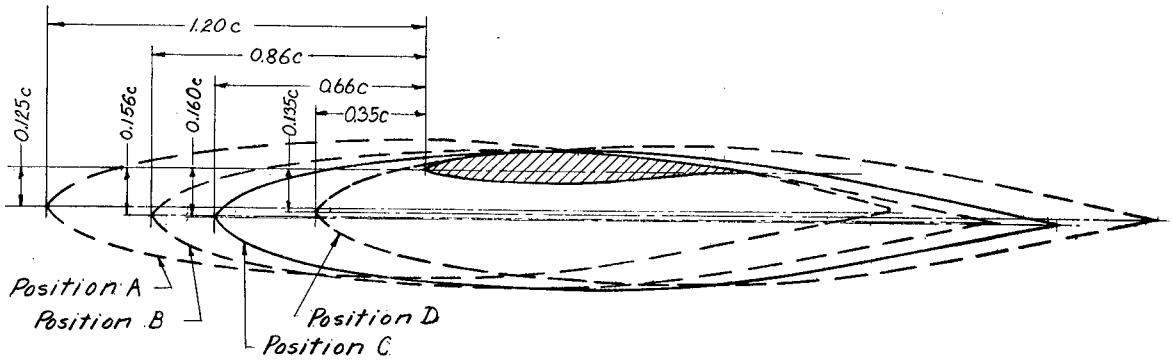


(b) Longitudinal variations of nacelle positions.

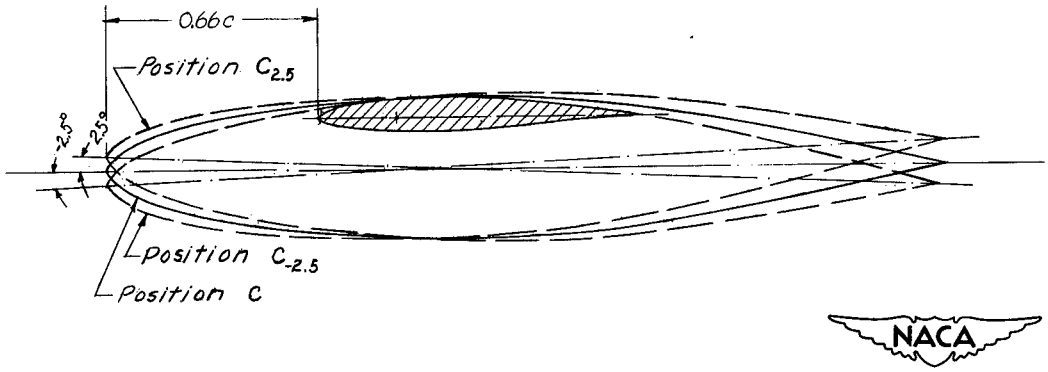


(c) Variation of nacelle angle of incidence.

Figure 2.- Nacelle positions.

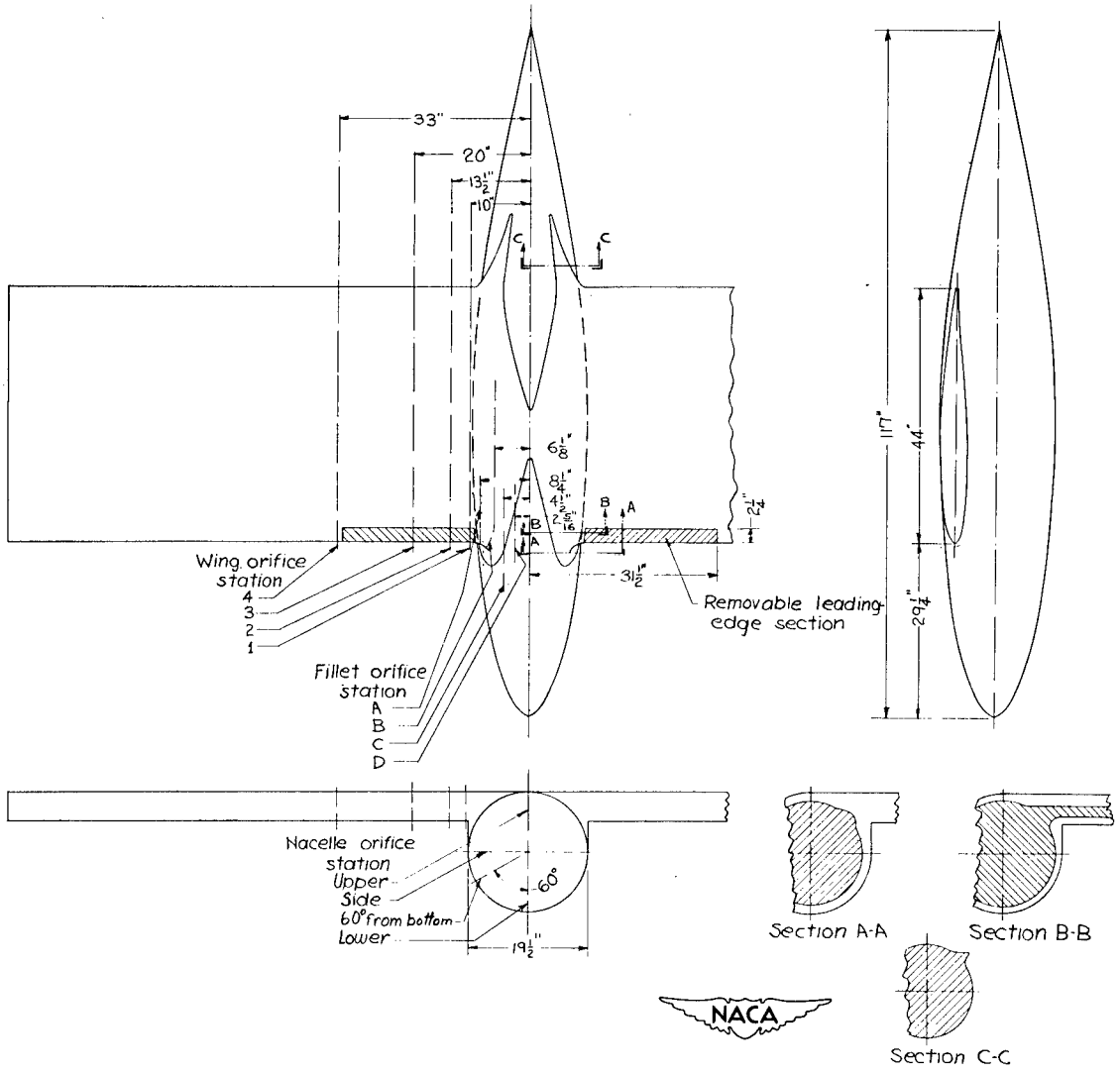


Figure 3.- Model with the nacelle in position C showing the pressure-orifice locations.

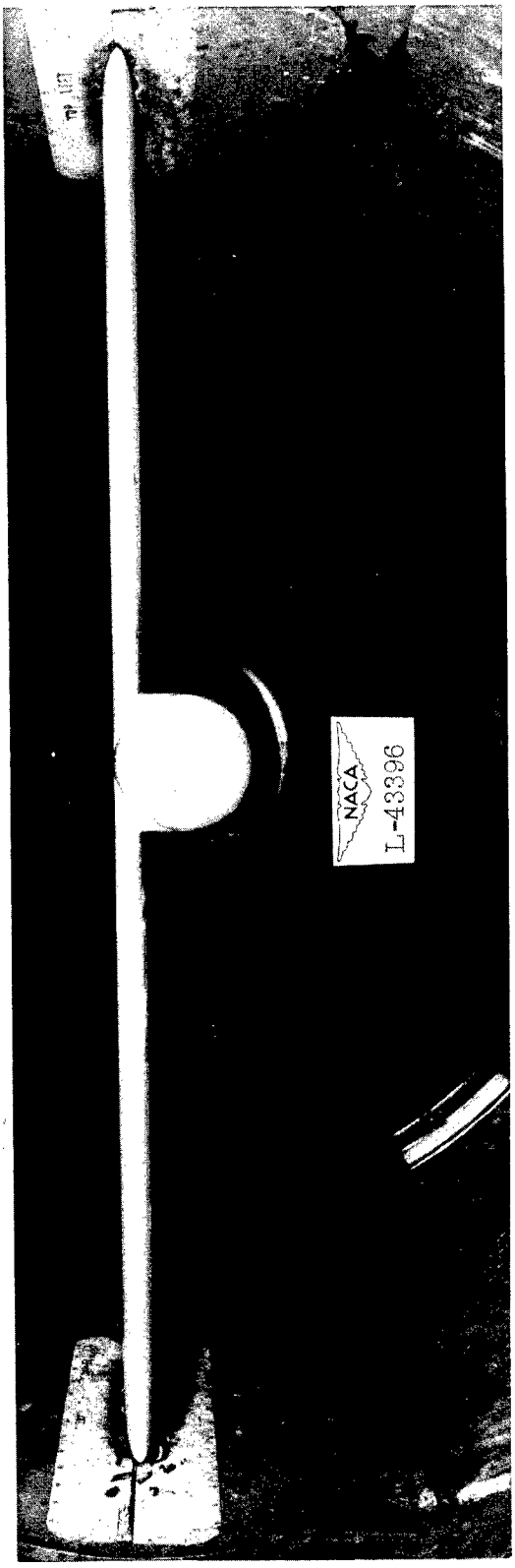


Figure 4.- Front view of model in the tunnel with nacelle in position C.

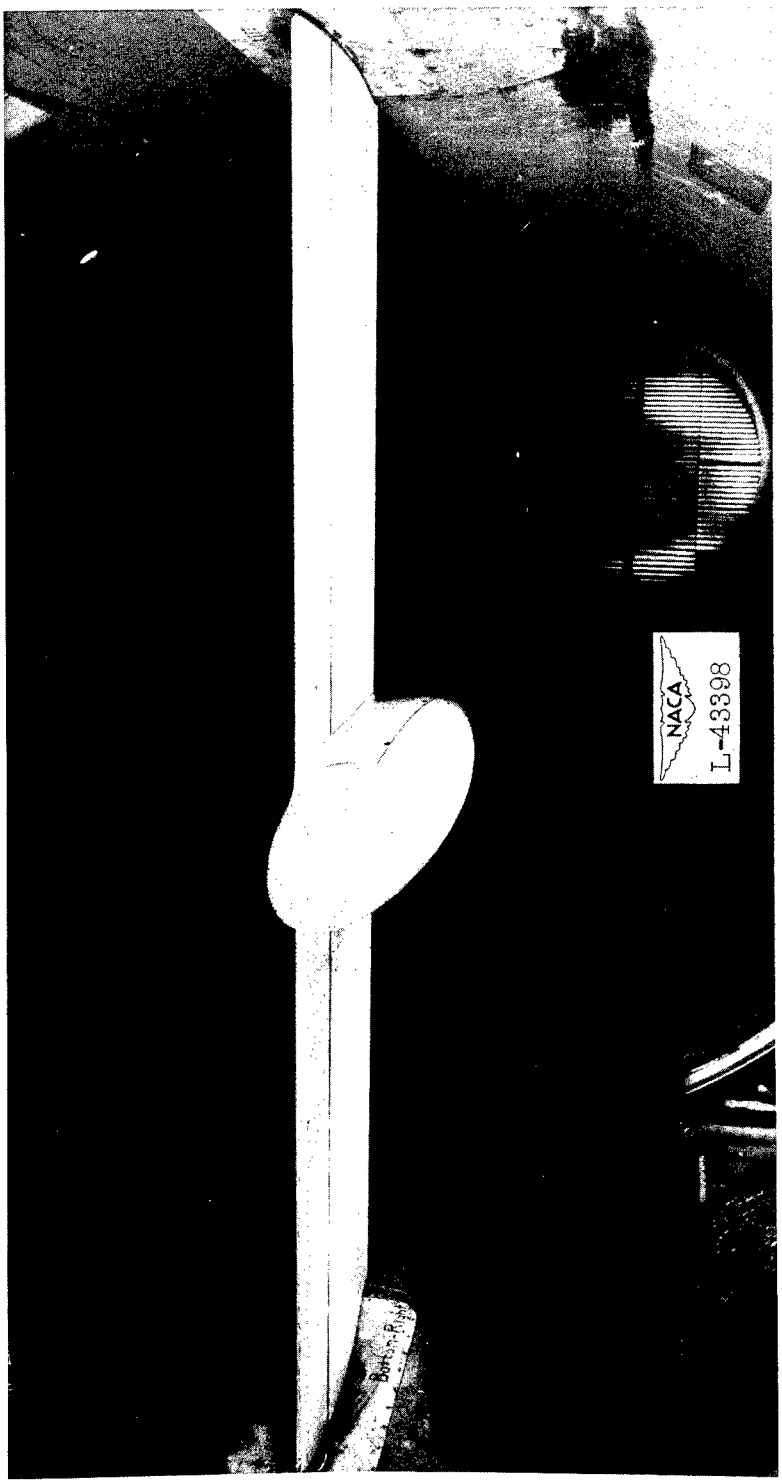


Figure 5.- Three-quarter front view of model with nacelle in position C.

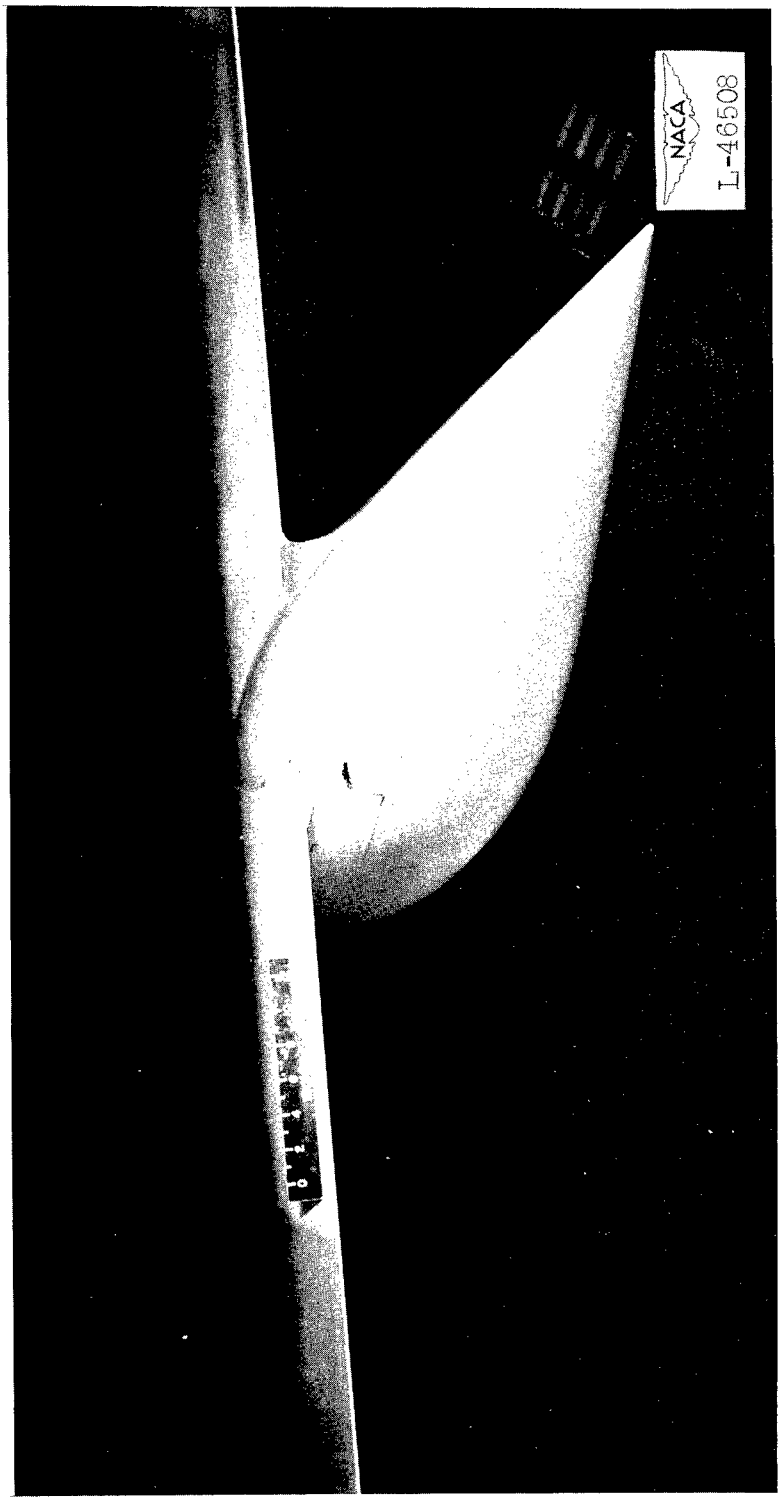


Figure 6.- Three-quarter rear view of model with nacelle in position C showing typical trailing-edge fillet.

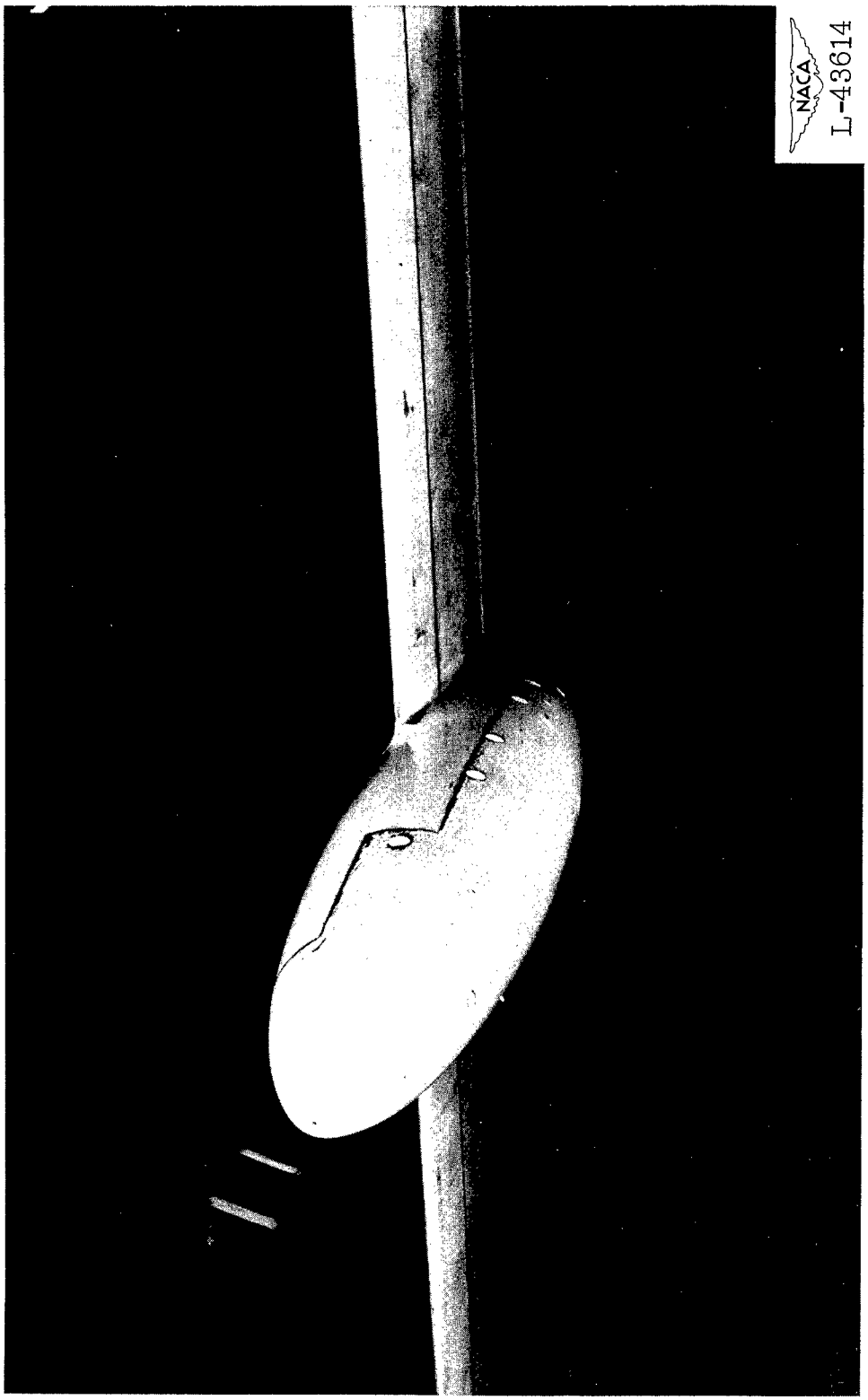


Figure 7.- Three-quarter front view of model with nacelle in position A

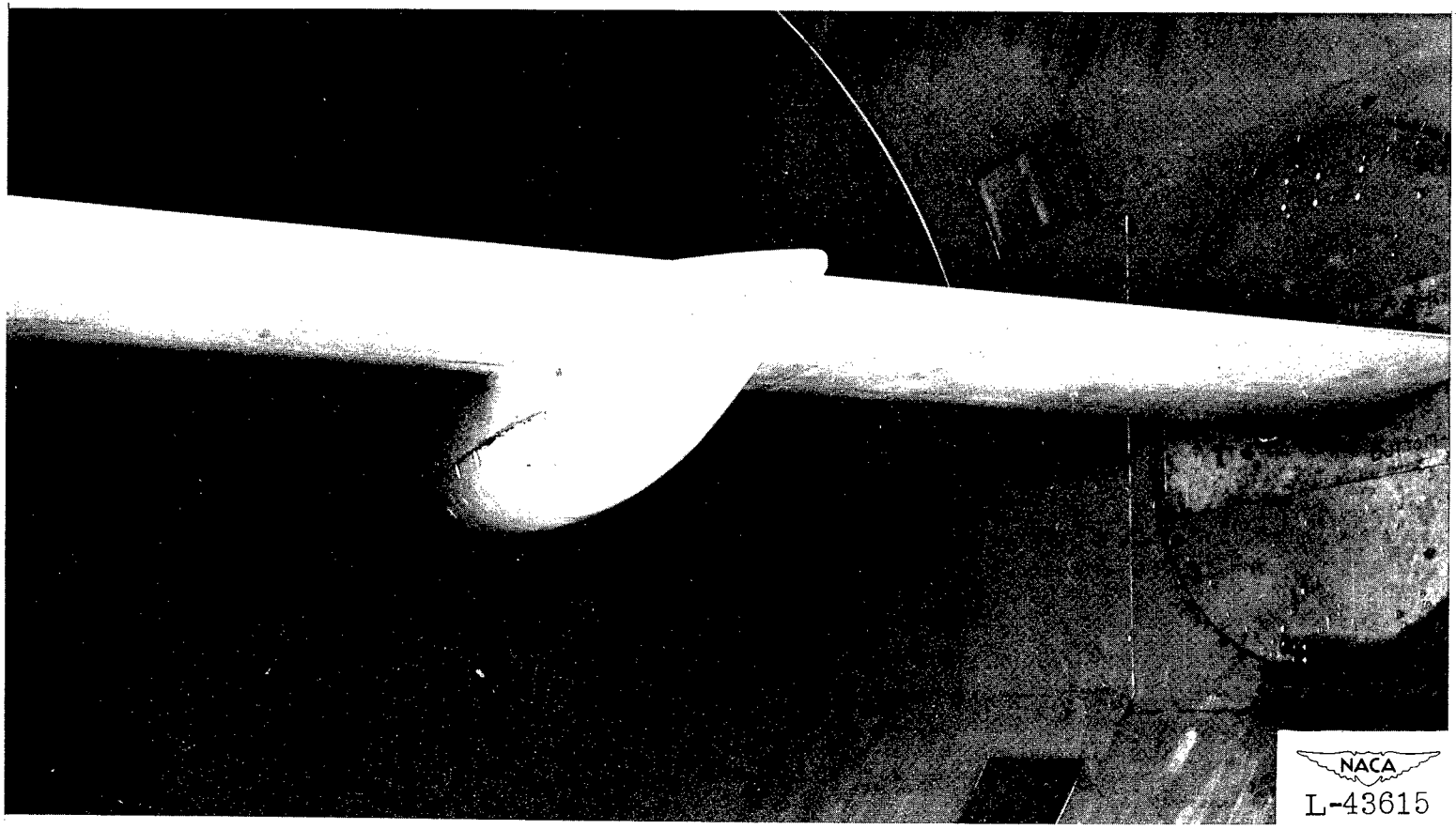


Figure 8.- Three-quarter rear view of model with nacelle in position A.

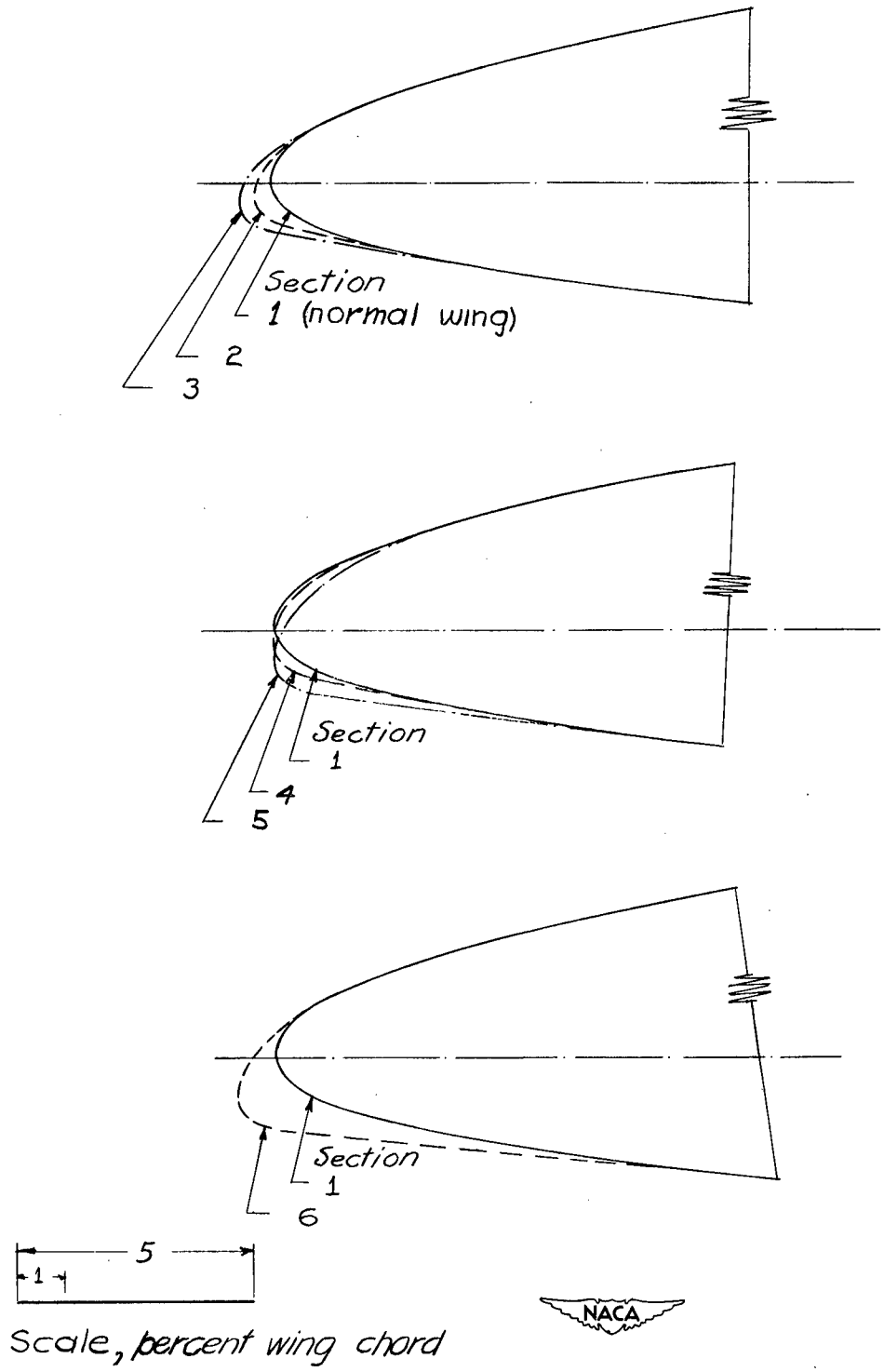


Figure 9.- Modified leading-edge sections at wing orifice station 1.

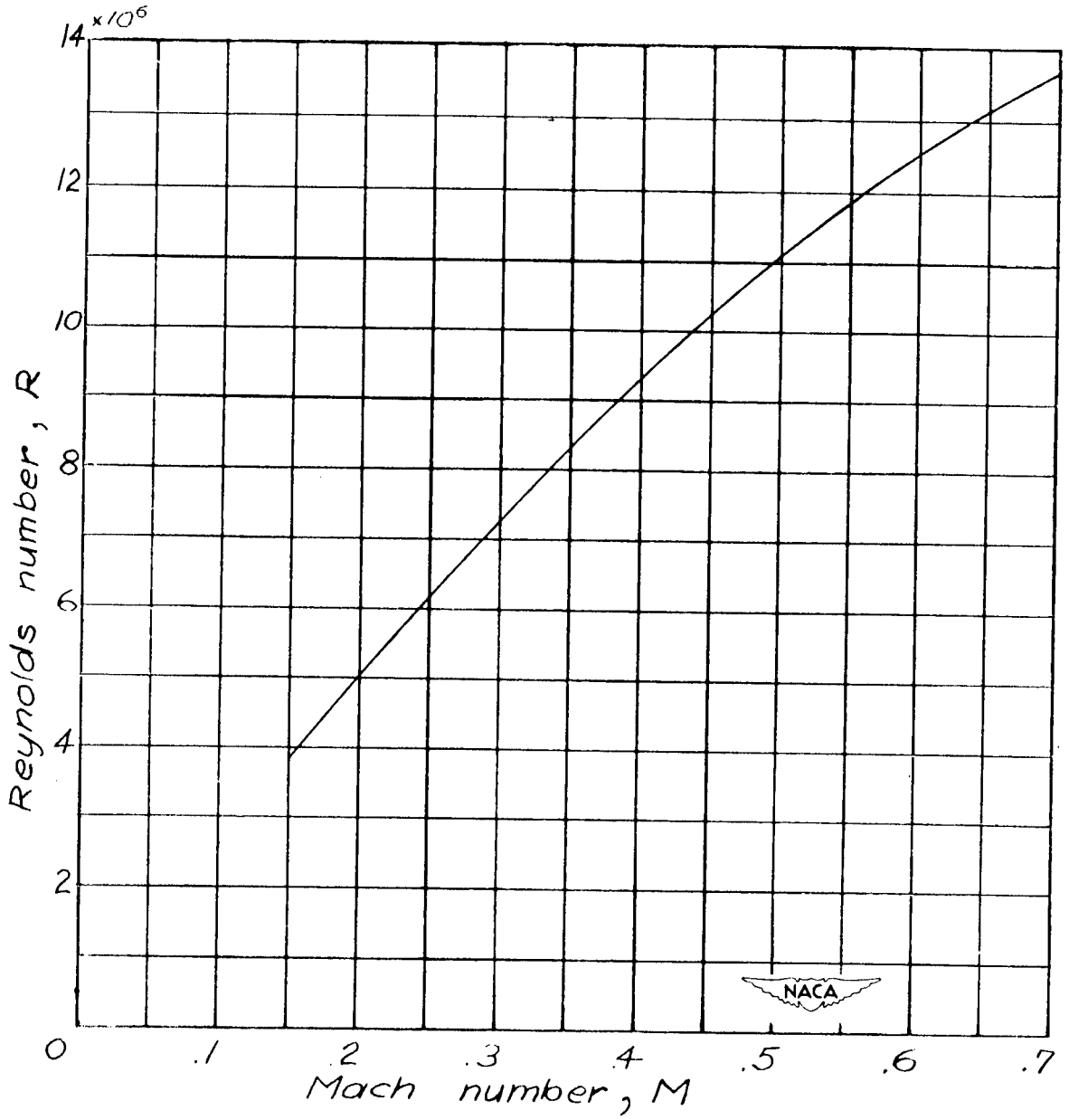


Figure 10.- Variation of average Reynolds number with Mach number during test.

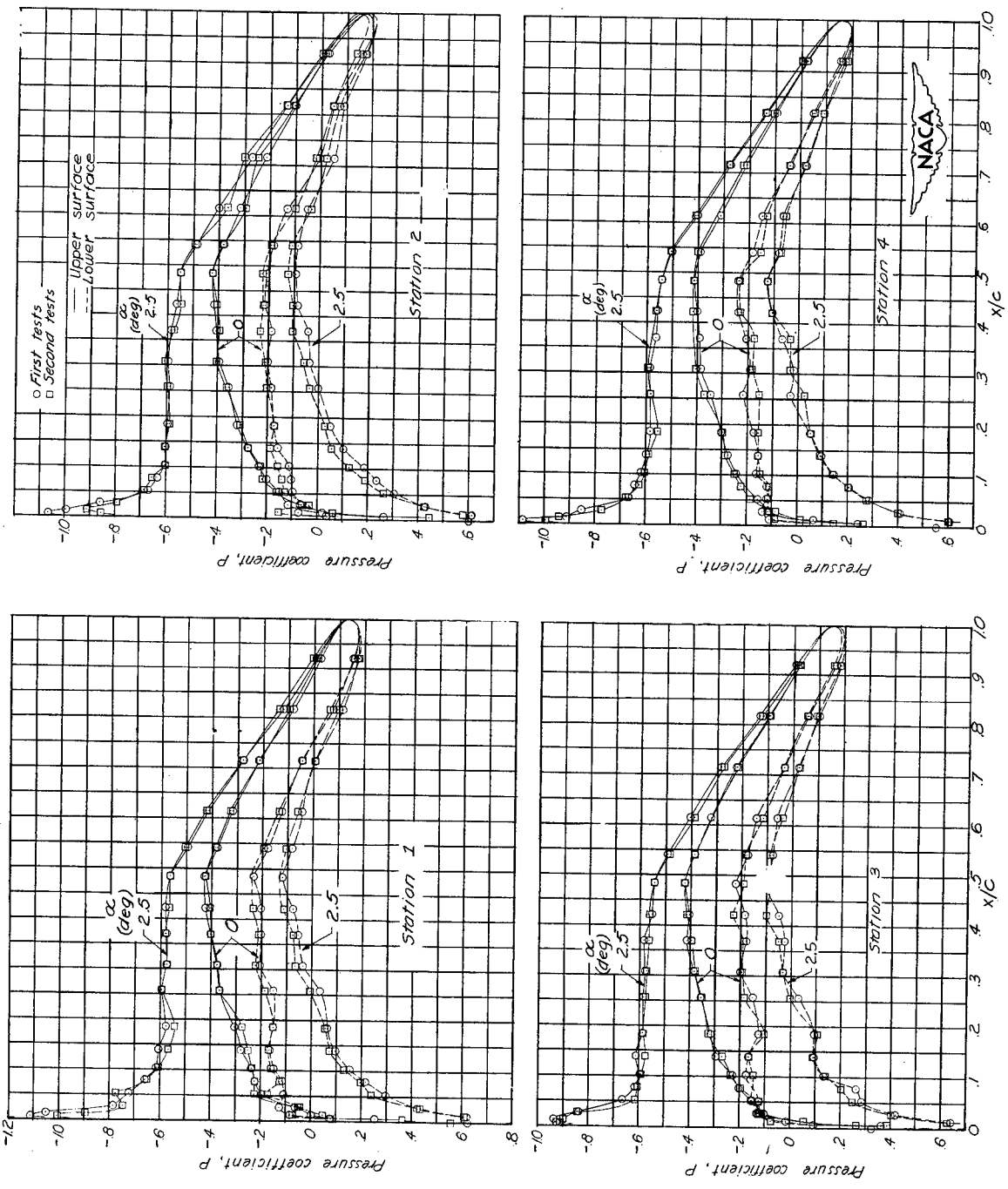


Figure 11.- Pressure distributions about the wing for wing-alone condition at M = 0.4.

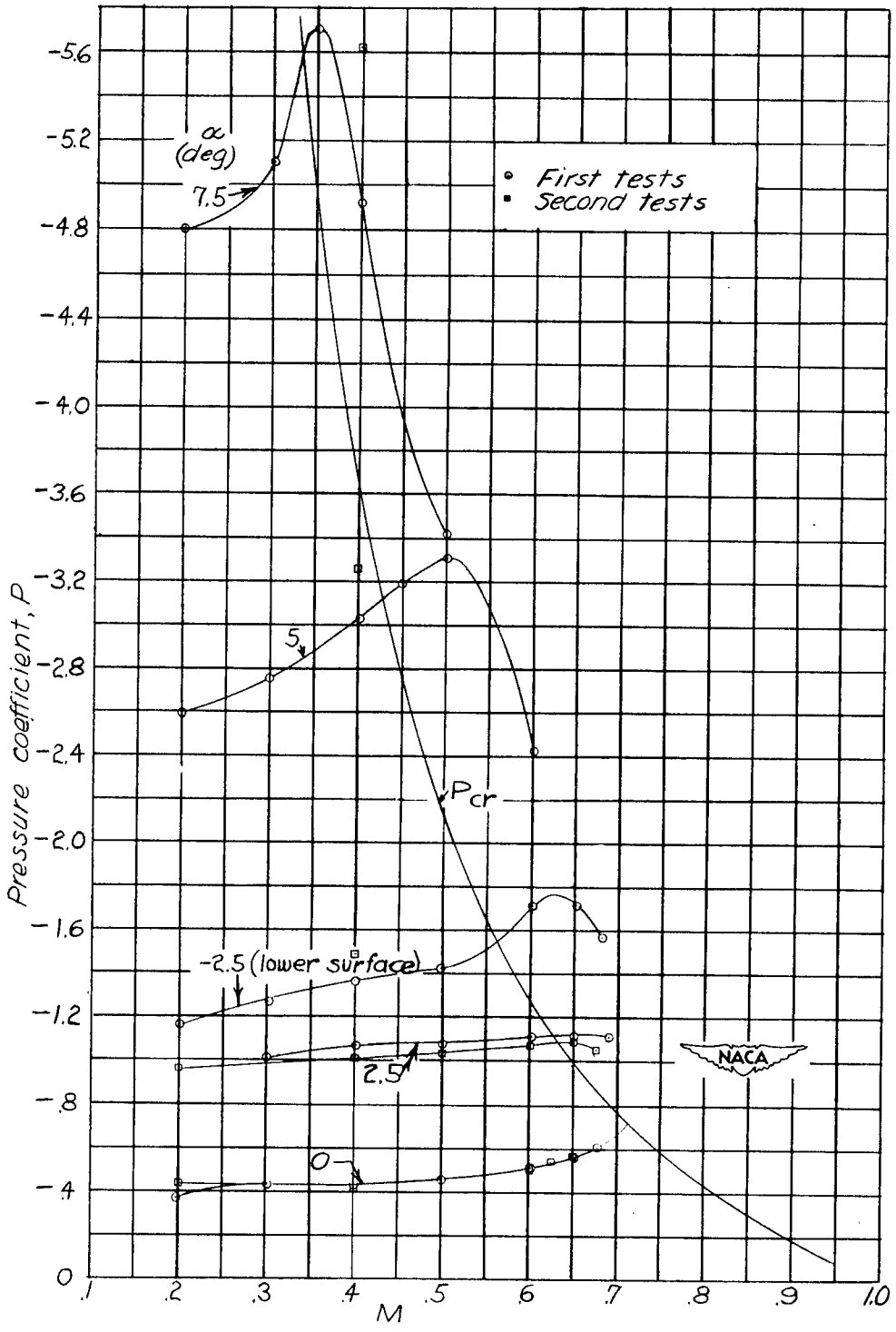


Figure 12.- Variation with Mach number of peak negative pressure coefficients on wing for wing-alone condition.

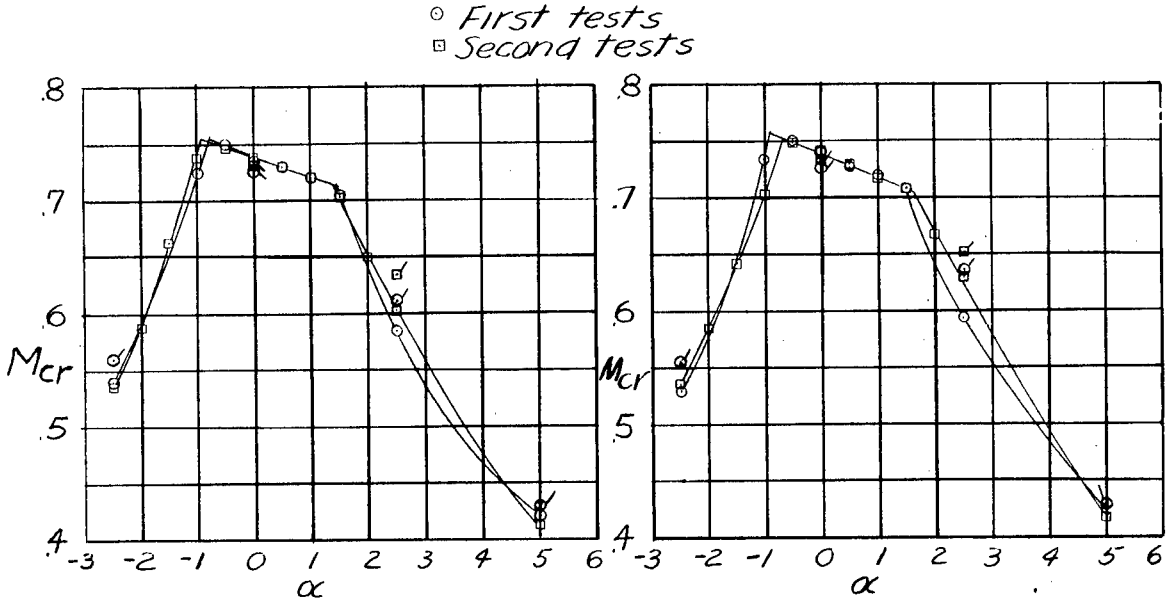


(a) Station 1.

(b) Station 2.

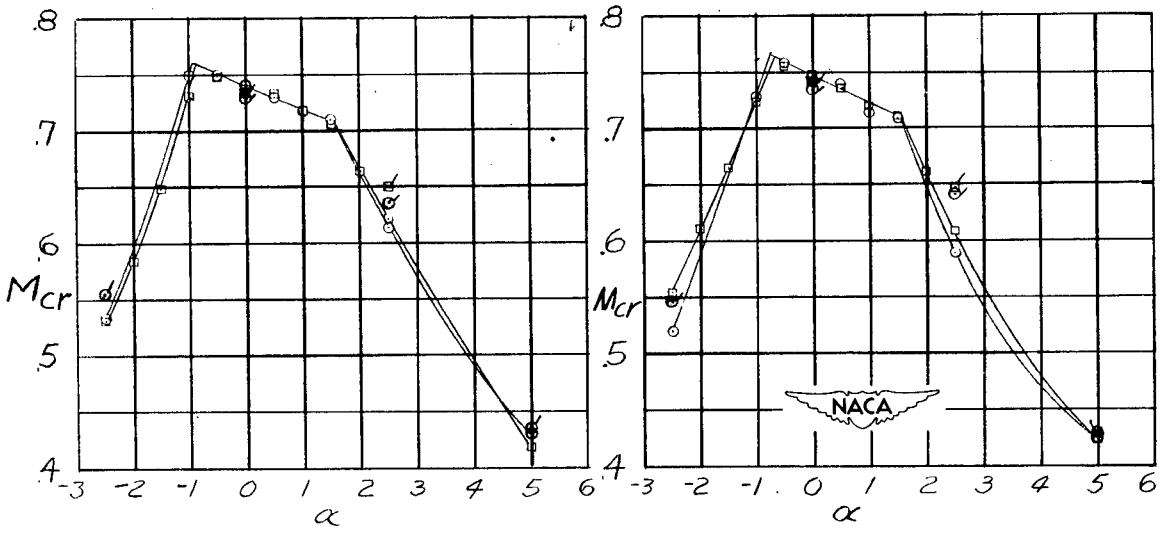


(c) Station 3.

(d) Station 4.

Figure 13.- Variation of critical Mach number with angle of attack for wing alone. Untailed symbols refer to points extrapolated from M = 0.4 results.

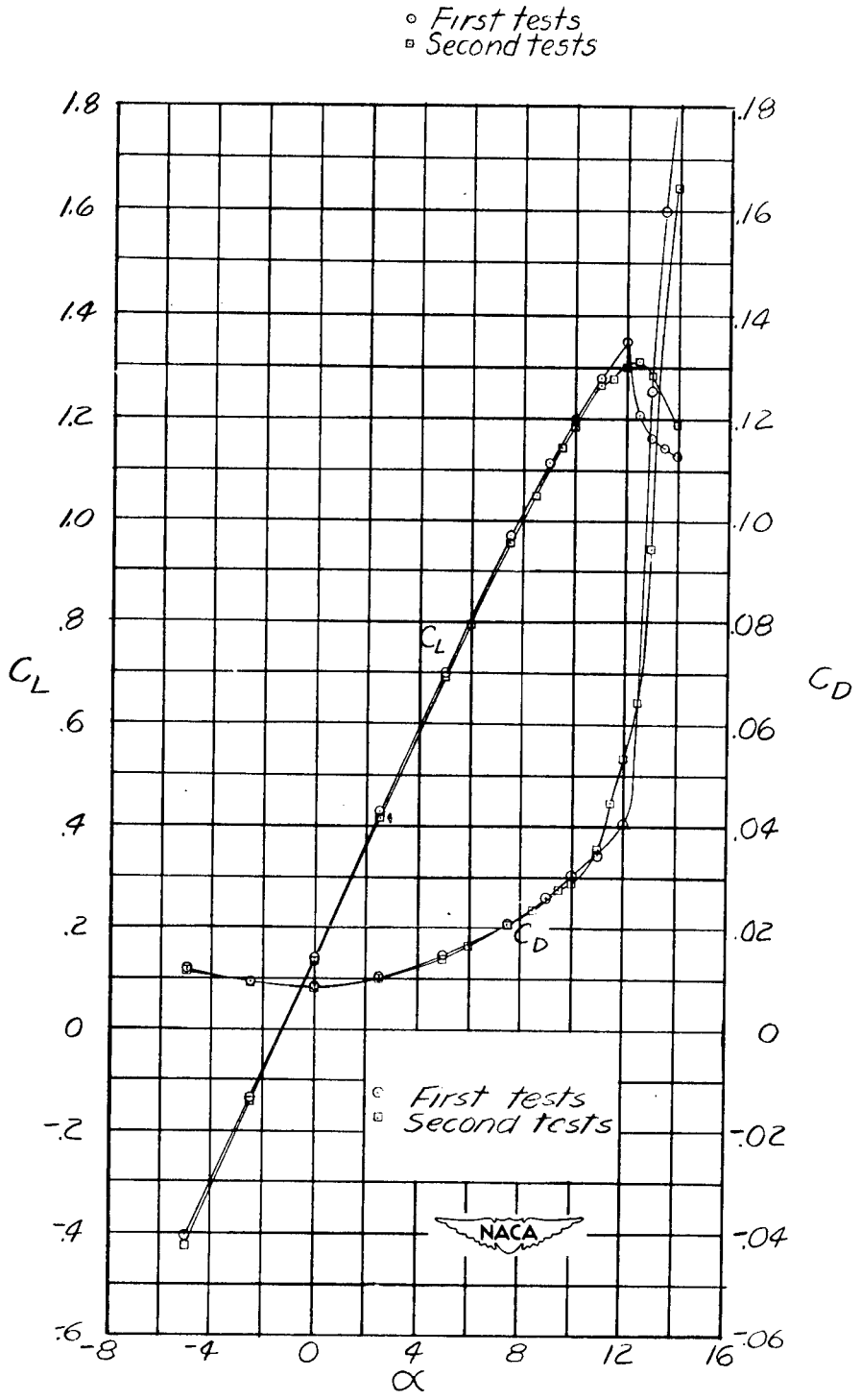


Figure 14.- Wing-alone characteristics. M = 0.2.

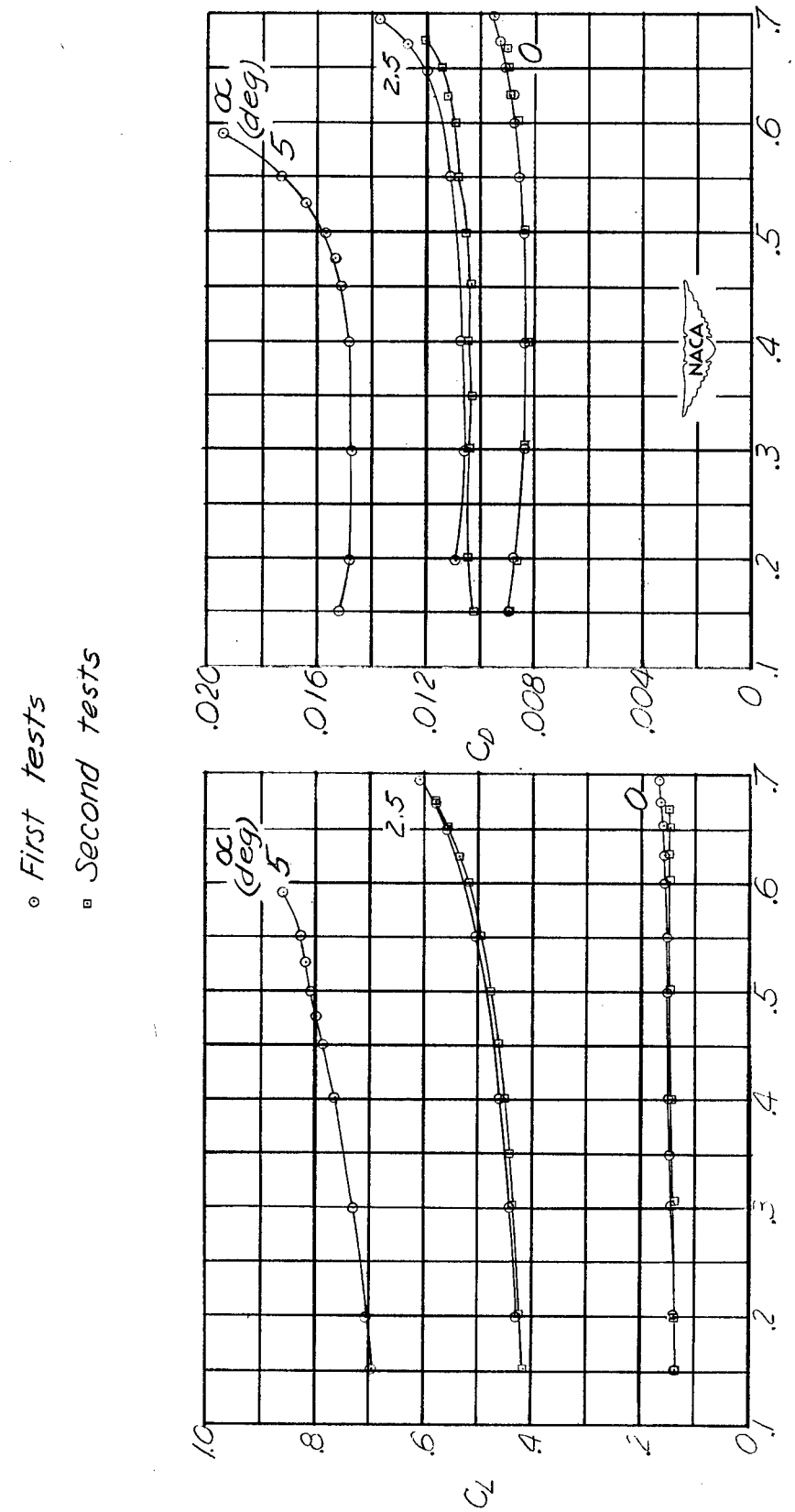


(a) Lift. (b) Drag.

Figure 15.- Variation of wing-alone lift and drag coefficients with Mach number.

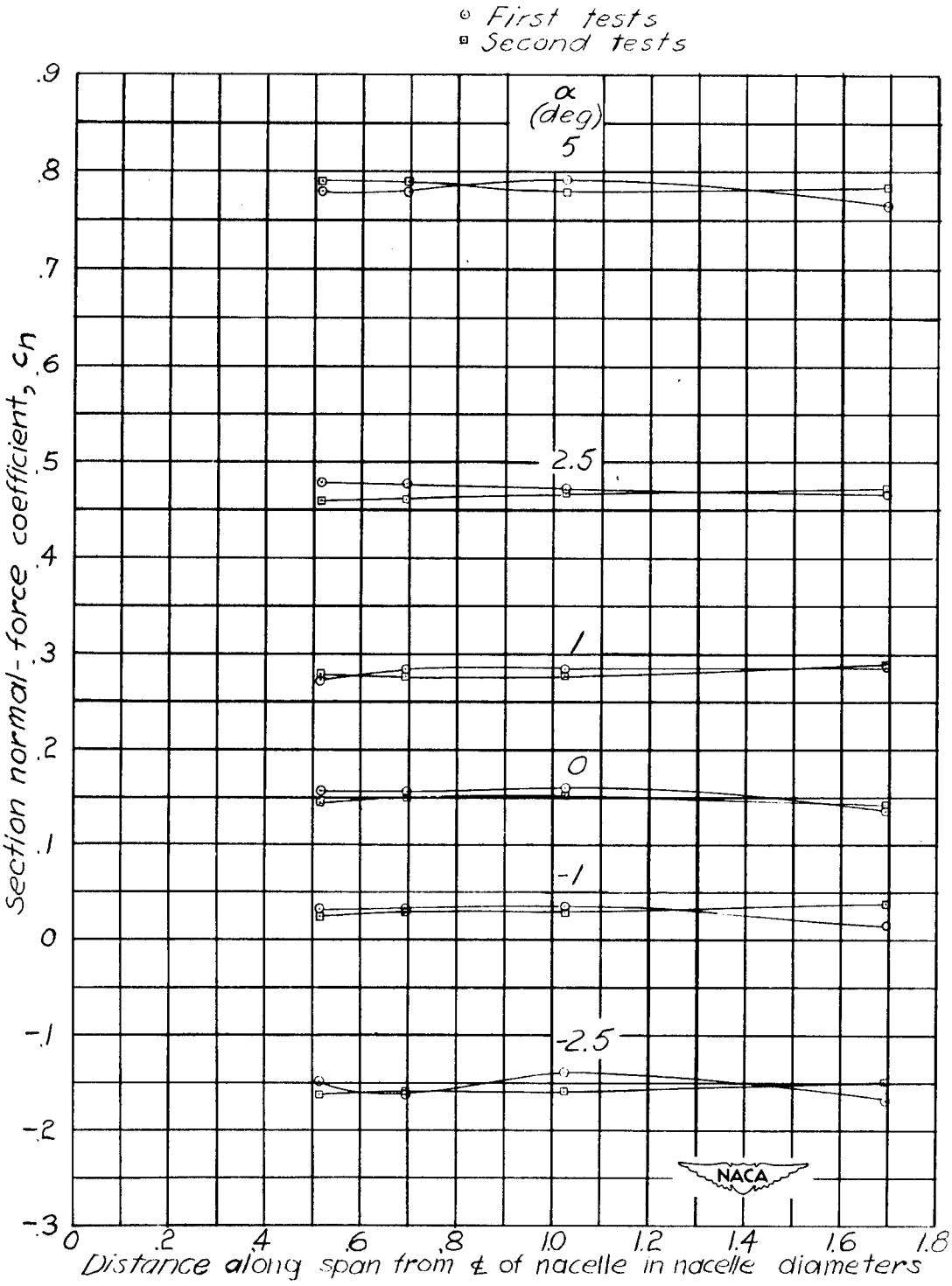


Figure 16.- Spanwise variation of normal-force coefficients for wing alone. M = 0.4.

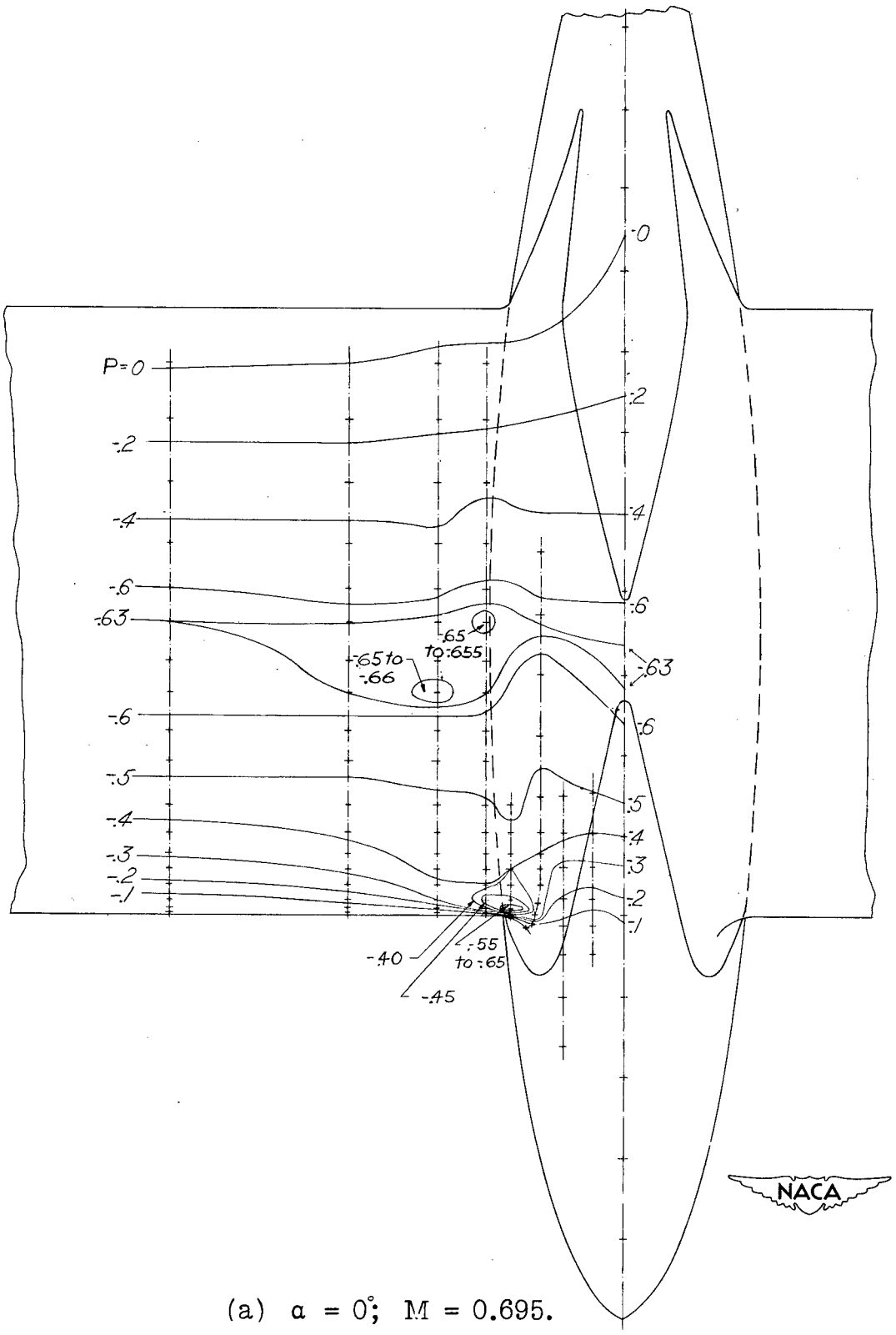


(a) $\alpha = 0^\circ$; $M = 0.695$.

Figure 17.- Pressure contours on upper surface of wing and nacelle with nacelle in position C.

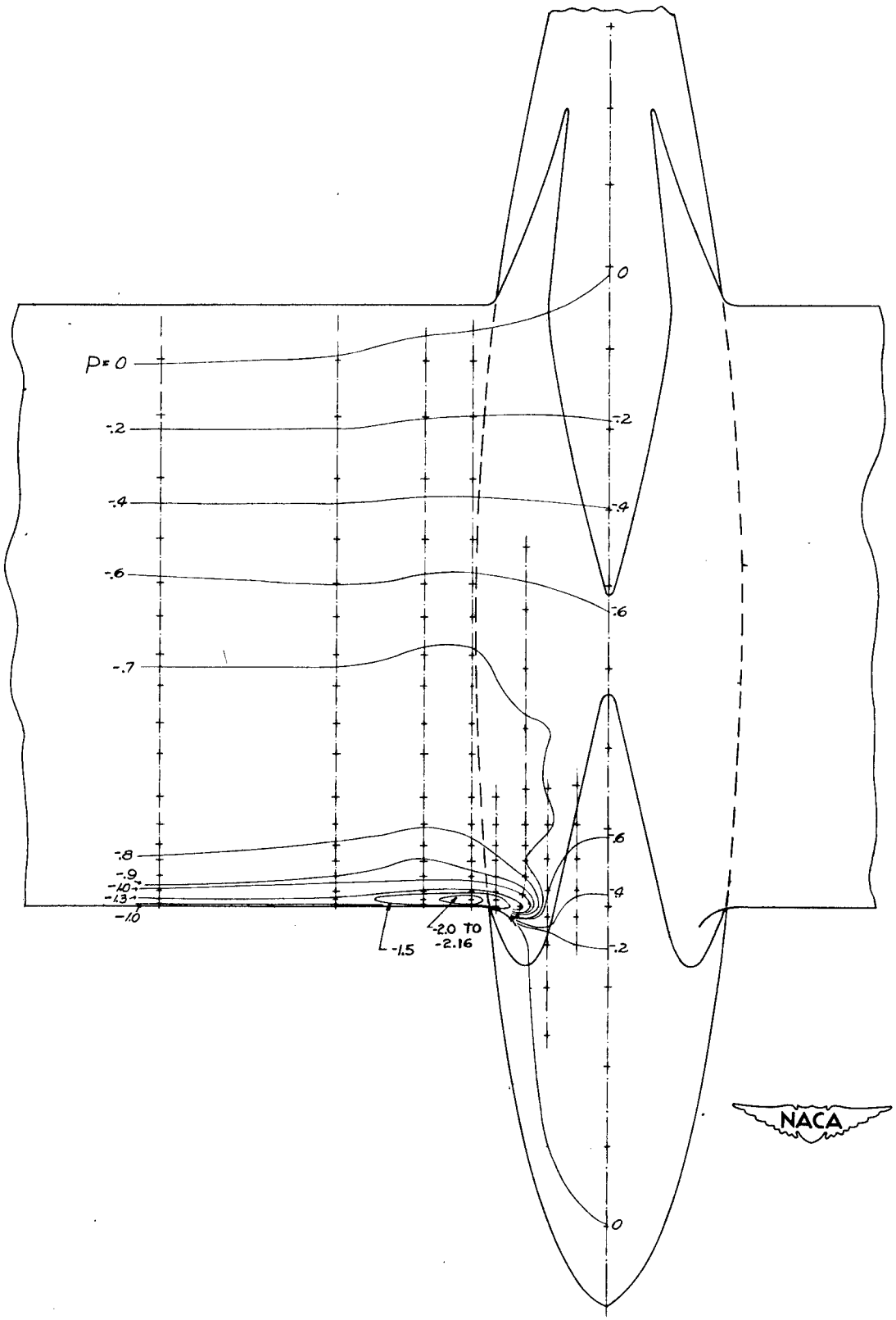


(b) $\alpha = 2.5^{\circ}$; M = 0.6.

Figure 17.- Continued.

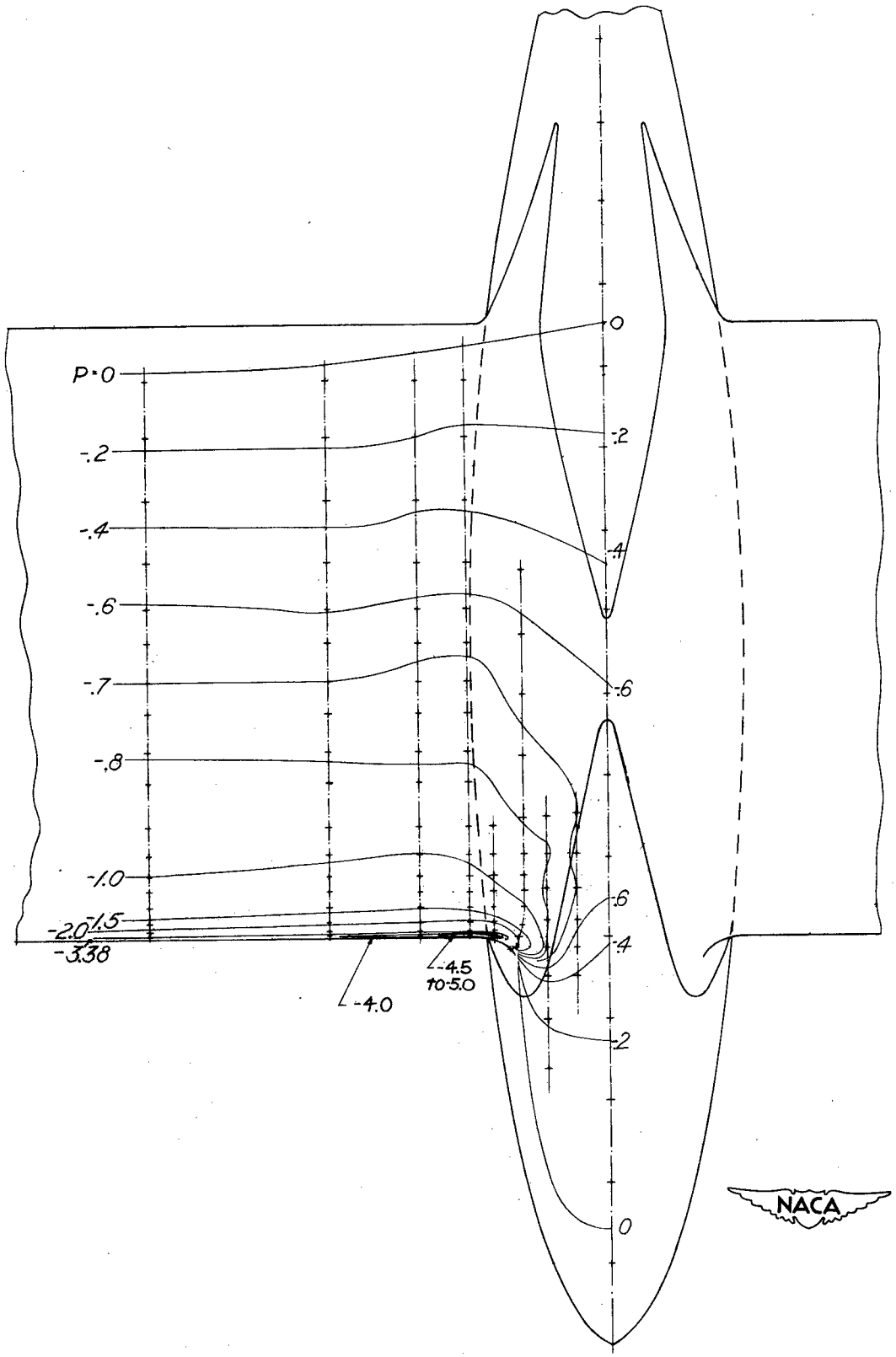


(c) $\alpha = 5^{\circ}$; M = 0.4.

Figure 17.- Concluded.

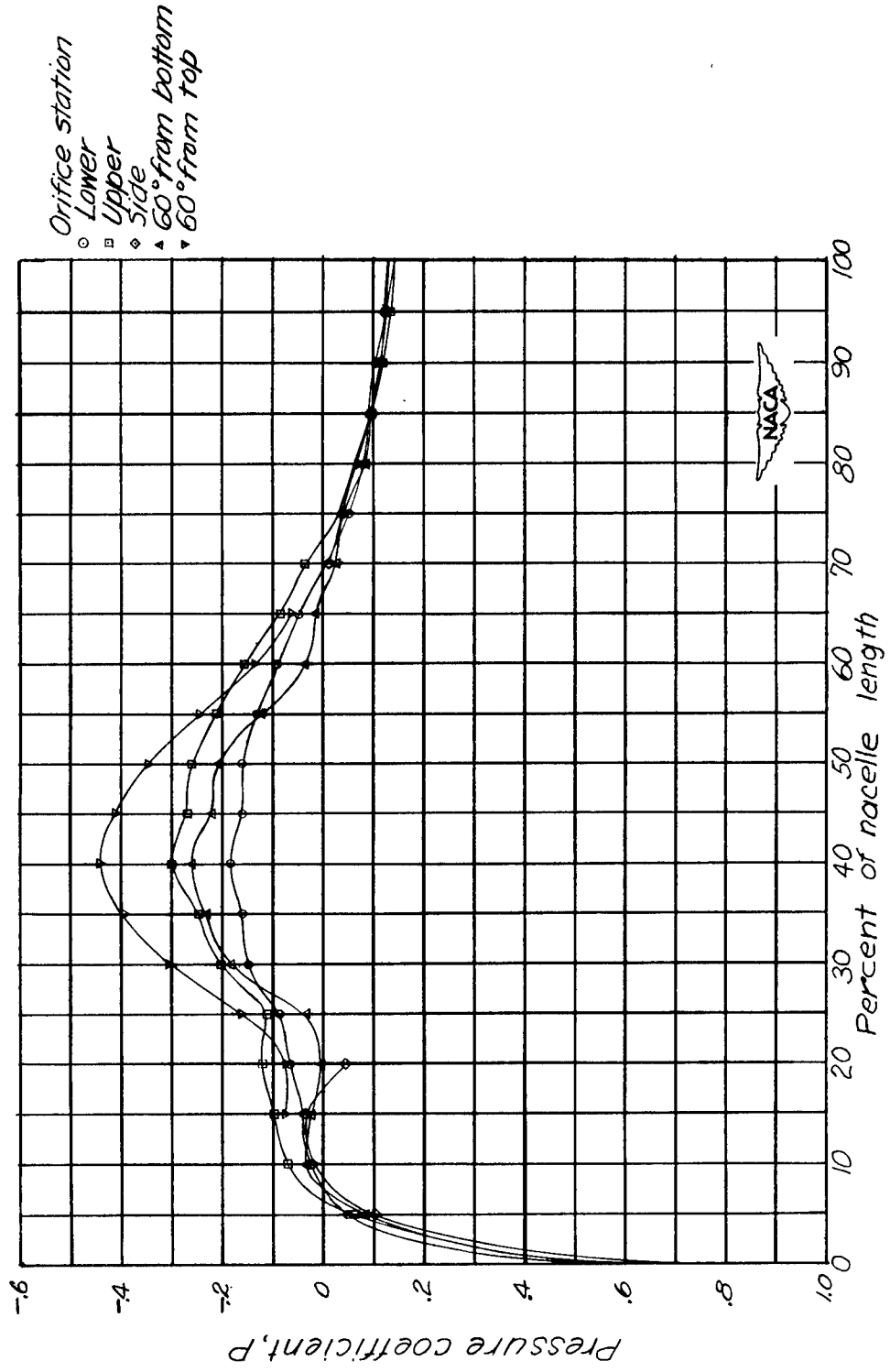


Figure 18.- Pressure-coefficient distributions over nacelle in position $C_3$. $\alpha = 0°$; $M = 0.4$.

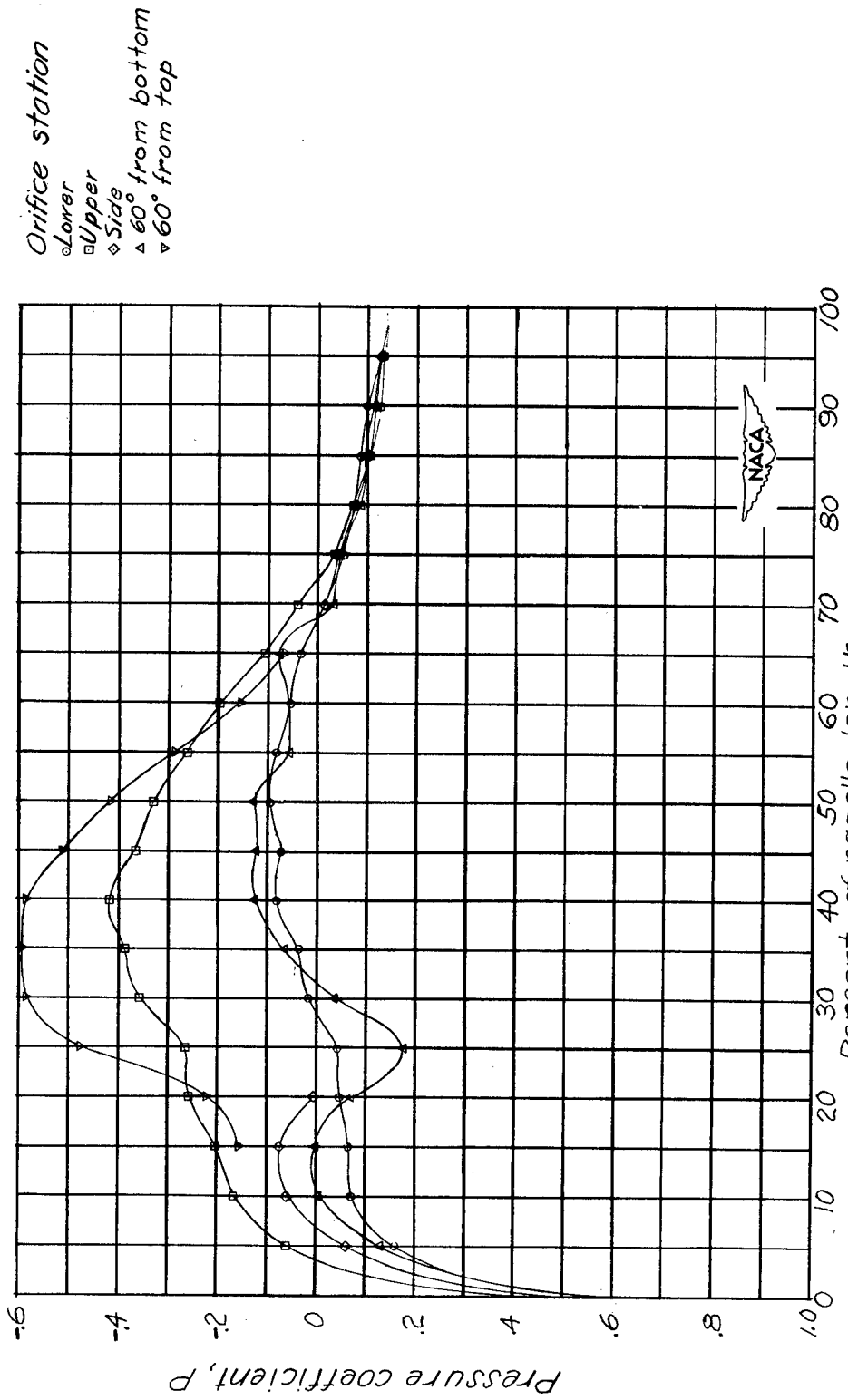


Figure 19.- Pressure-coefficient distributions over nacelle in position $C_3$. $\alpha = 2.5^\circ$; M = 0.4.

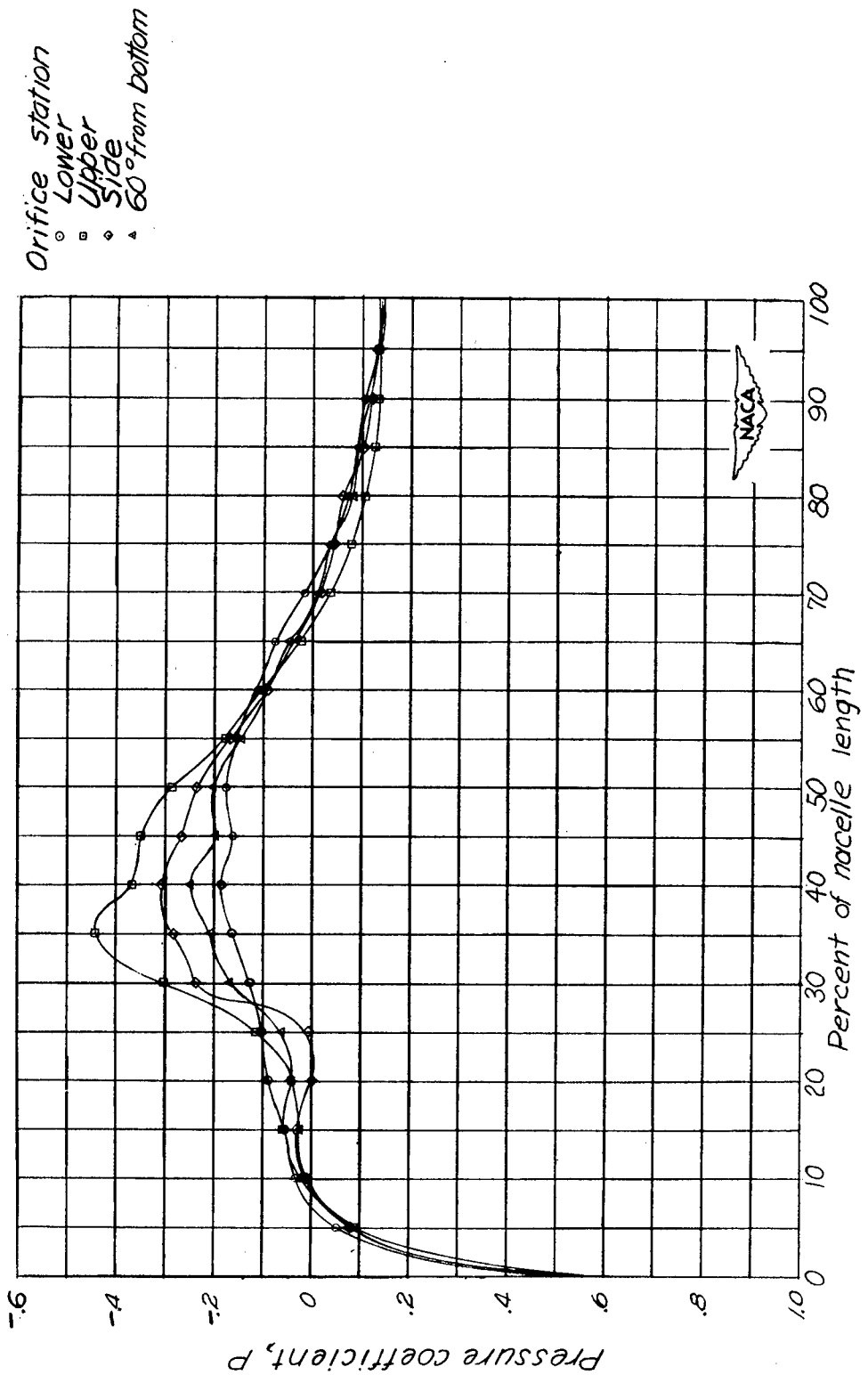


Figure 20.- Pressure-coefficient distributions over nacelle in position C. $\alpha = 0^{\circ}$; M = 0.4.

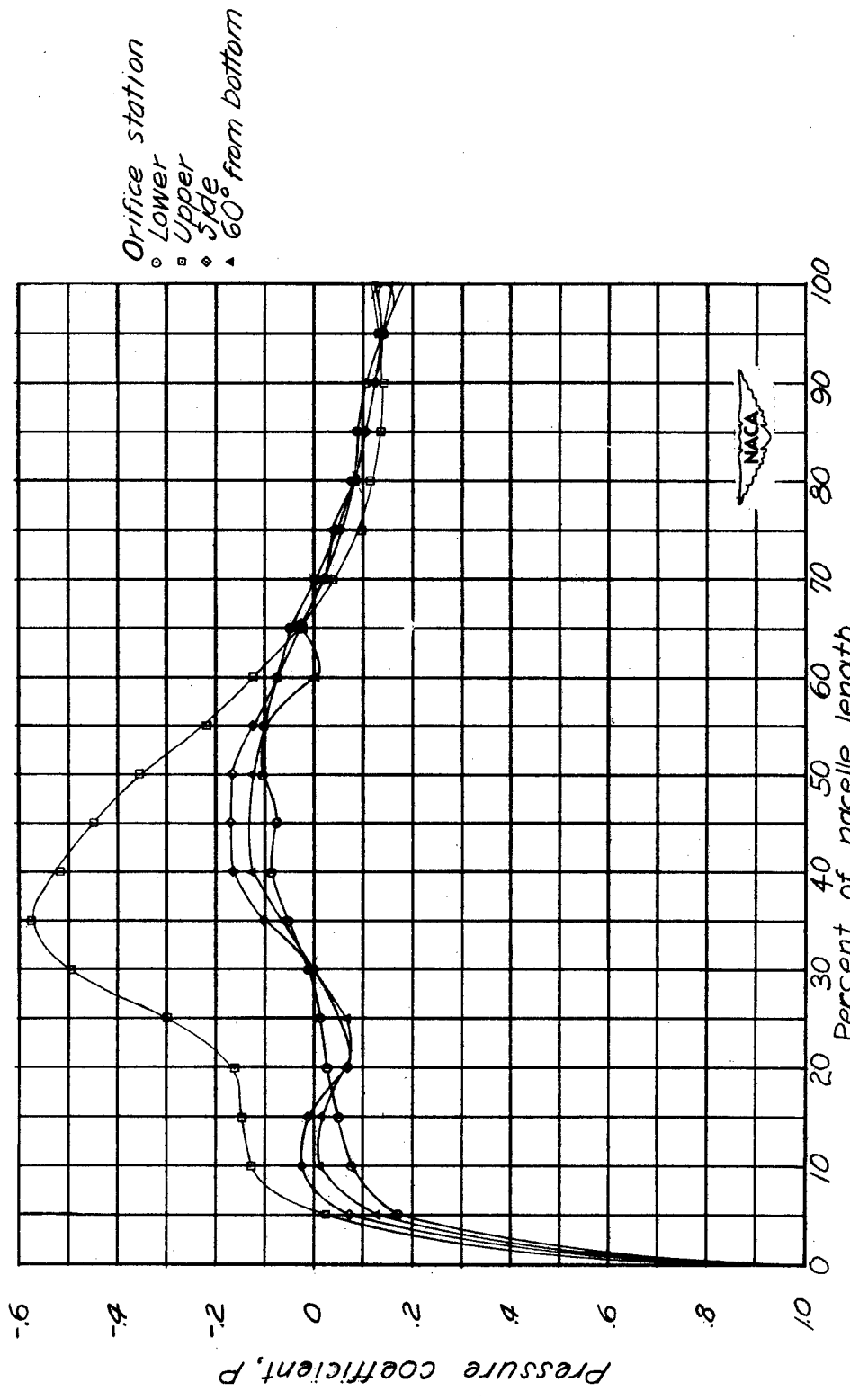


Figure 21.- Pressure-coefficient distributions over nacelle in position C. $\alpha = 2.5^{\circ}$; M = 0.4.

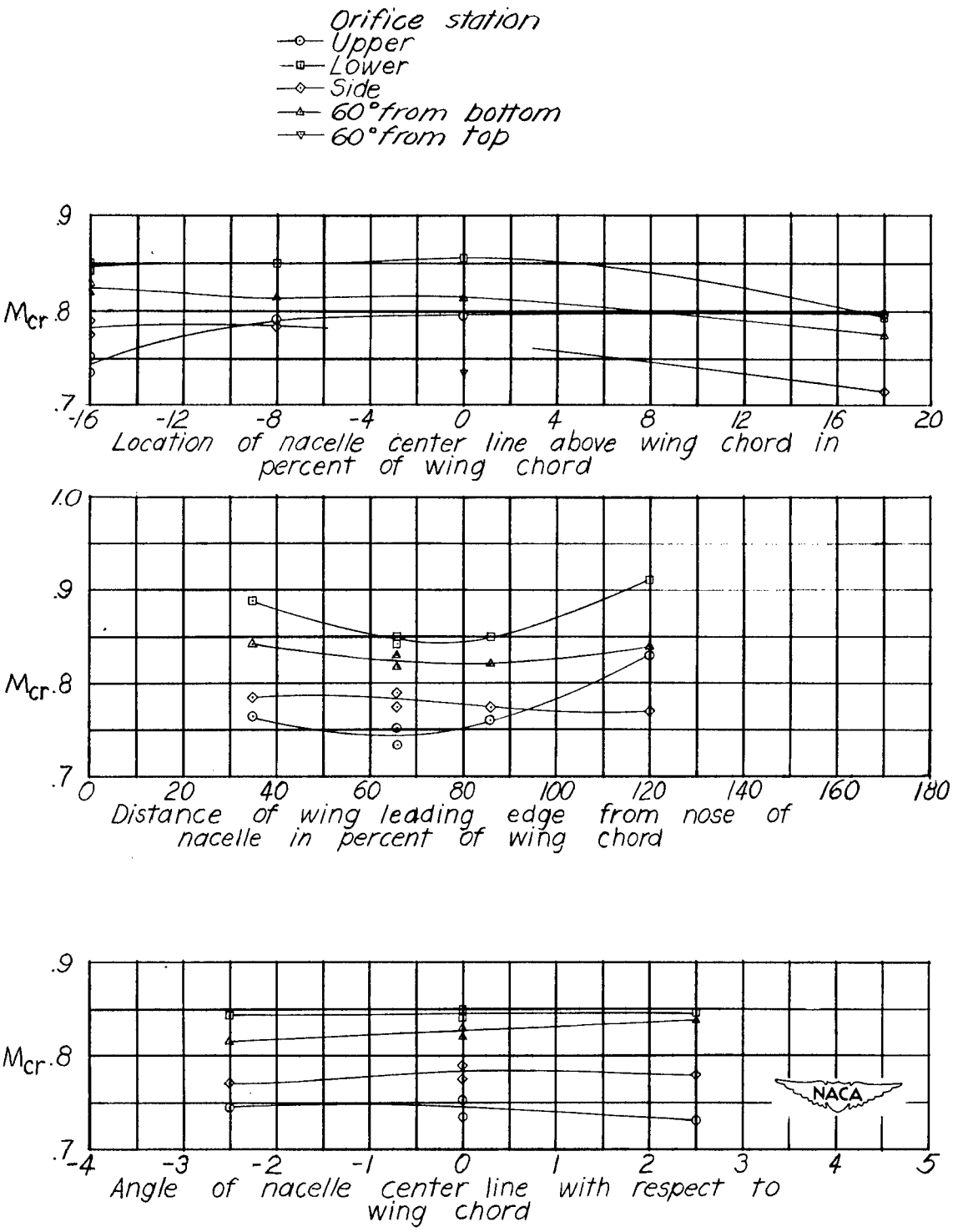


(a) $\alpha = 0^{\circ}$. Wing-alone critical Mach number is approximately 0.73.

Figure 22.- Variation of nacelle critical Mach number with nacelle position.

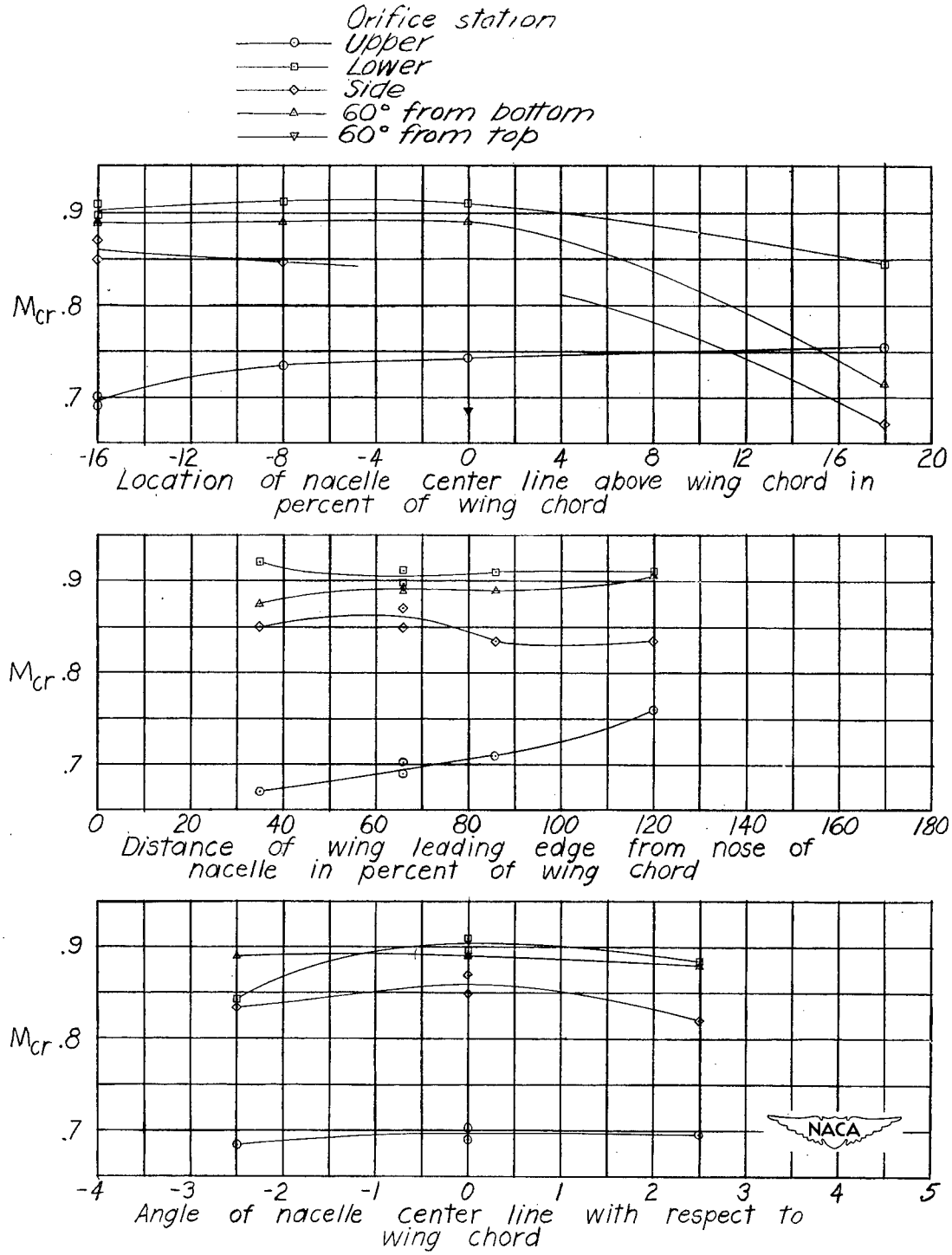


(b) $\alpha = 2.5^{\circ}$. Wing-alone critical Mach number is approximately 0.6.

Figure 22.- Concluded.

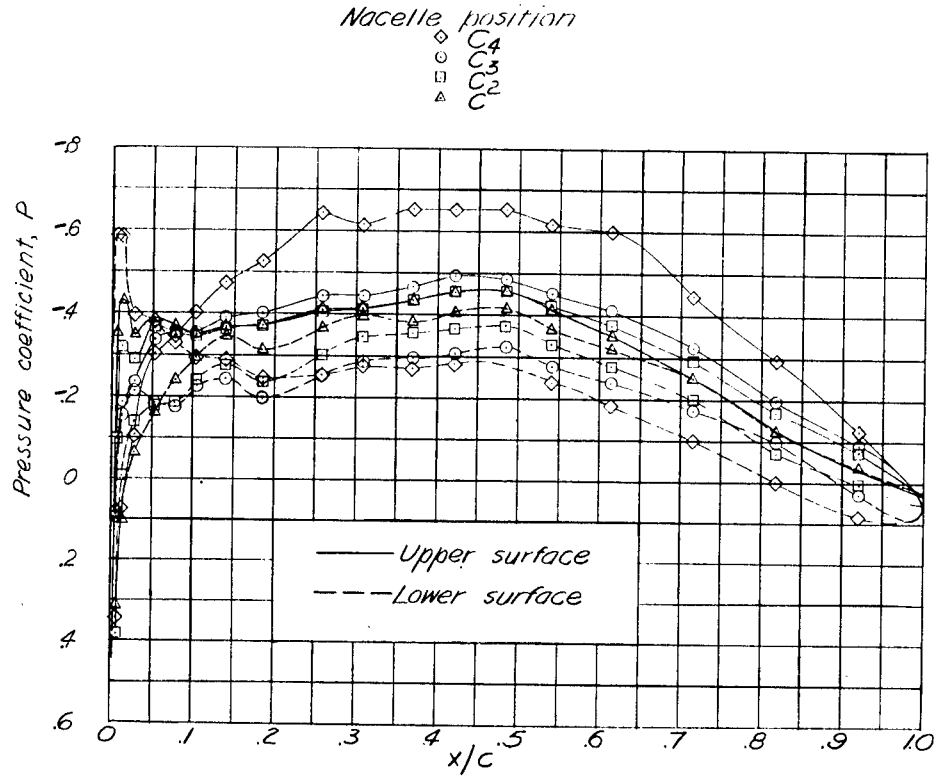


(a) Station 1.

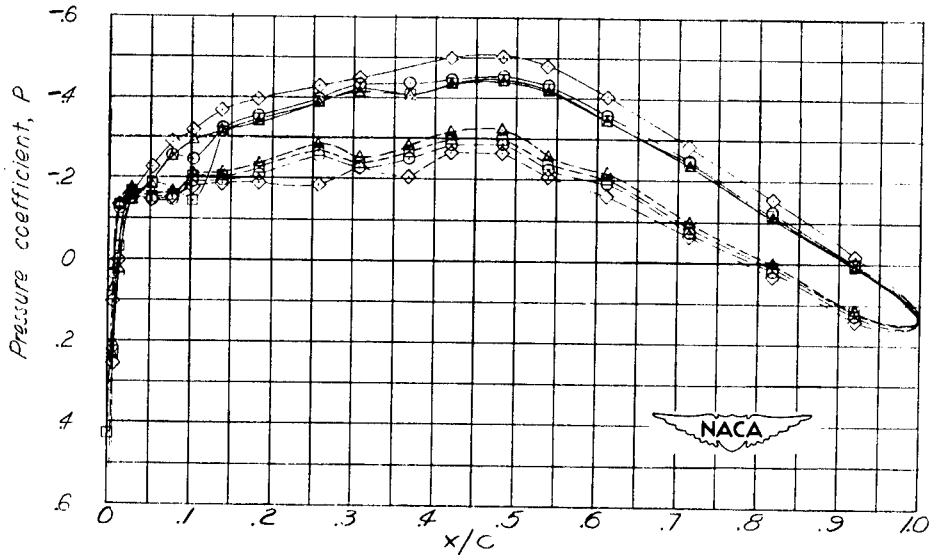


(b) Station 4.

Figure 23.- Pressure distributions over the wing with four vertical nacelle positions. $\alpha = 0^{\circ}$; $M = 0.4$.

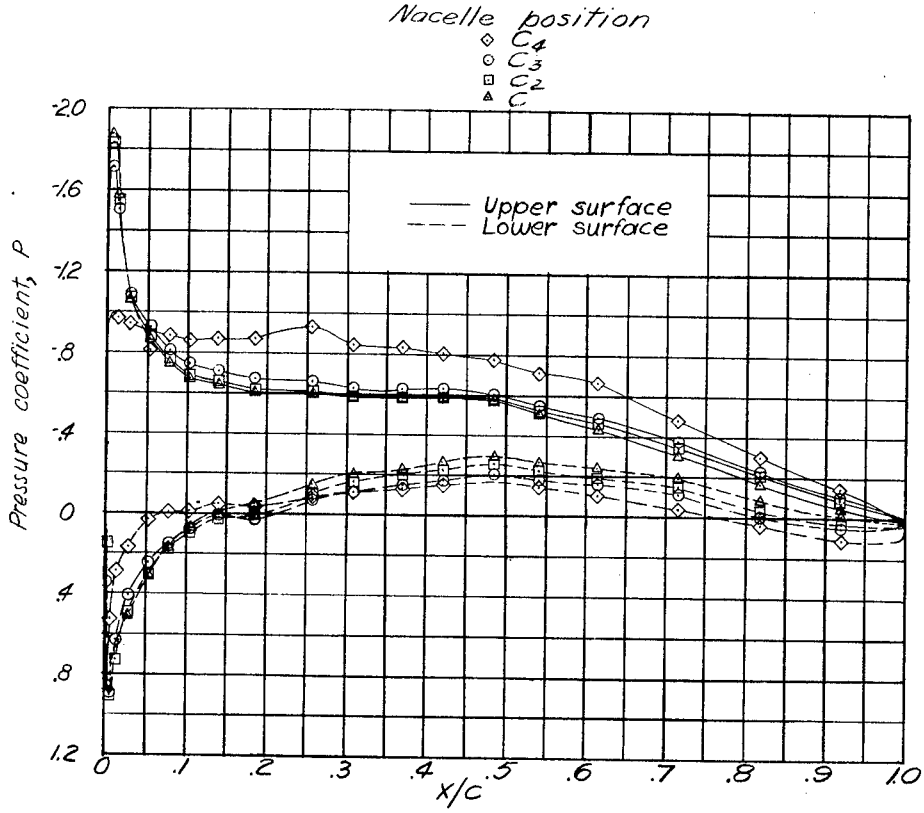


(a) Station 1.

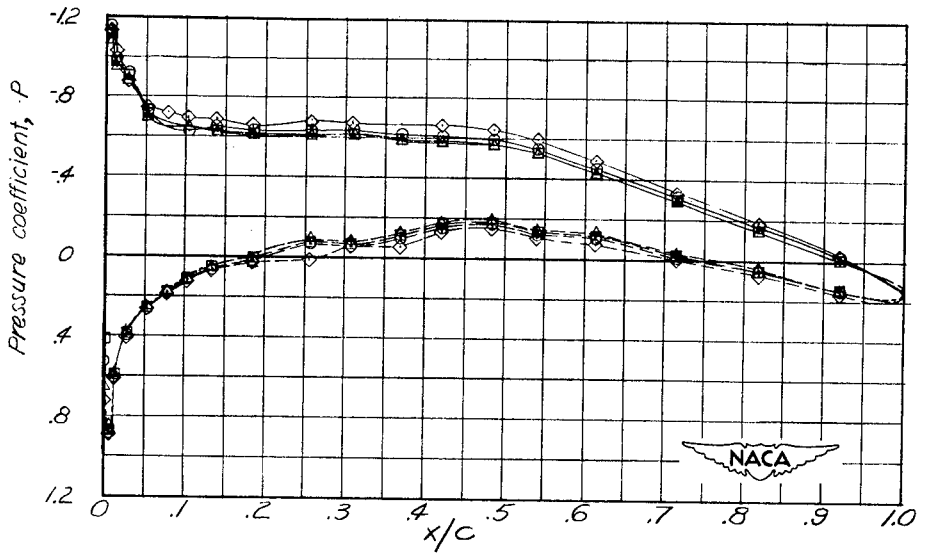


(b) Station 4.

Figure 24.- Pressure distributions over the wing with four vertical nacelle positions. $\alpha = 2.5^{\circ}$; $M = 0.4$.

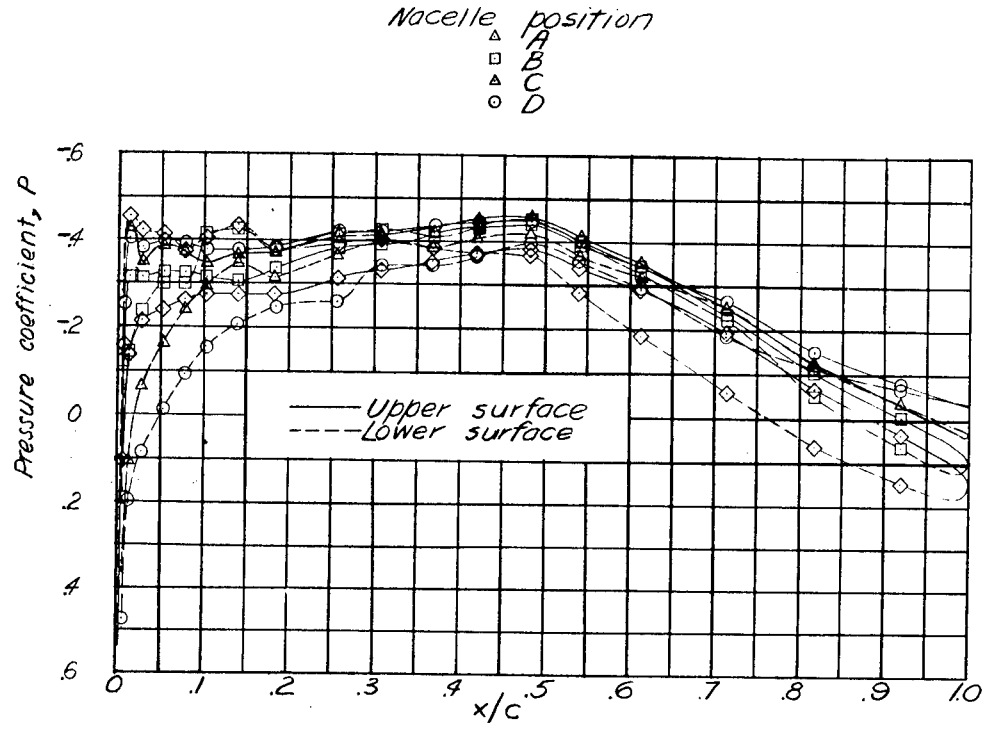


(a) Station 1.

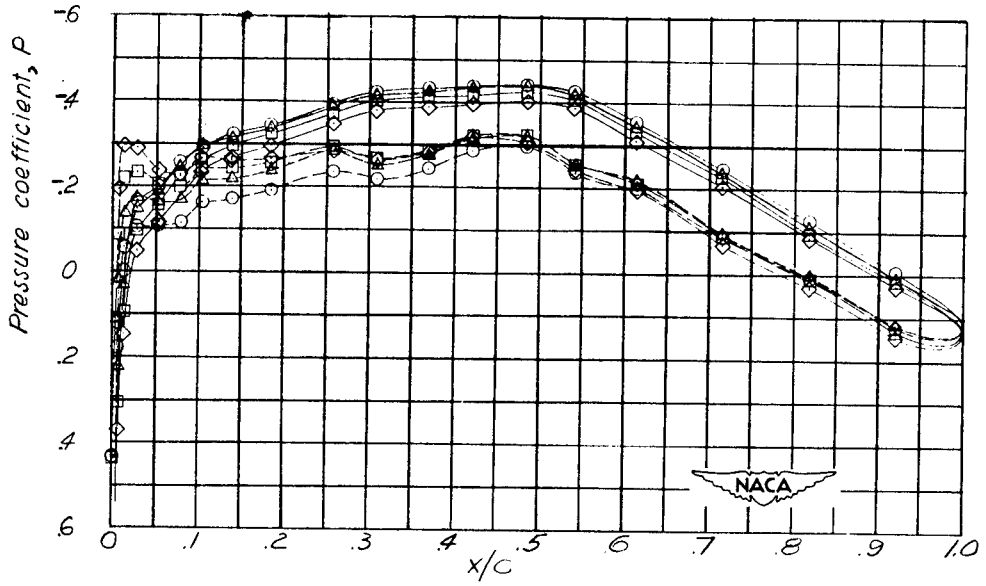


(b) Station 4.

Figure 25.- Pressure distributions over the wing with four horizontal nacelle positions. $\alpha = 0^{\circ}$; $M = 0.4$.

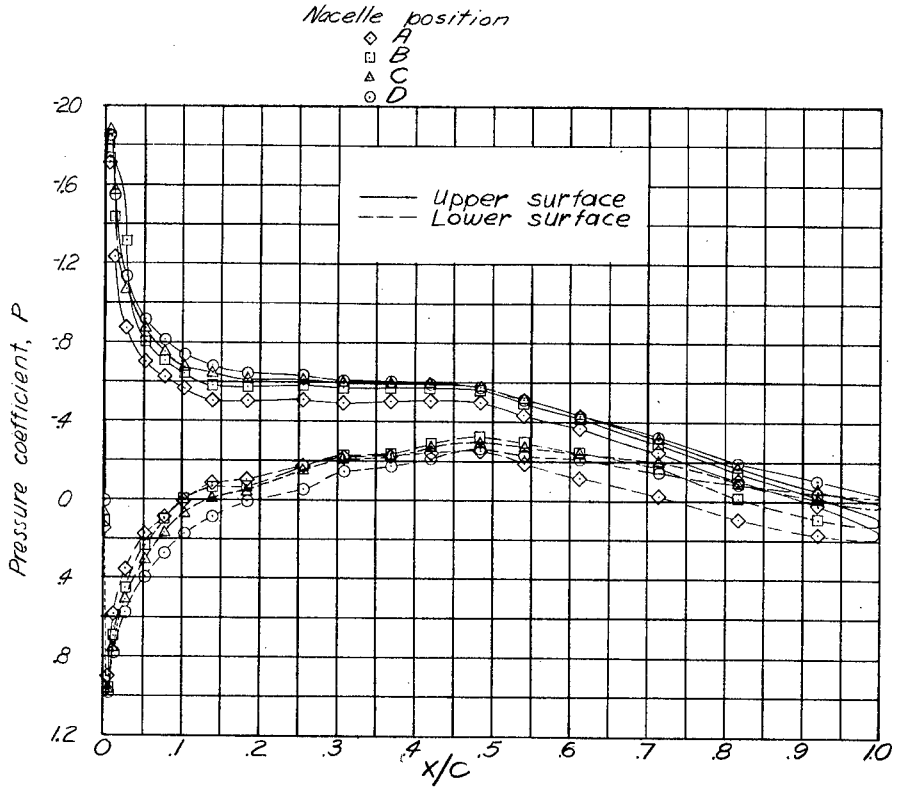


(a) Station 1.

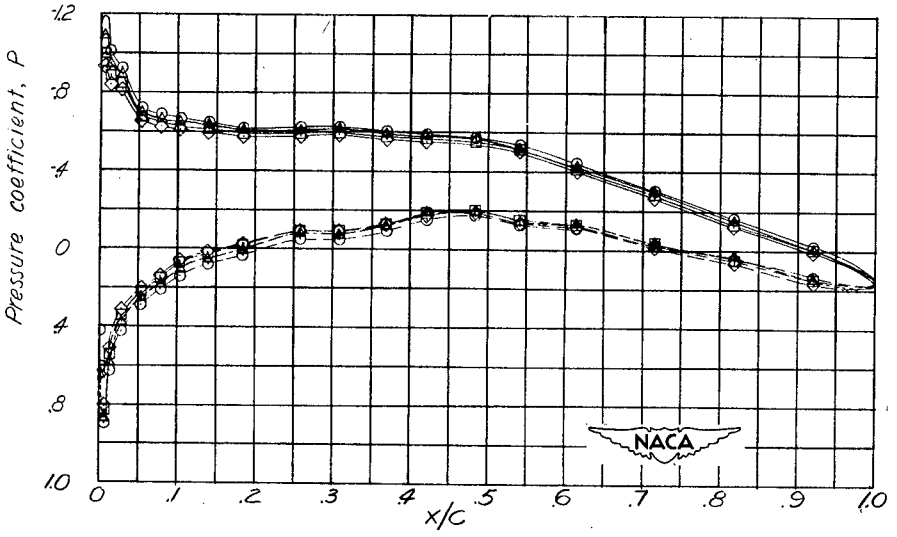


(b) Station 4.

Figure 26.- Pressure distributions over the wing with four horizontal nacelle positions. $\alpha = 2.5^{\circ}$; $M = 0.4$.

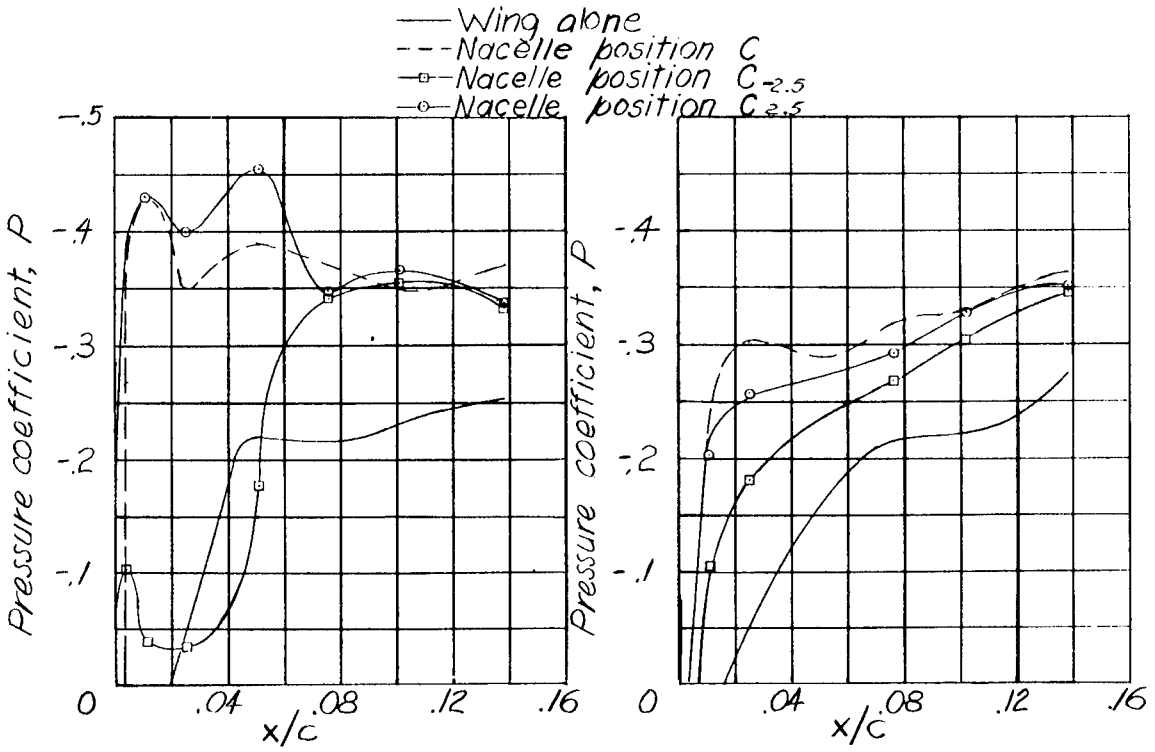


(a) Station 1.

(b) Station 2.

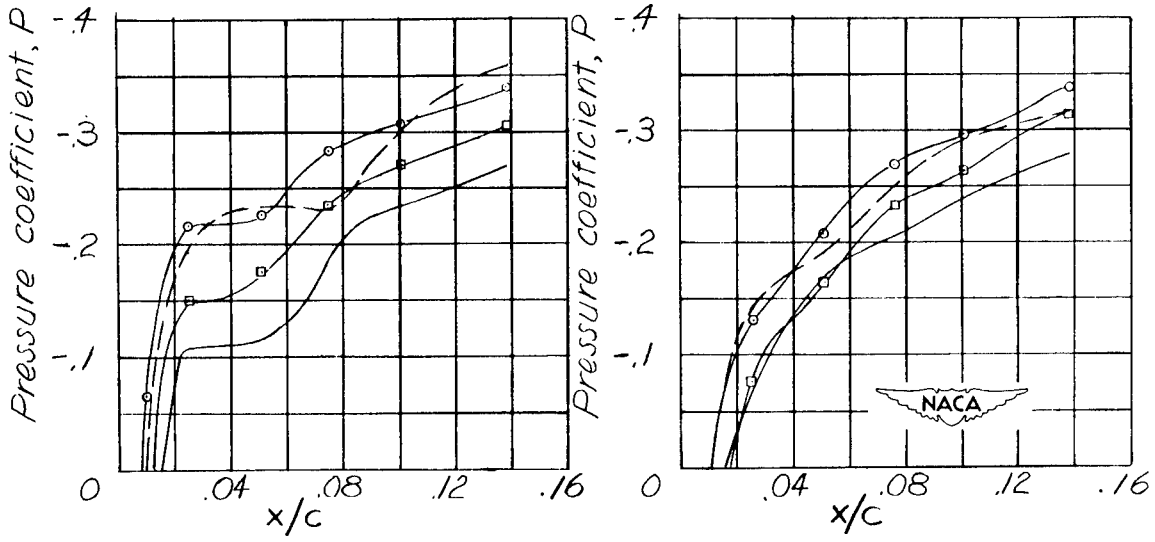


(c) Station 3.

(d) Station 4.

Figure 27.- Pressure distributions over the upper surface of the leading edge of the wing with three angular nacelle positions. $\alpha = 0^{\circ}$; M = 0.4.

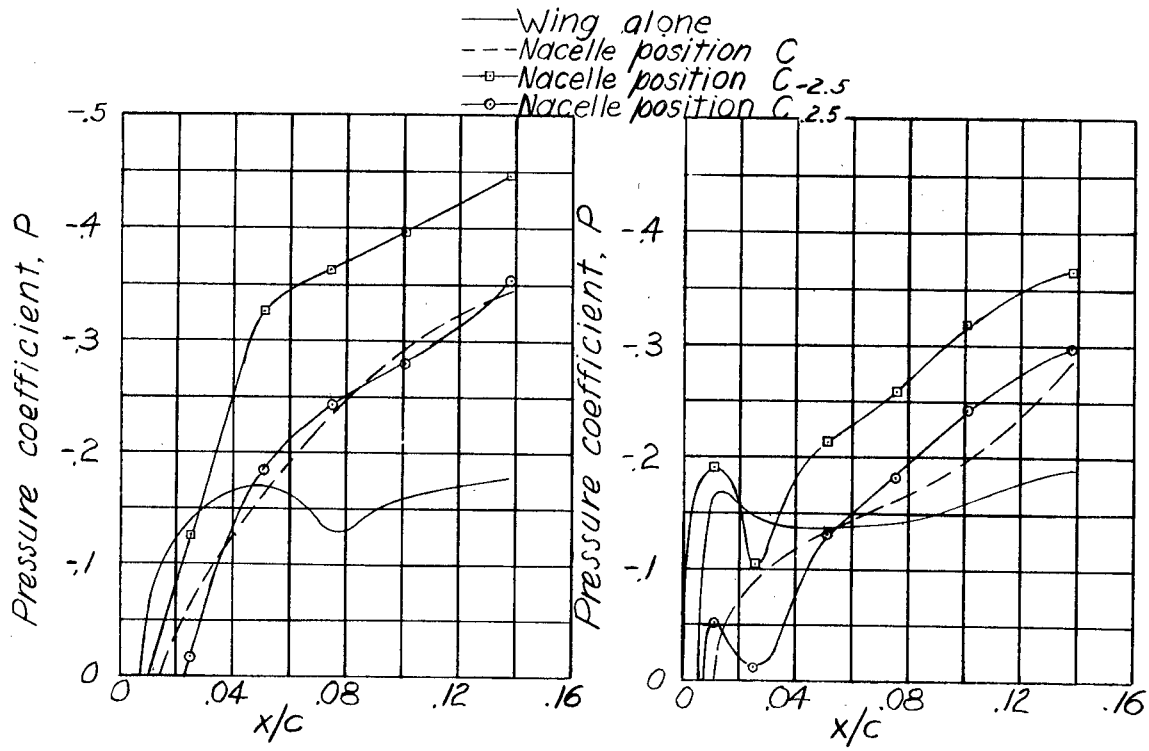


(a) Station 1.

(b) Station 2.

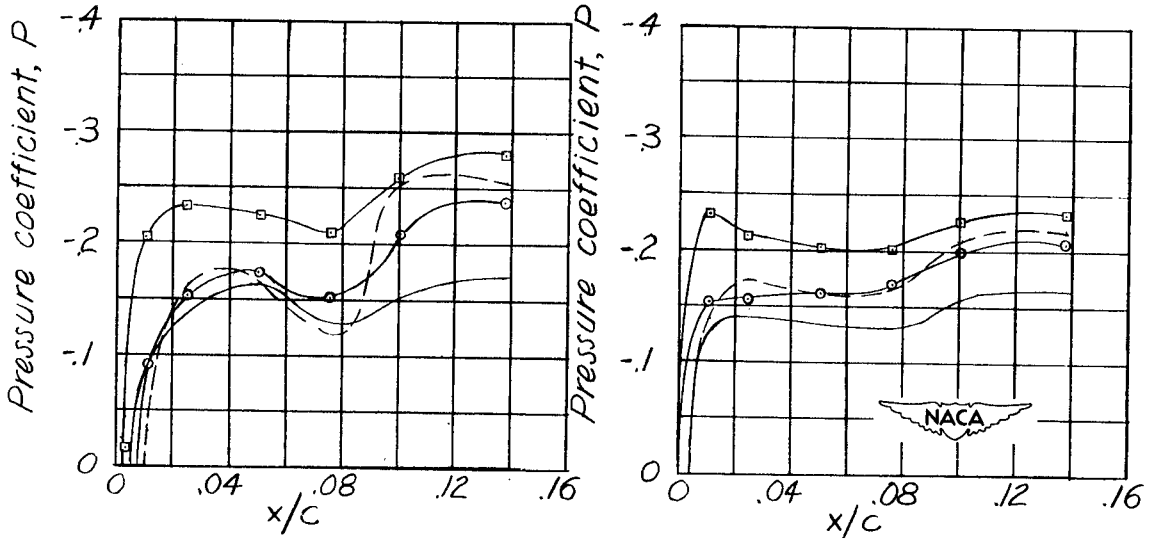


(c) Station 3.

(d) Station 4.

Figure 28.- Pressure distributions over the lower surface of the leading edge of the wing with three angular nacelle positions. $\alpha = 0^{\circ}$; M = 0.4.

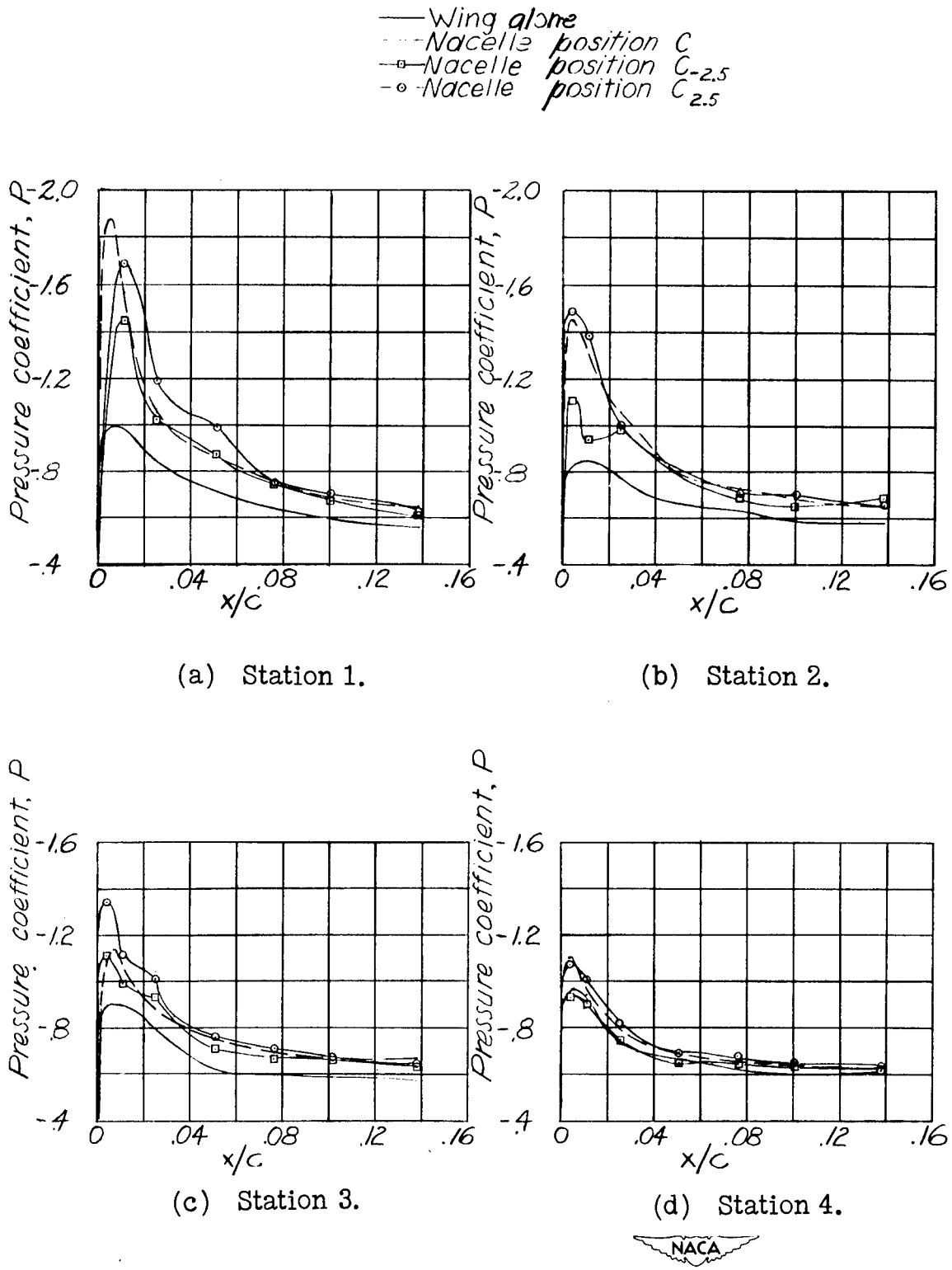


(a) Station 1.

(b) Station 2.

(c) Station 3.

(d) Station 4.

Figure 29.- Pressure distributions over the upper surface of the leading edge of the wing with three angular nacelle positions. $\alpha = 2.5^{\circ}$; M = 0.4.

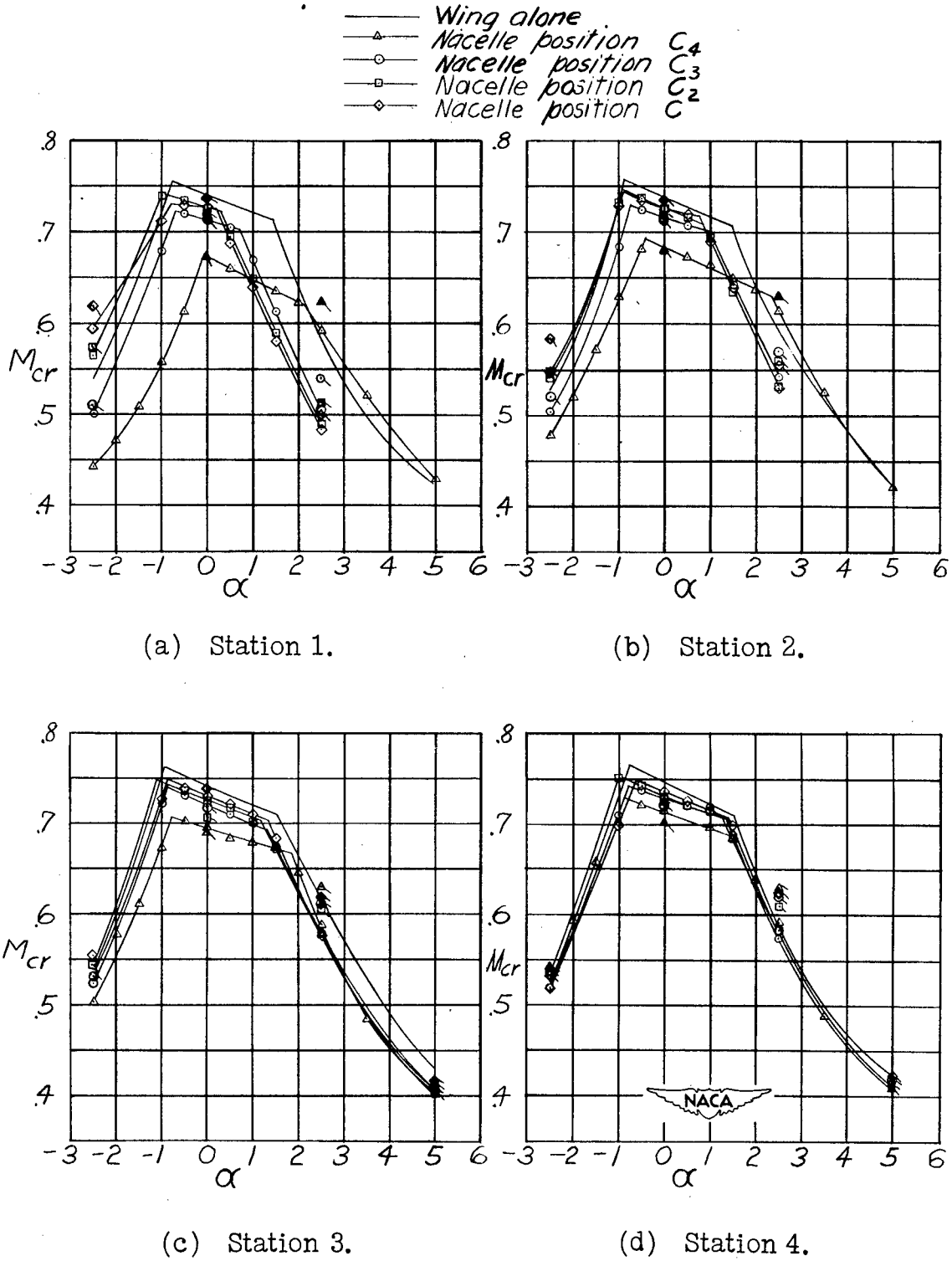


(a) Station 1.

(b) Station 2.

(c) Station 3.

(d) Station 4.

Figure 30.- Variation of critical Mach number with angle of attack for the wing with four vertical nacelle positions. Untailed symbols refer to points extrapolated from M = 0.4 results.

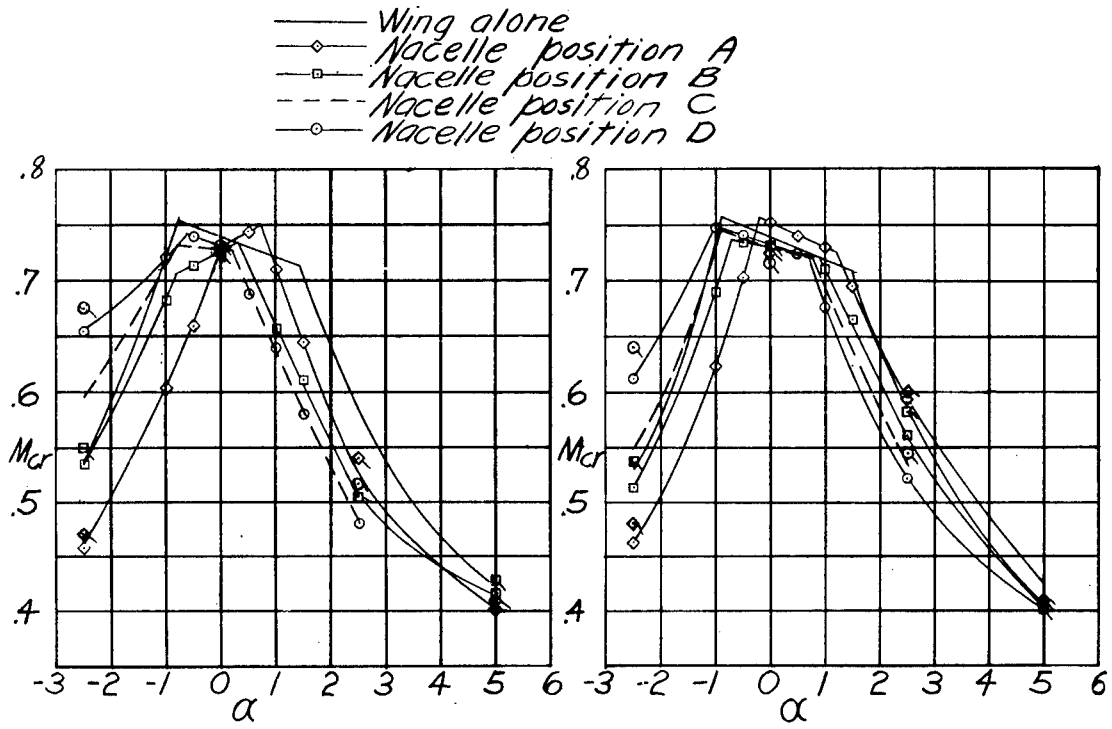


(a) Station 1.

(b) Station 2.

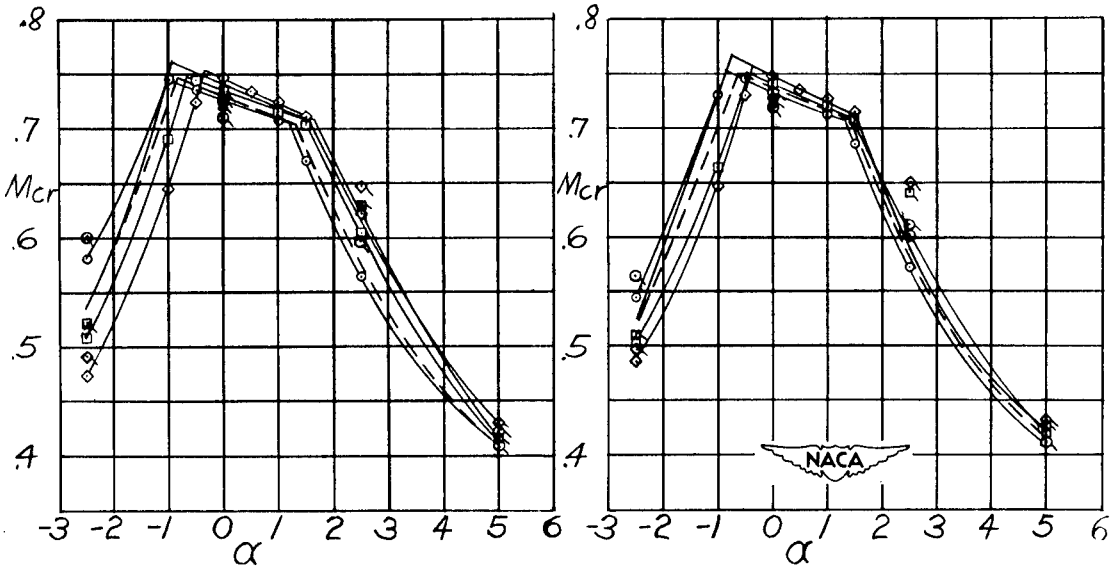


(c) Station 3.

(d) Station 4.

Figure 31.- Variation of critical Mach number with angle of attack for the wing with four horizontal nacelle positions. Untailed symbols refer to points extrapolated from M = 0.4 results.

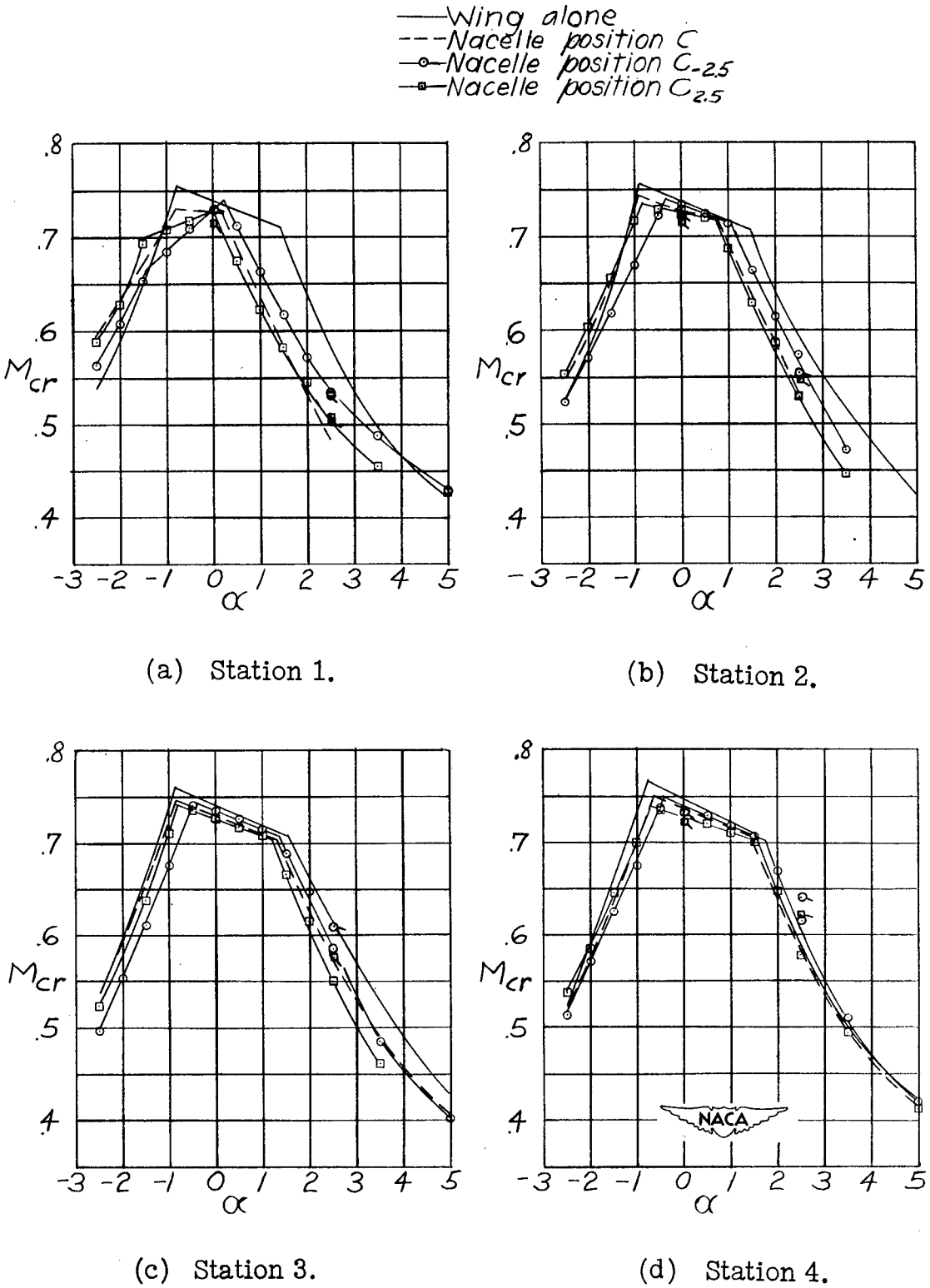


(a) Station 1.

(b) Station 2.

(c) Station 3.

(d) Station 4.

Figure 32.- Variation of critical Mach number with angle of attack for the wing with three angular nacelle positions. Untailed symbols refer to points extrapolated from M = 0.4 results.

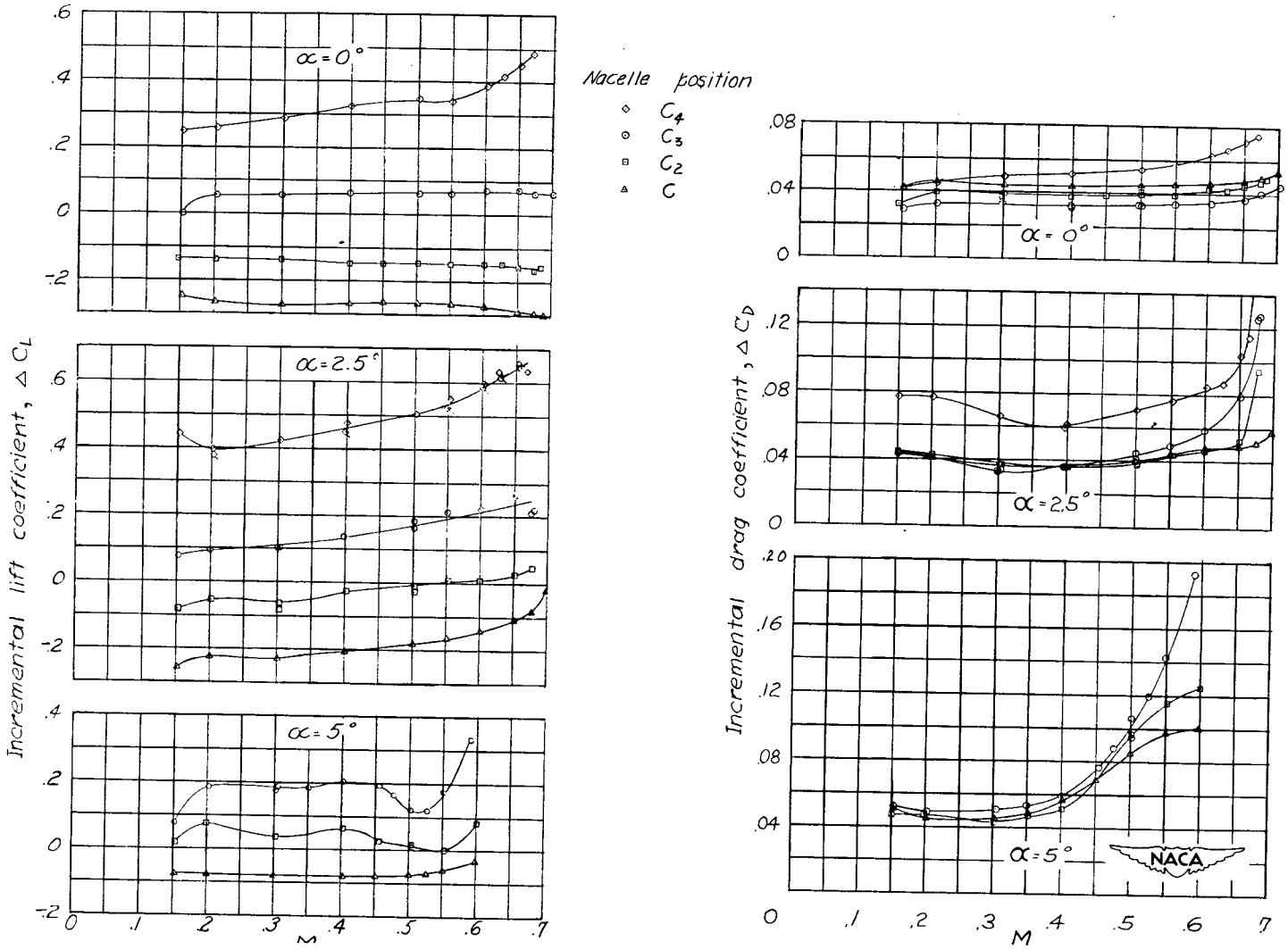


(a) Lift.

(b) Drag.

Figure 33.- Variation with Mach number of the incremental lift and drag for four vertical nacelle positions.

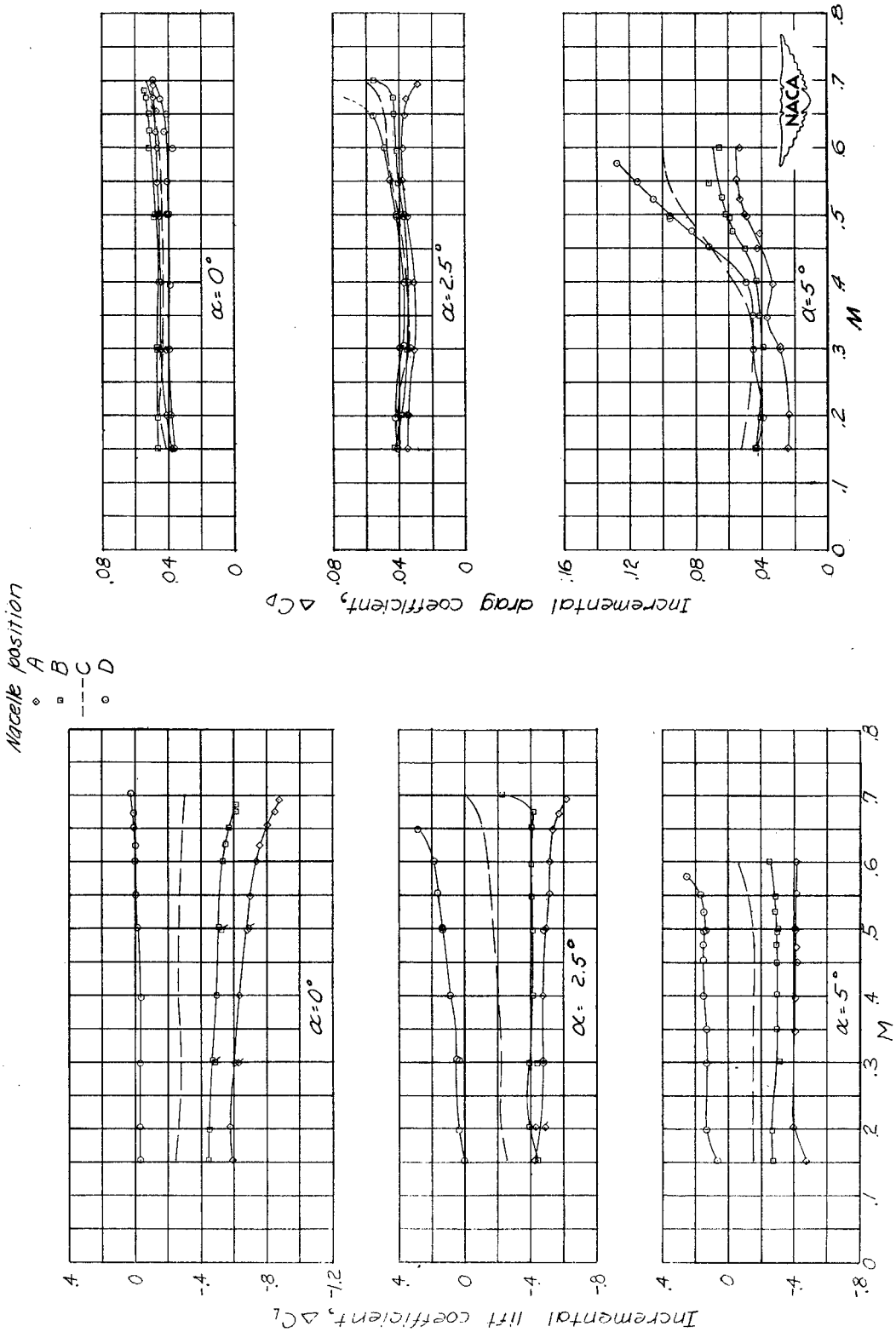


(a) Lift. (b) Drag.

Figure 34.- Variation with Mach number of the incremental lift and drag for four horizontal nacelle positions.

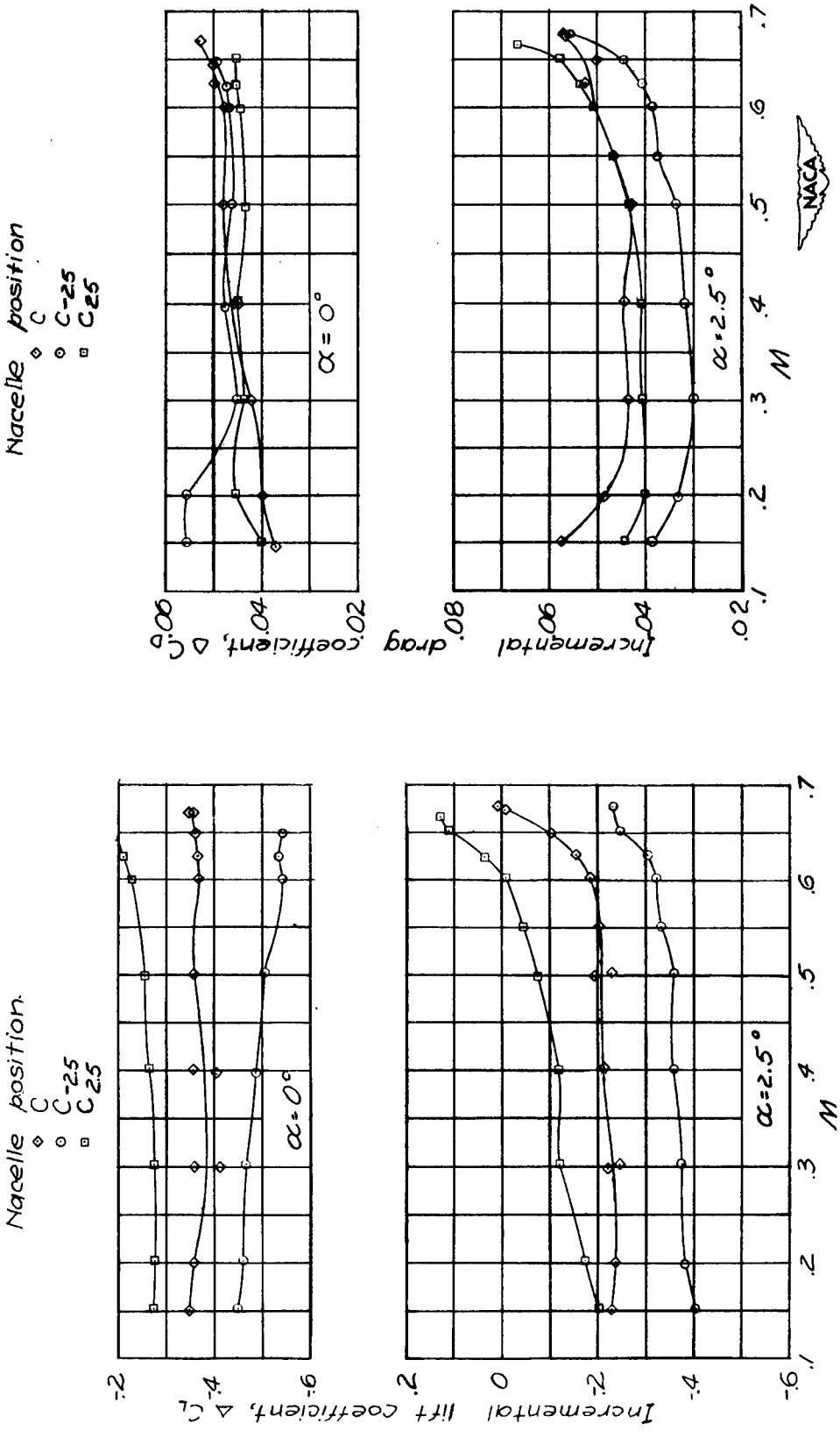


(a) Lift.

(b) Drag.

Figure 35.- Variation with Mach number of the incremental lift and drag for three angular nacelle positions.

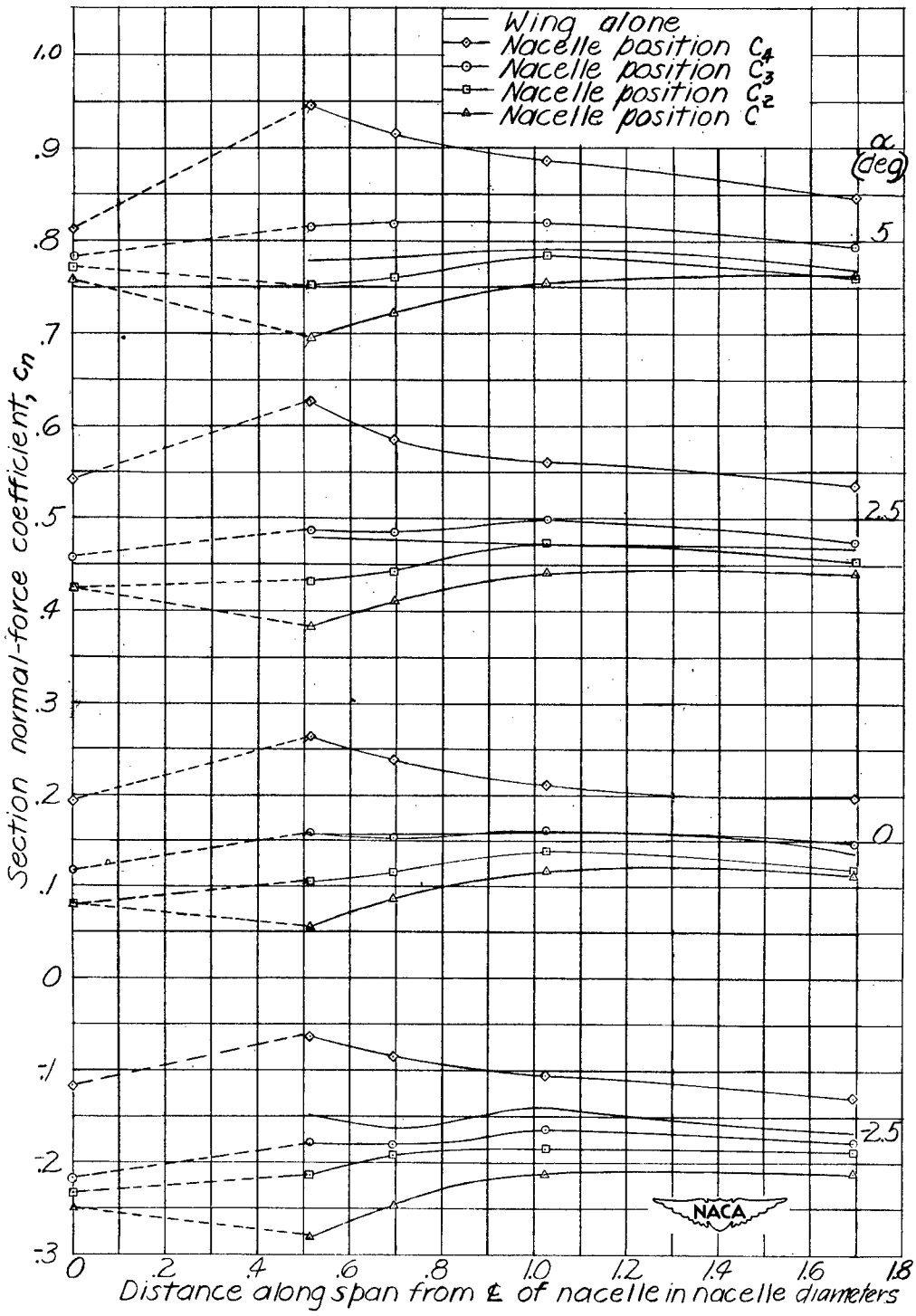


Figure 36.- Spanwise variation of section normal-force coefficients for four vertical nacelle positions. M = 0.4.

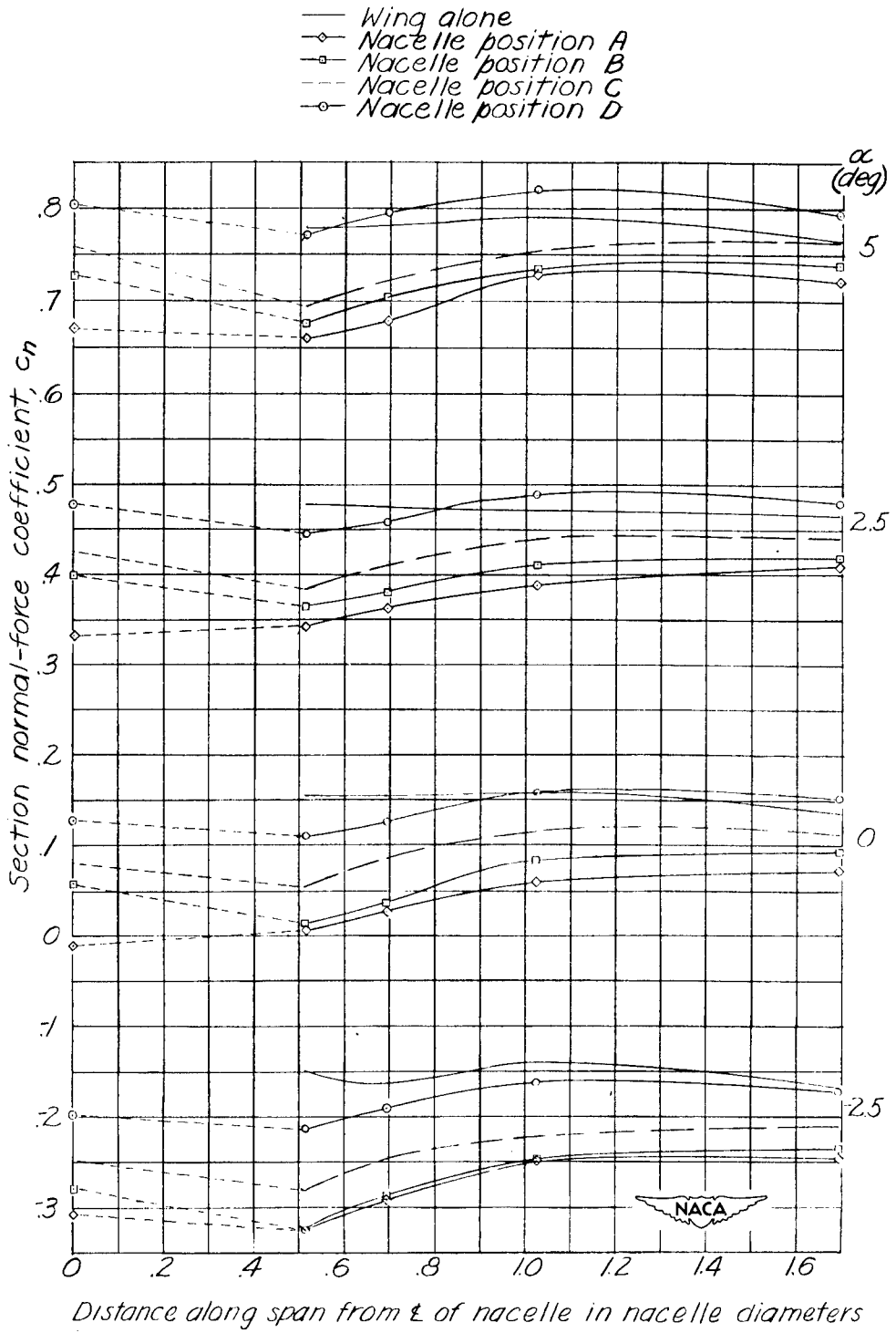


Figure 37.- Spanwise variation of section normal-force coefficients for four horizontal positions. M = 0.4.

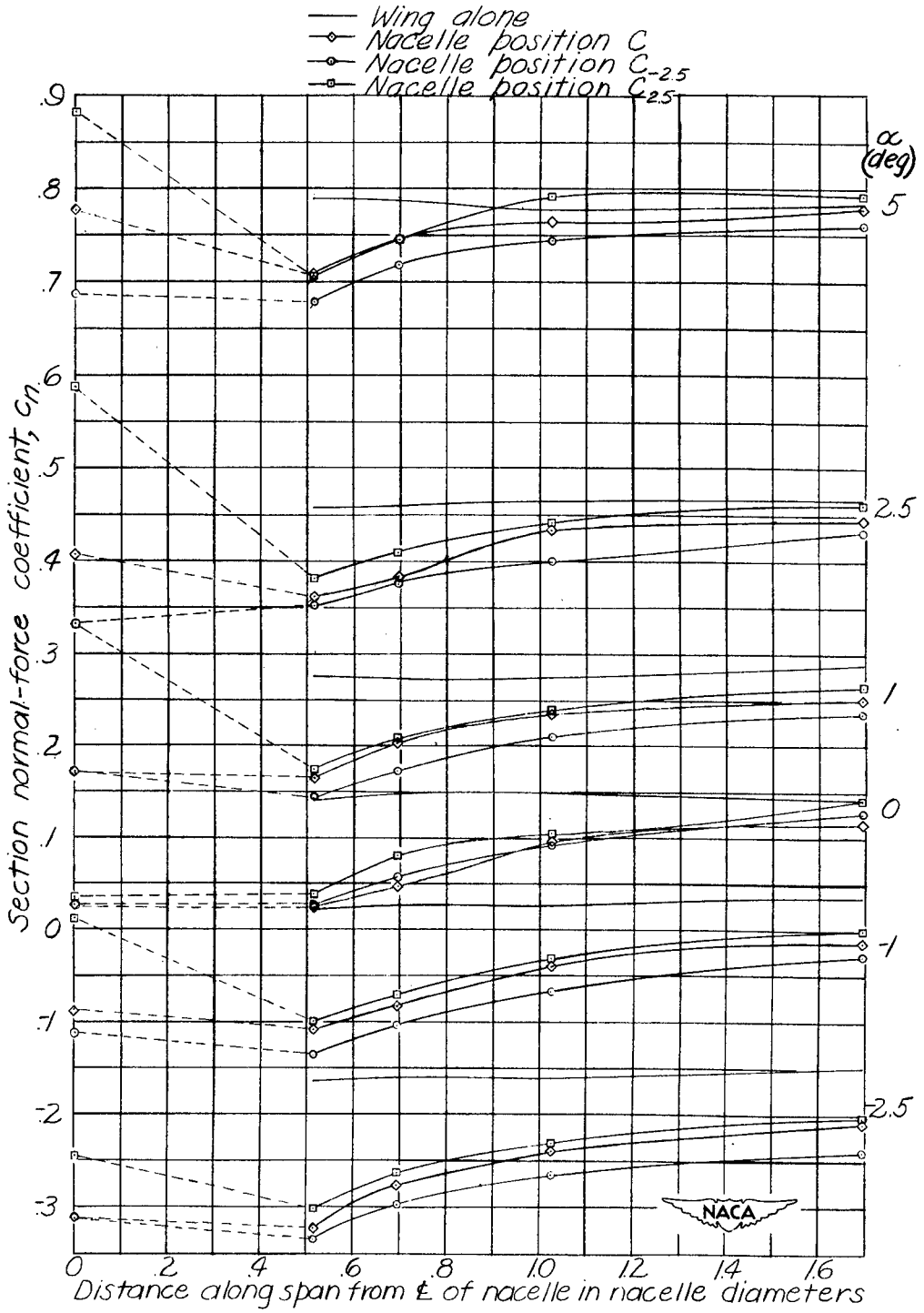


Figure 38.- Spanwise variation of section normal-force coefficients for three angular positions. M = 0.4.

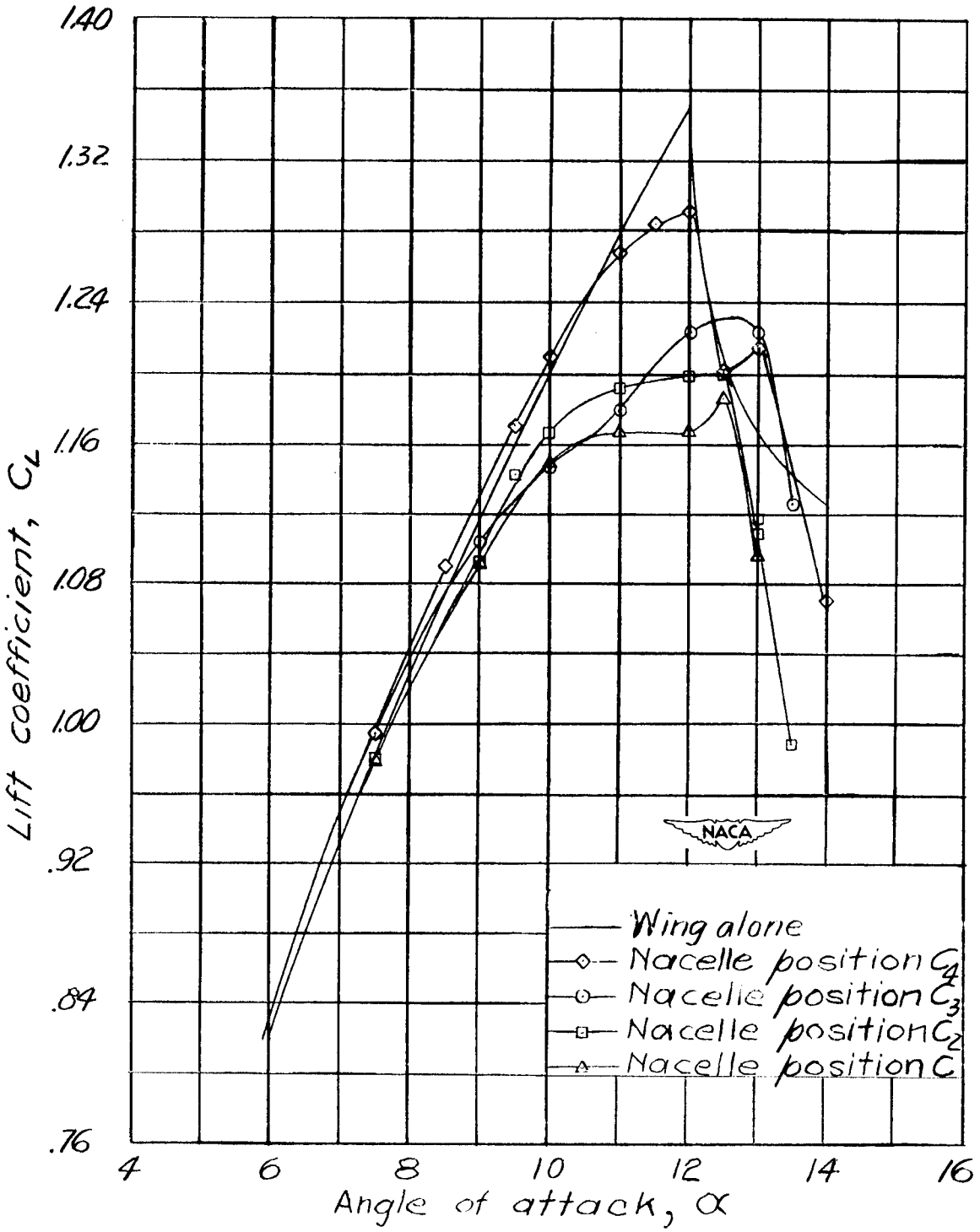


Figure 39.- Variation of lift coefficient with angle of attack for four vertical nacelle positions. M = 0.2. (First series of tests.)

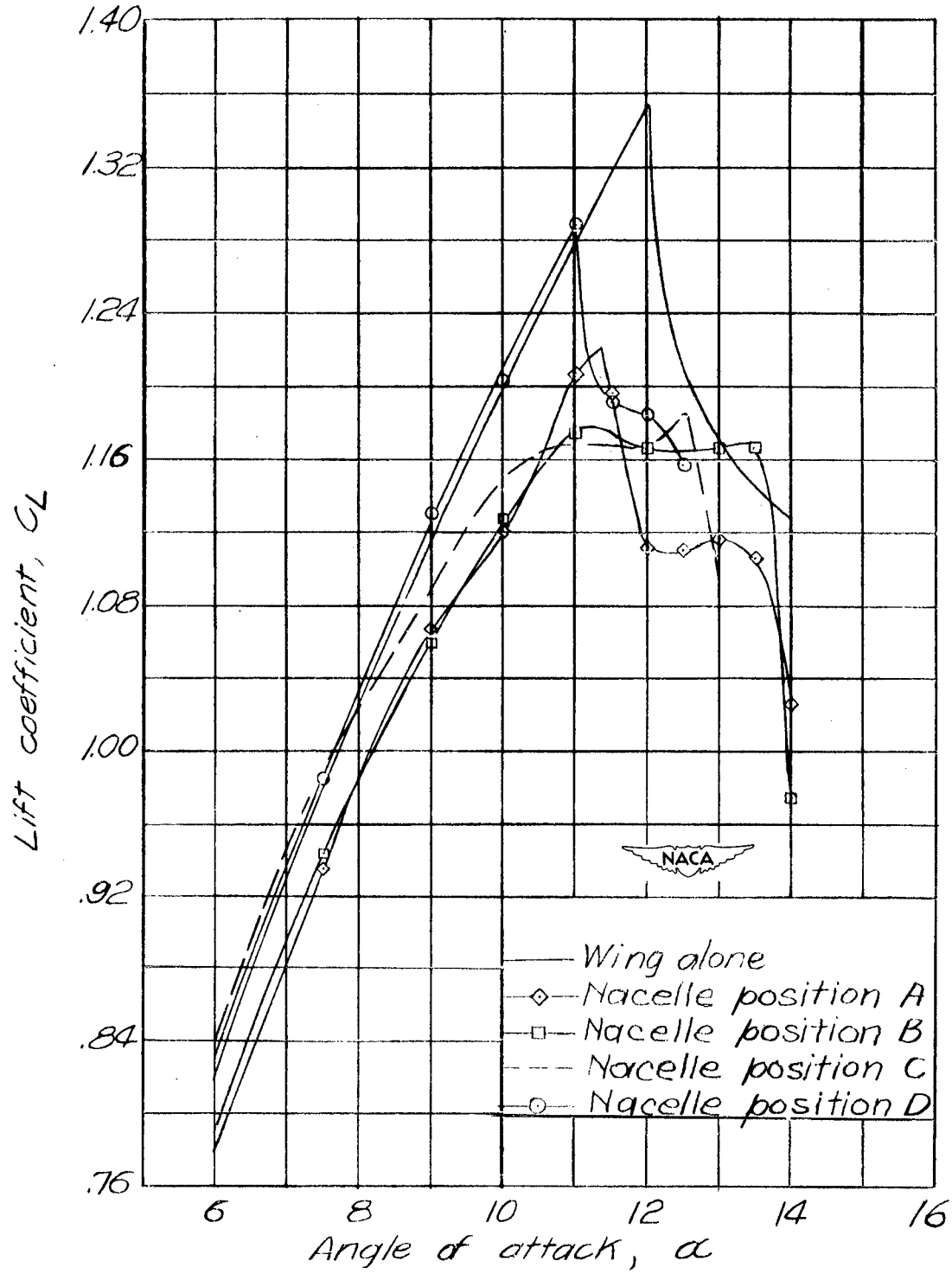


Figure 40.- Variation of lift coefficient with angle of attack for four horizontal nacelle positions. M = 0.2. (First series of tests.)

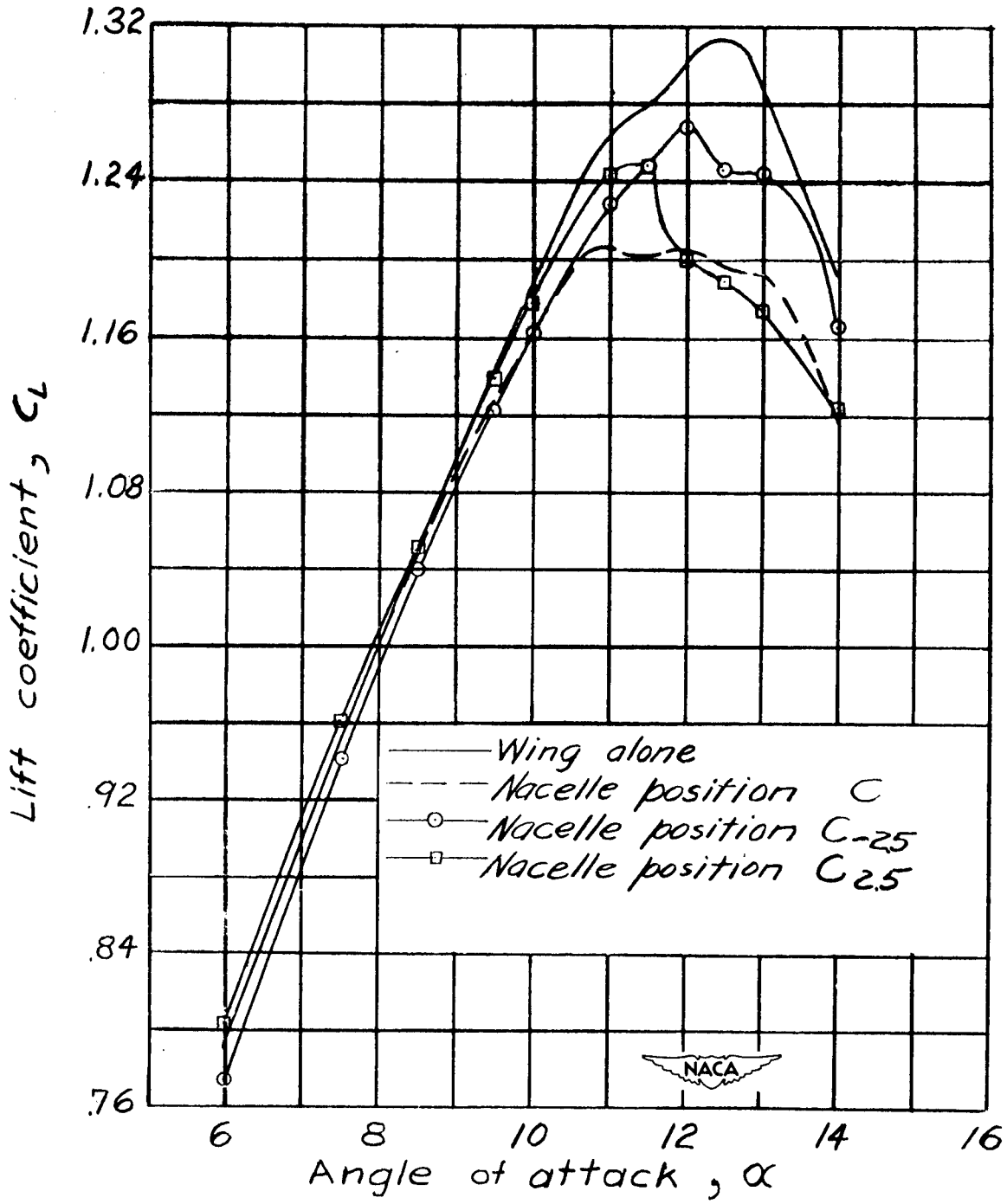


Figure 41.- Variation of lift coefficient with angle of attack for three angular nacelle positions. M = 0.2. (Second series of tests.)

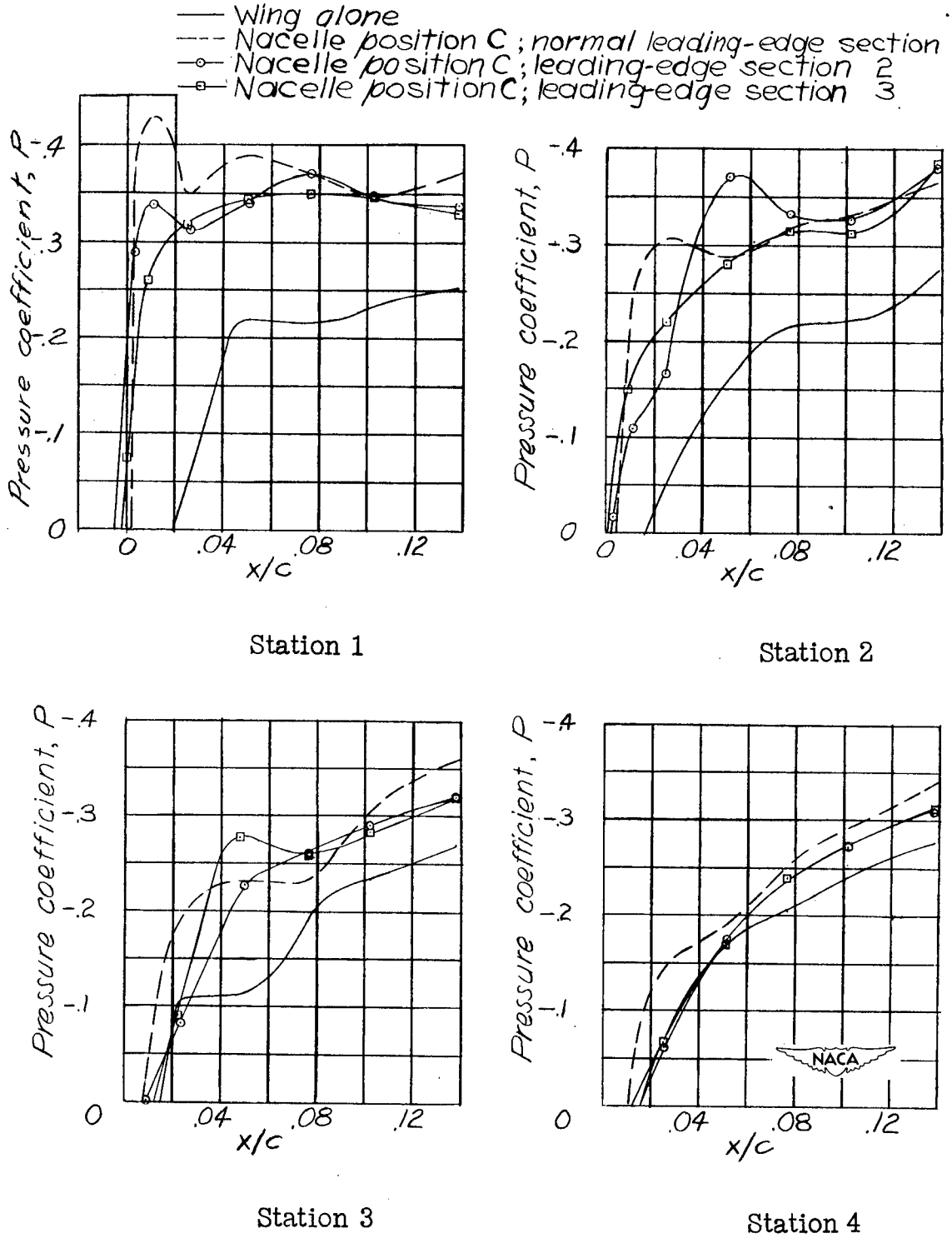


(a) Upper surface; $\alpha = 0^{\circ}$.

Figure 42.- Comparison of pressure distributions over leading-edge sections 2 and 3 with those over normal leading edge, nacelle in position C. M = 0.4.

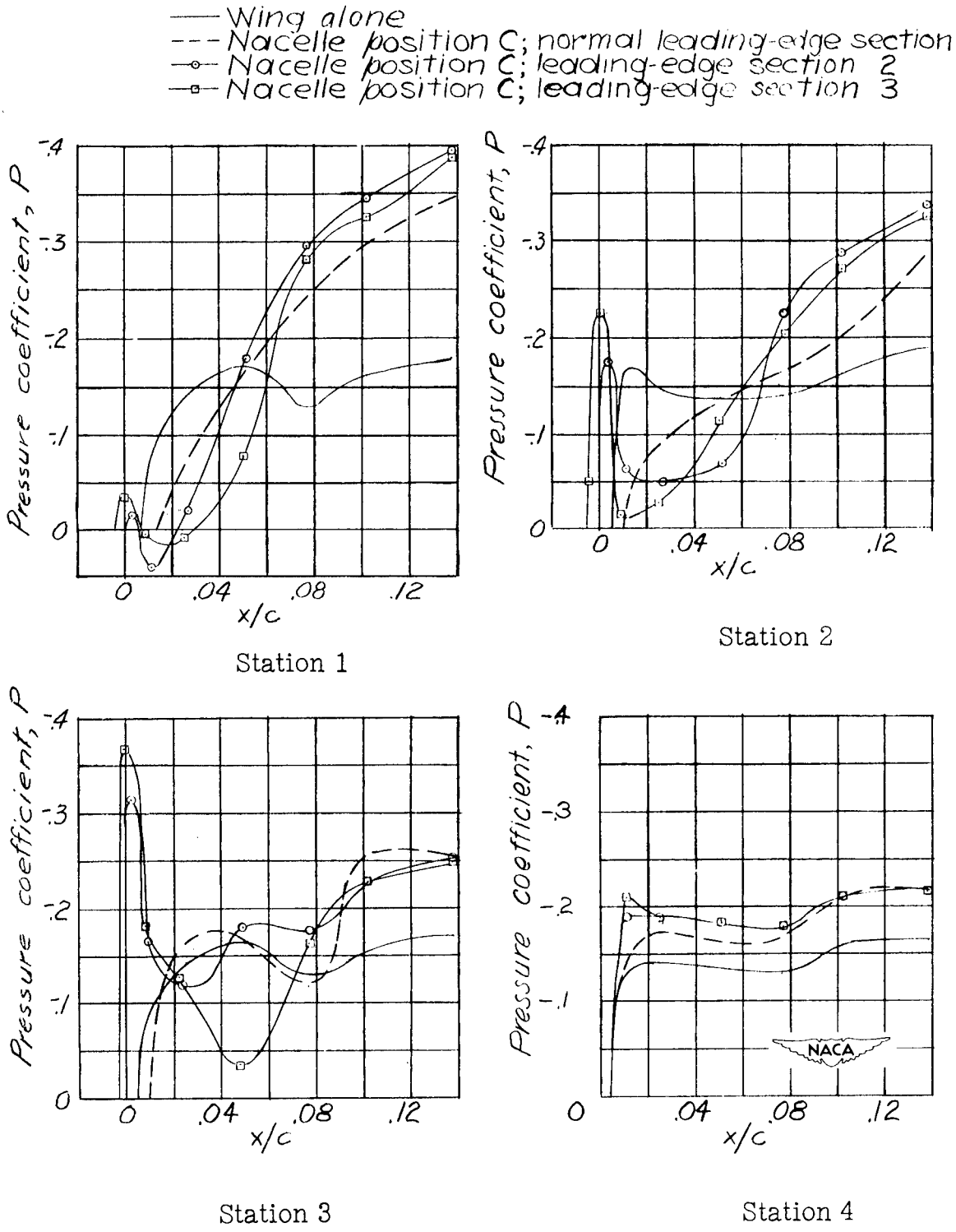


(b) Lower surface; $\alpha = 0^{\circ}$.

Figure 42.- Continued.

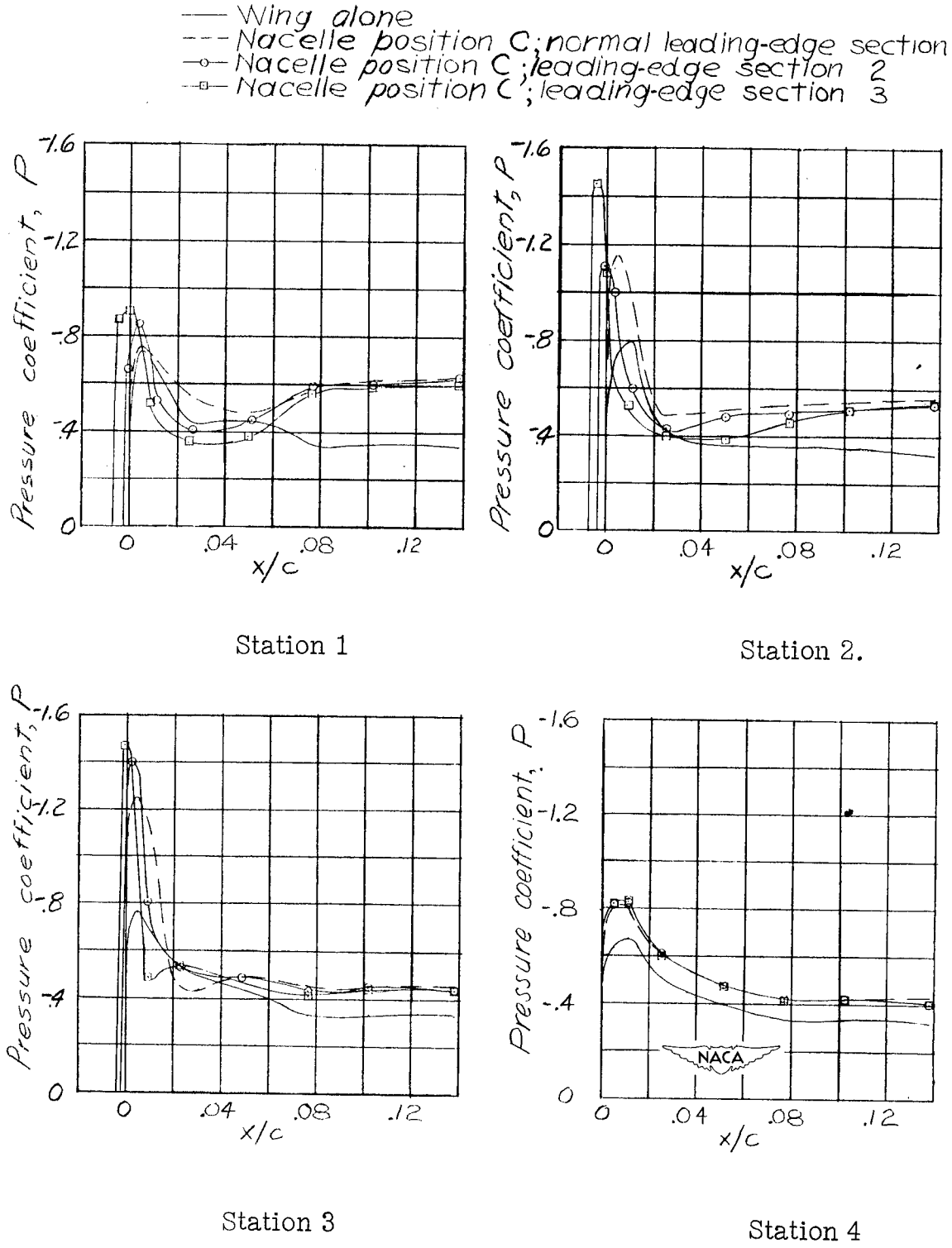


(c) Lower surface; $\alpha = -1.5^{\circ}$.

Figure 42.- Continued.

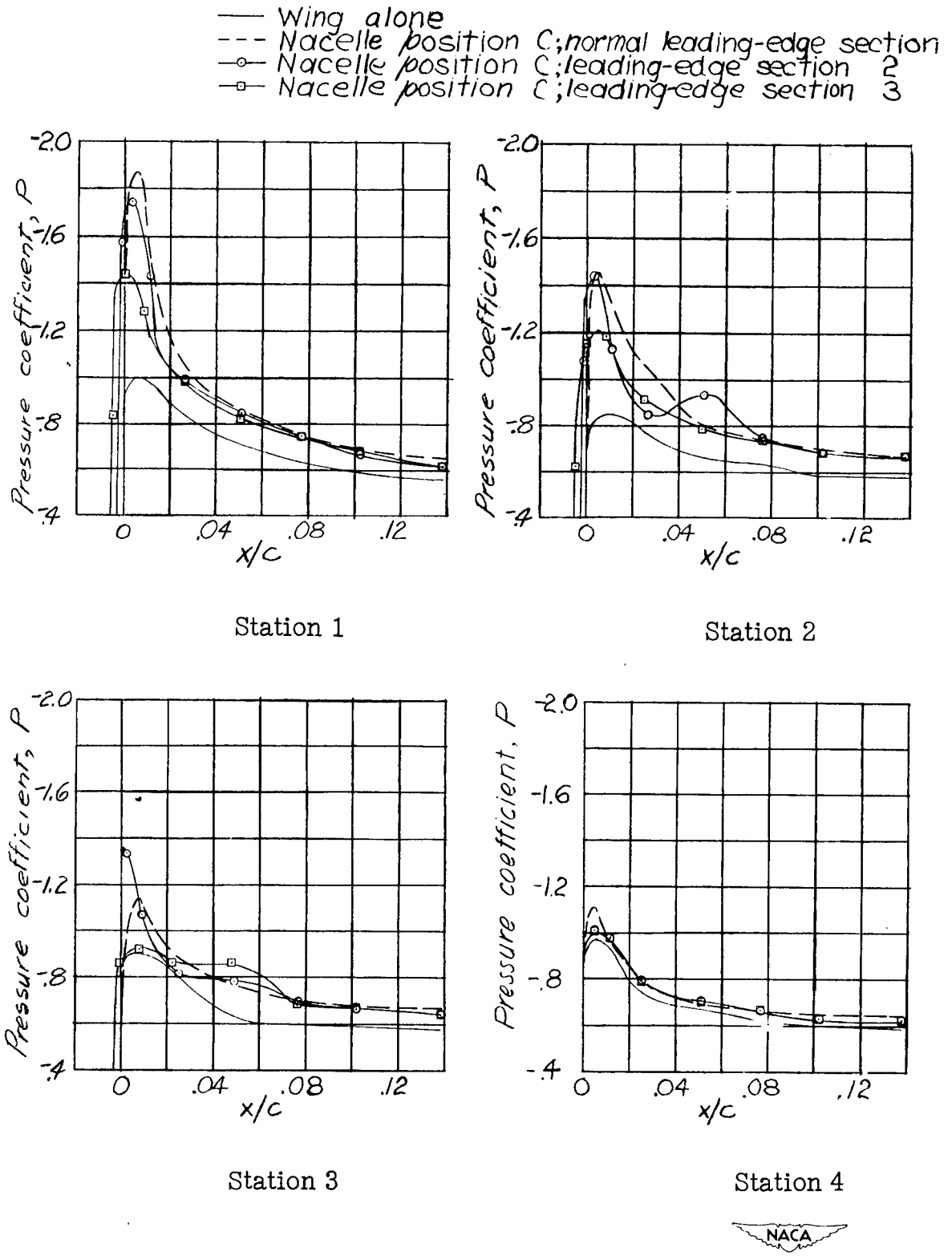


(d) Upper surface; $\alpha = 2.5^{\circ}$.

Figure 42.- Concluded.

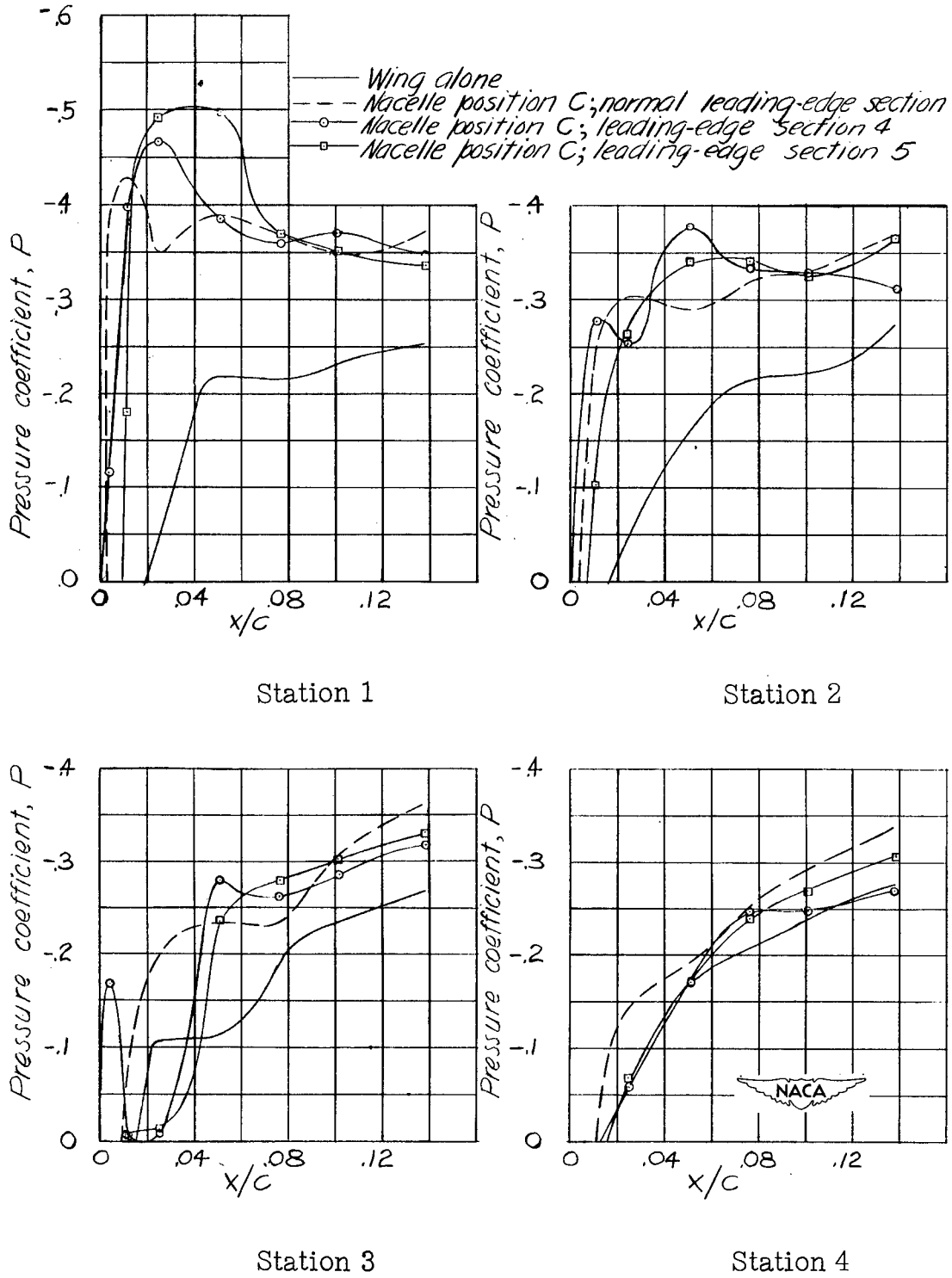


(a) Upper surface; $\alpha = 0^{\circ}$.

Figure 43.- Comparison of pressure distributions over leading-edge modifications 4 and 5 with those over normal leading edge, nacelle in position C. M = 0.4.

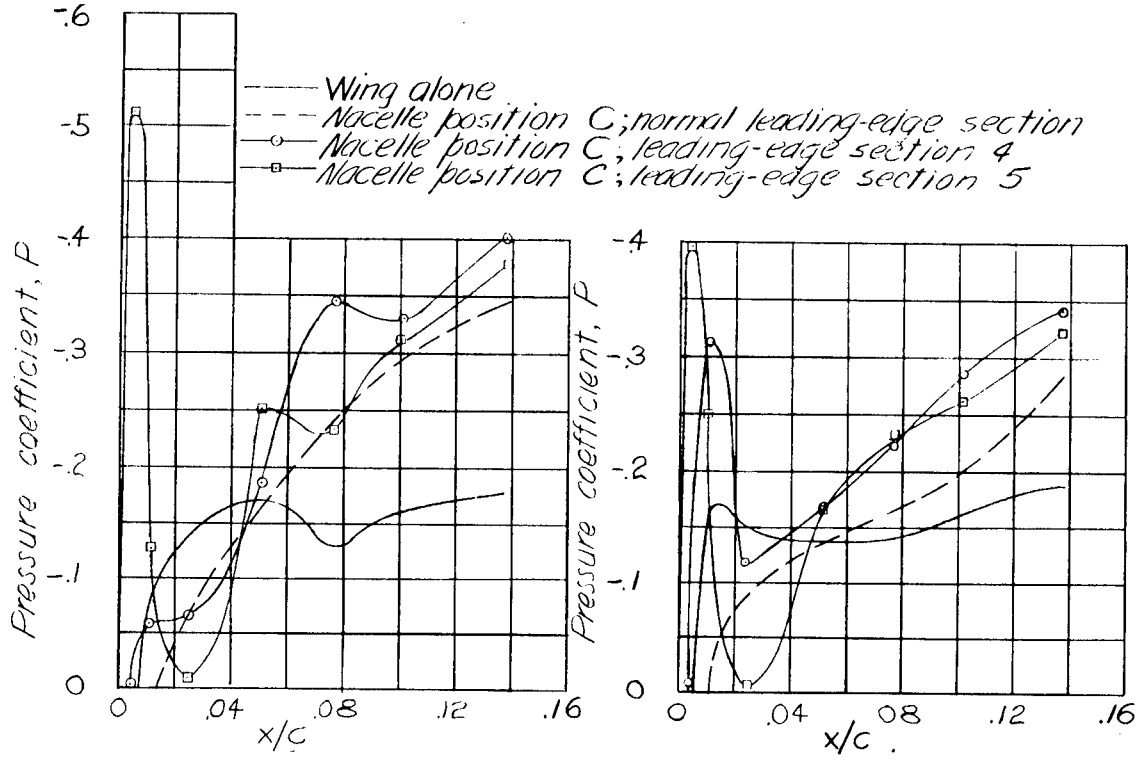


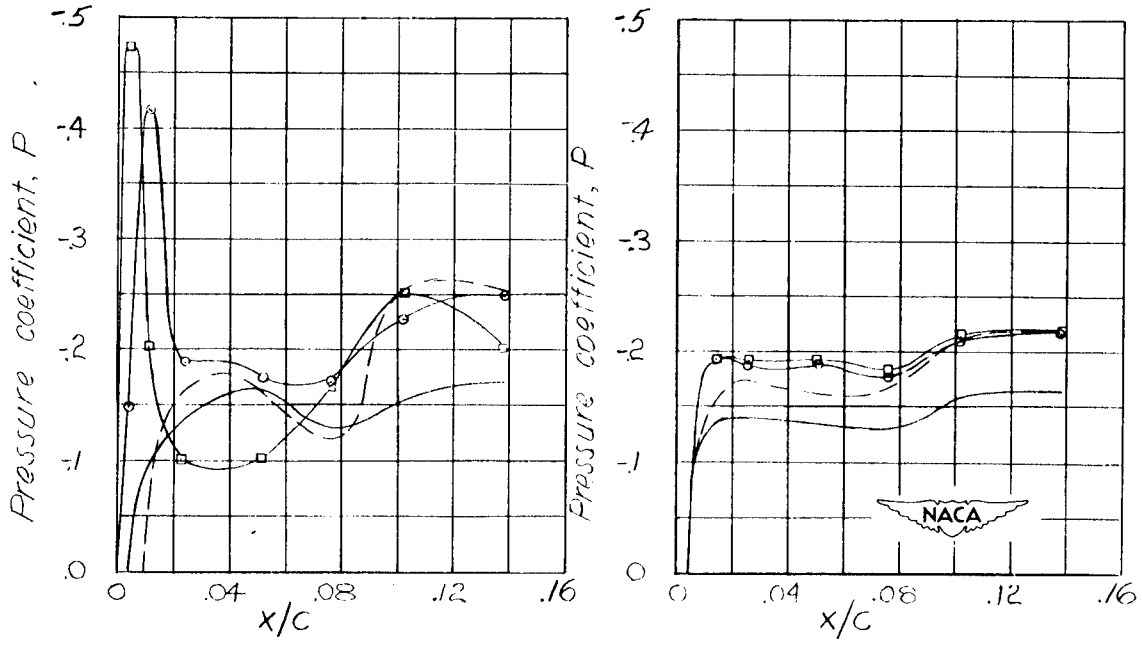


(b) Lower surface; $\alpha = 0^{\circ}$.

Figure 43.- Continued.

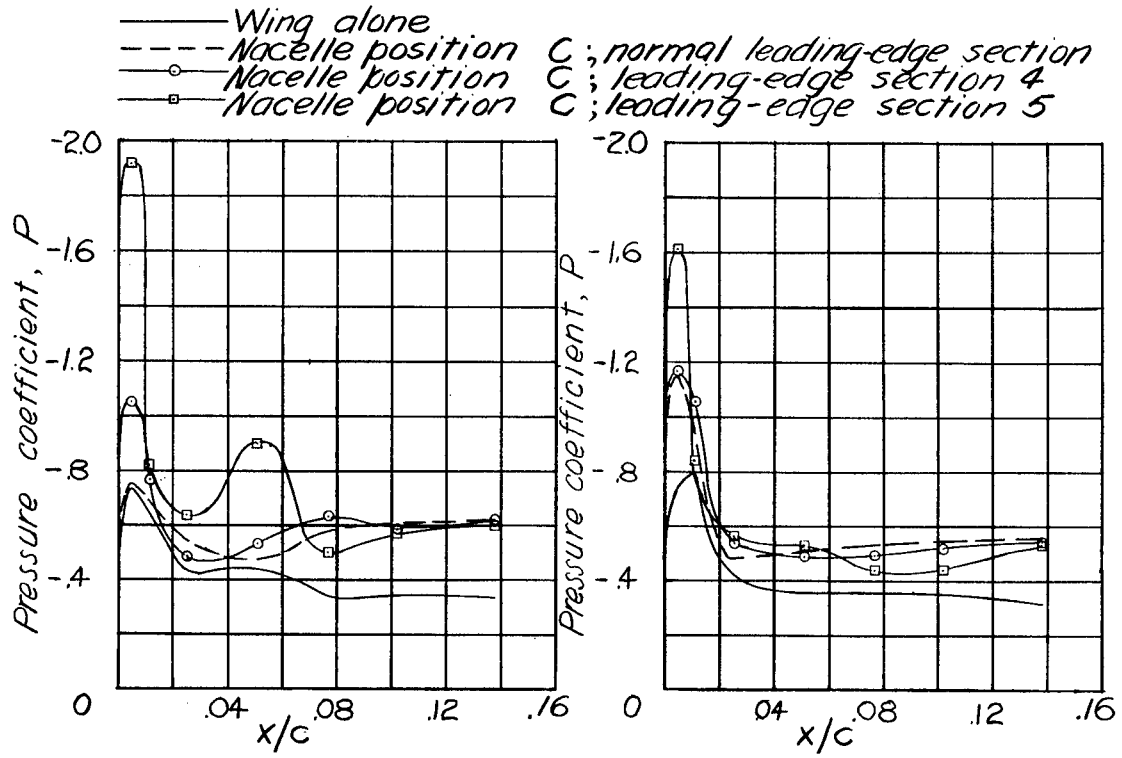


Station 1 Station 2

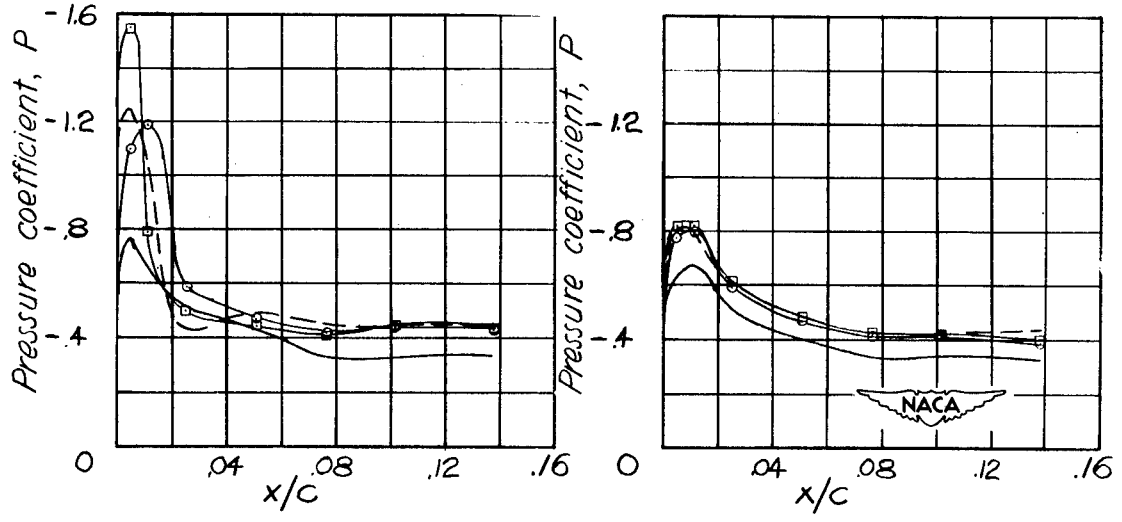


Station 3 Station 4.

(c) Lower surface; $\alpha = -1.5^{\circ}$.

Figure 43.- Continued.

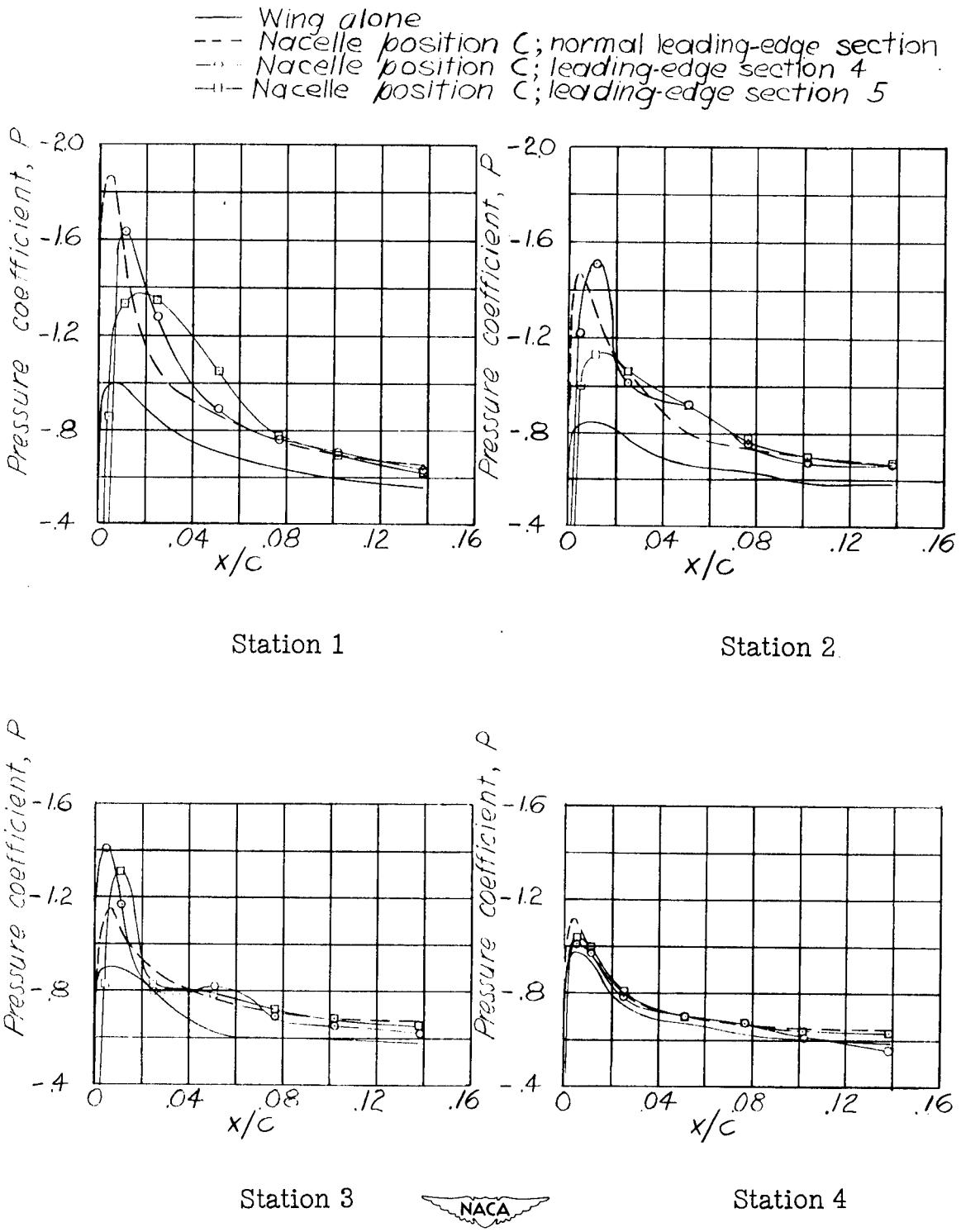


(d) Upper surface; $\alpha = 2.5^{\circ}$.

Figure 43.- Concluded.

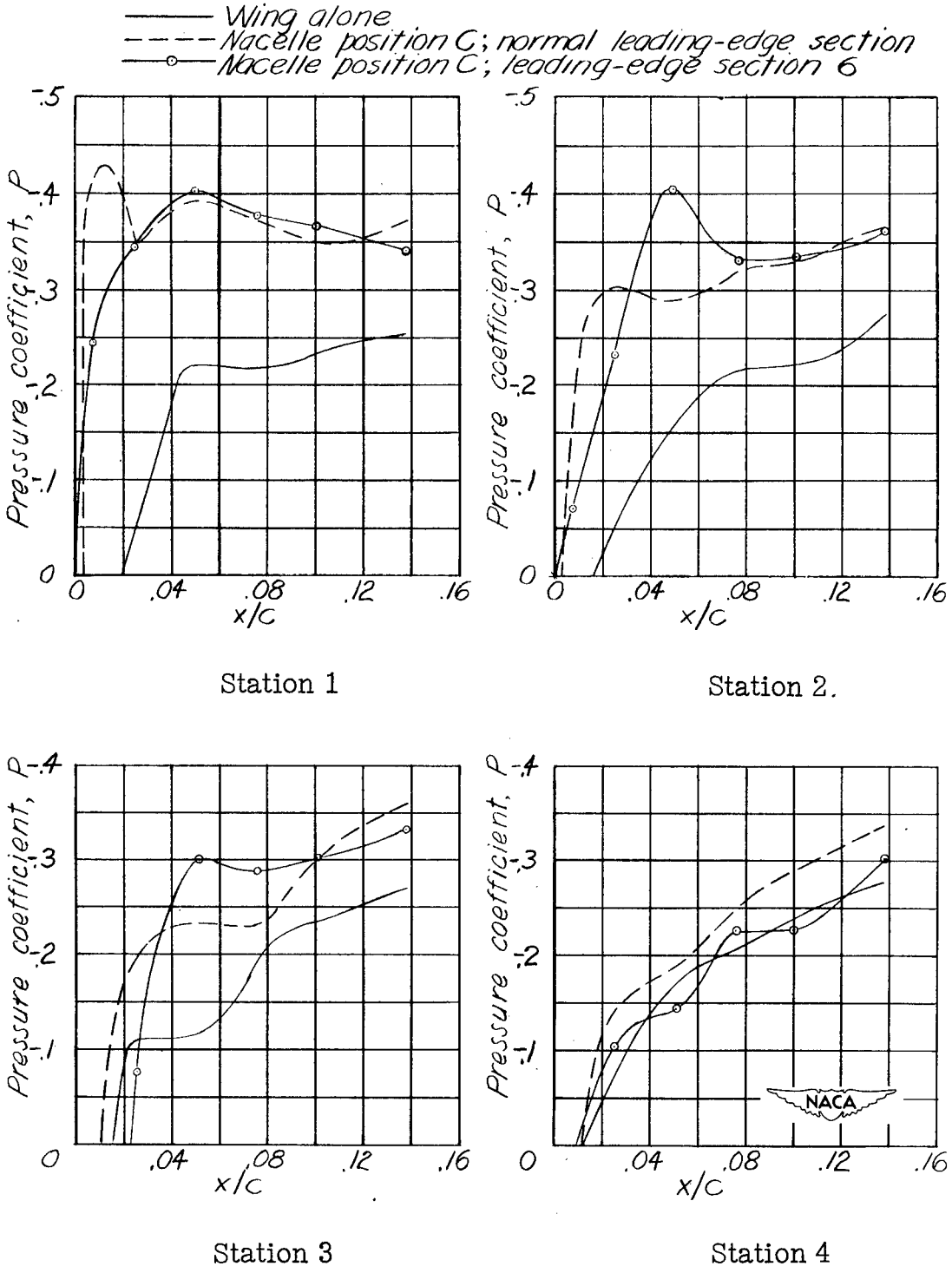


(a) Upper surface; $\alpha = 0^{\circ}$.

Figure 44.- Comparison of pressure distributions over leading-edge modification 6 with those over normal leading edge, nacelle in position C. M = 0.4.

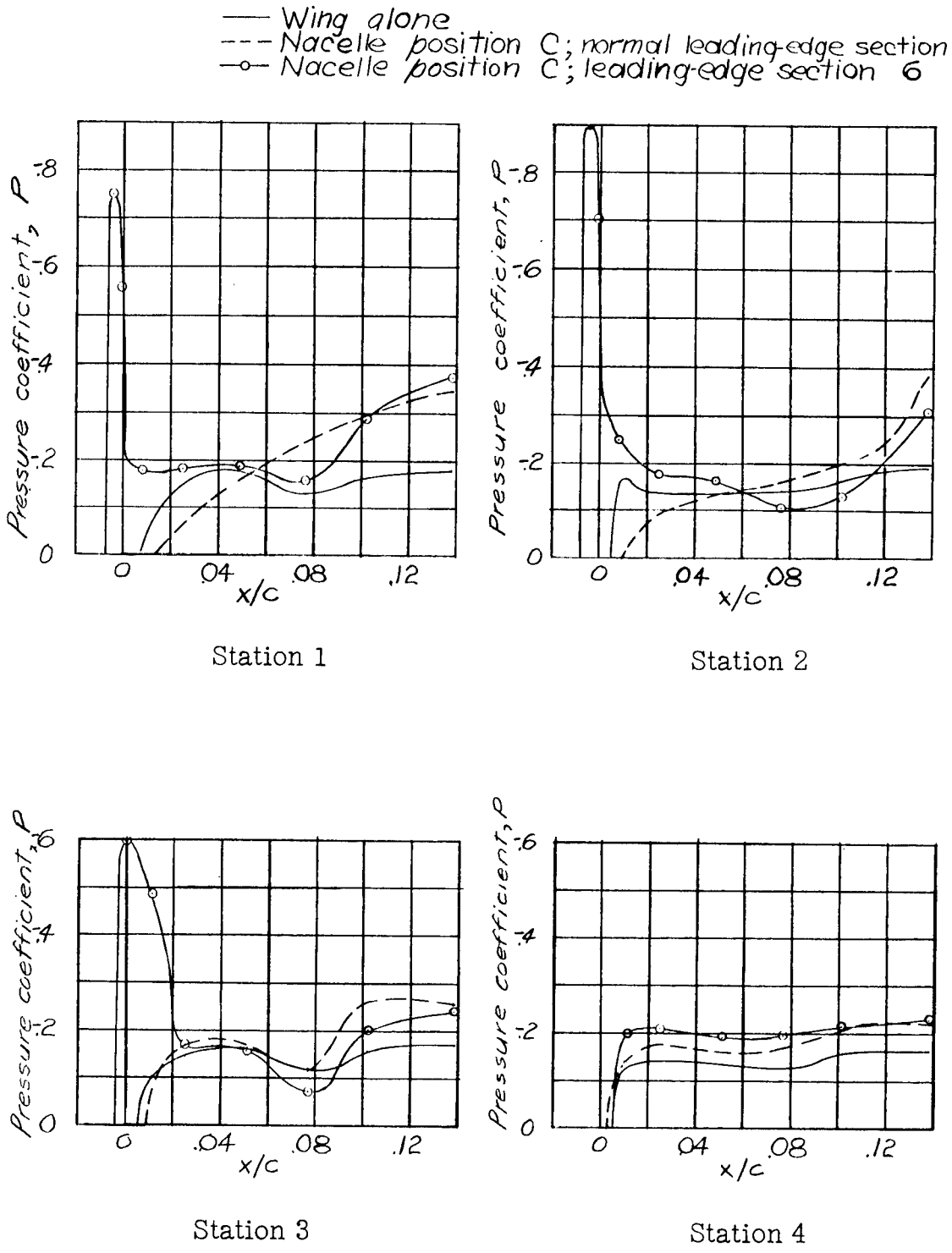


(b) Lower surface; $\alpha = 0^{\circ}$.

Figure 44.- Continued.

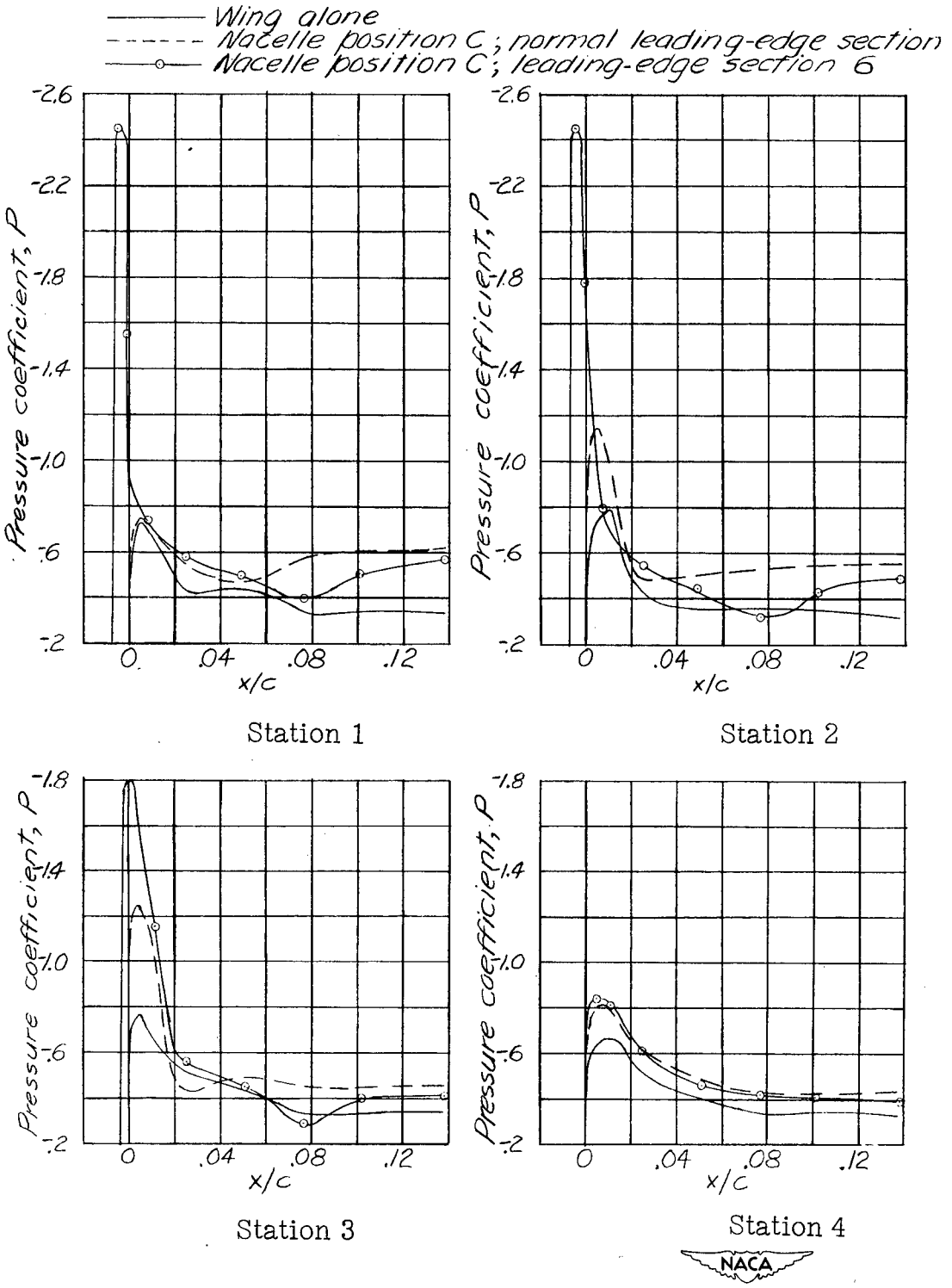


(c) Lower surface; $\alpha = -1.5^{\circ}$.

Figure 44.- Continued.

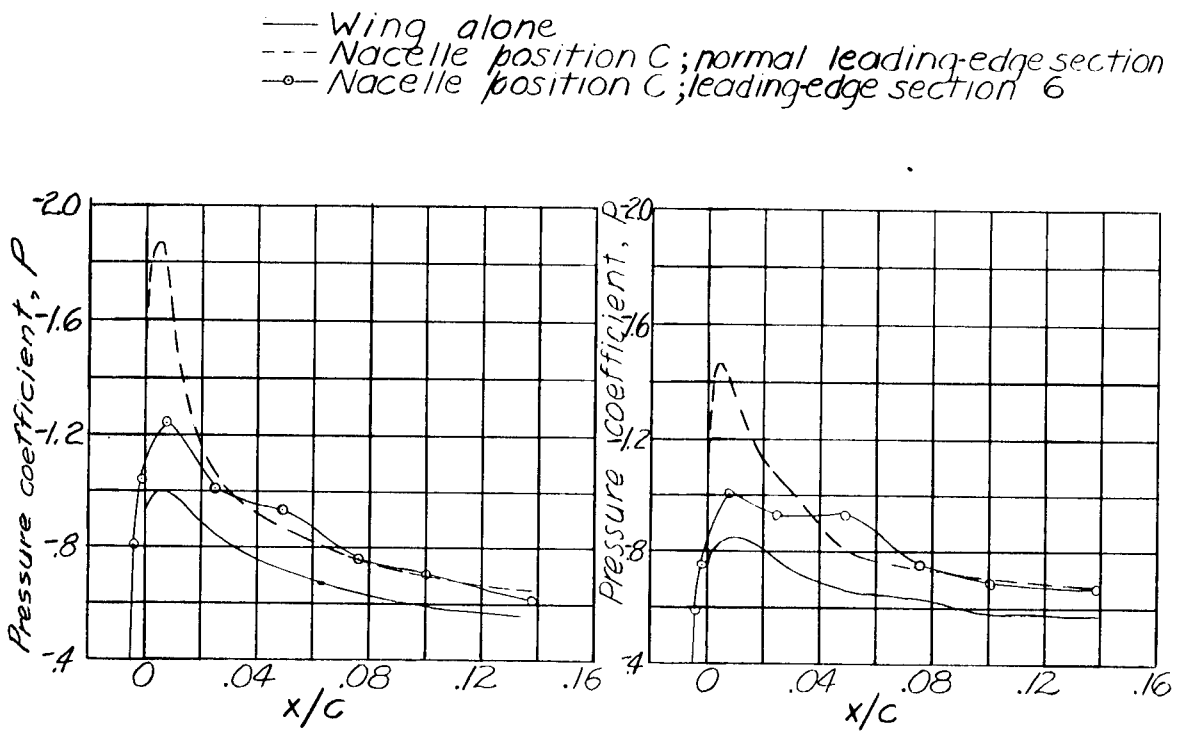


Station 1 Station 2

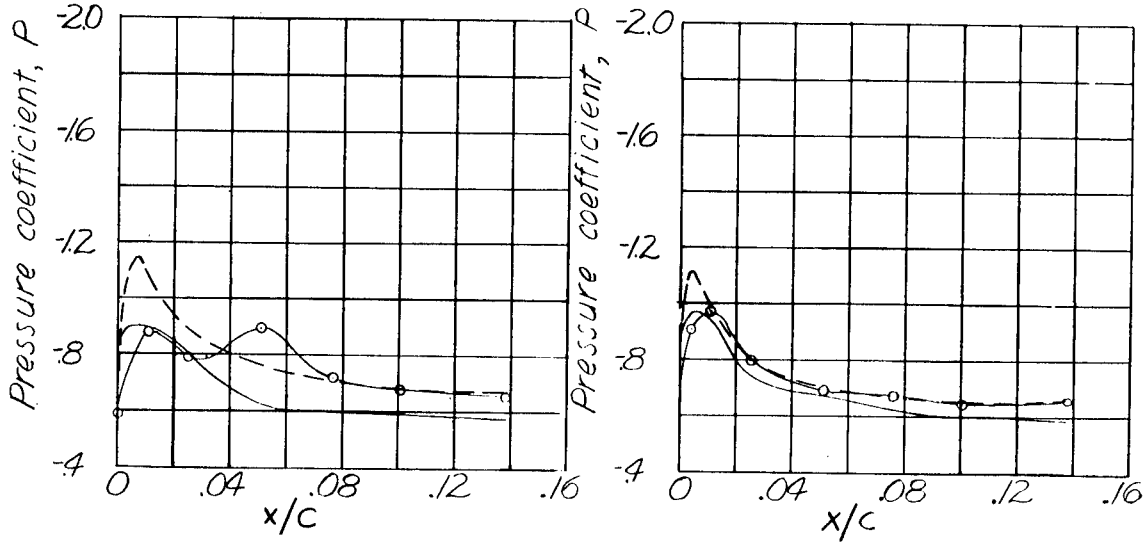


Station 3 Station 4

(d) Upper surface; $\alpha = 2.5^{\circ}$.

Figure 44.- Concluded.

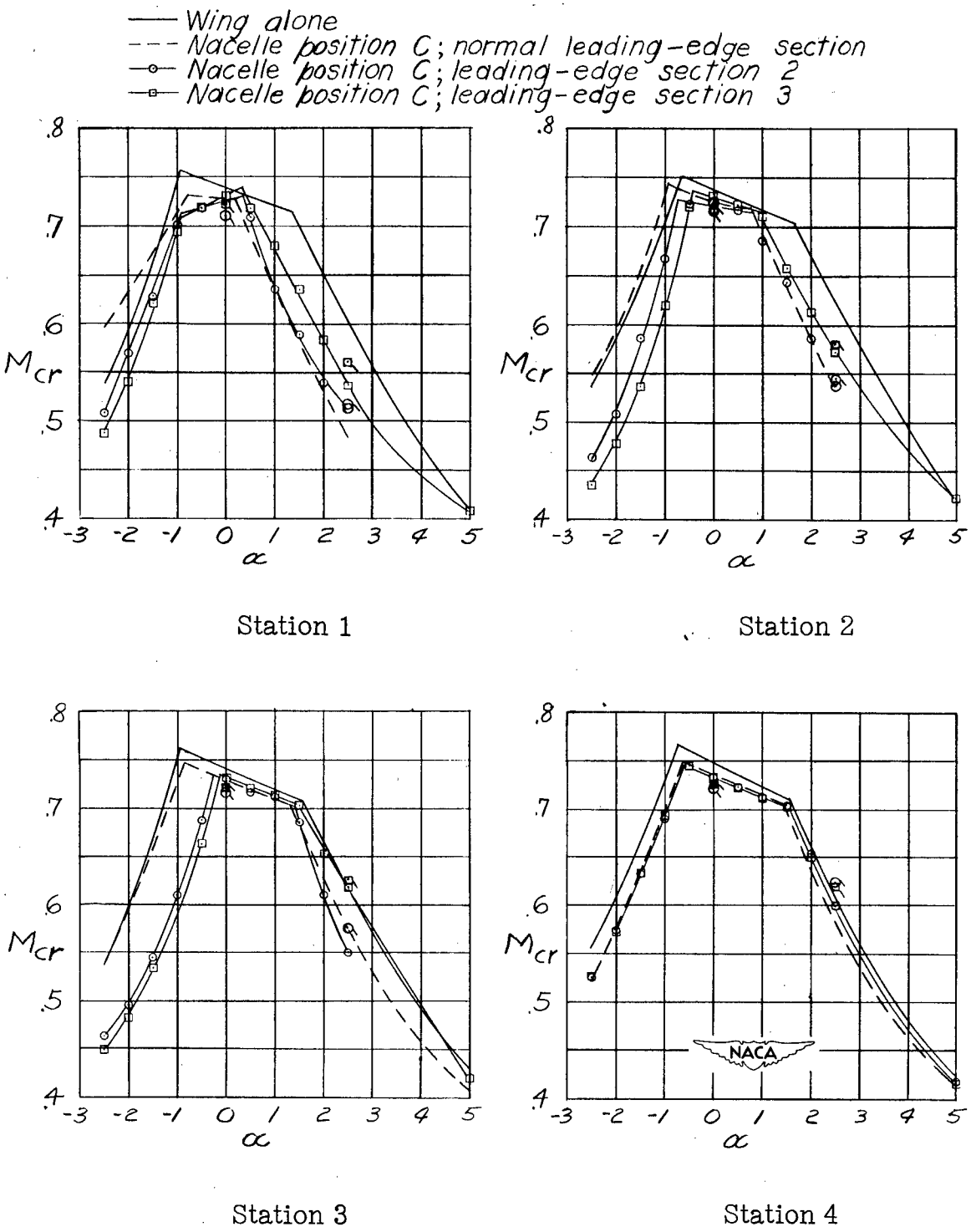


(a) Leading-edge sections 2 and 3.

Figure 45.- Comparison of critical Mach number characteristics for several leading-edge modifications with those for normal leading edge, nacelle in position C. Untailed symbols refer to results extrapolated from M = 0.4 results.

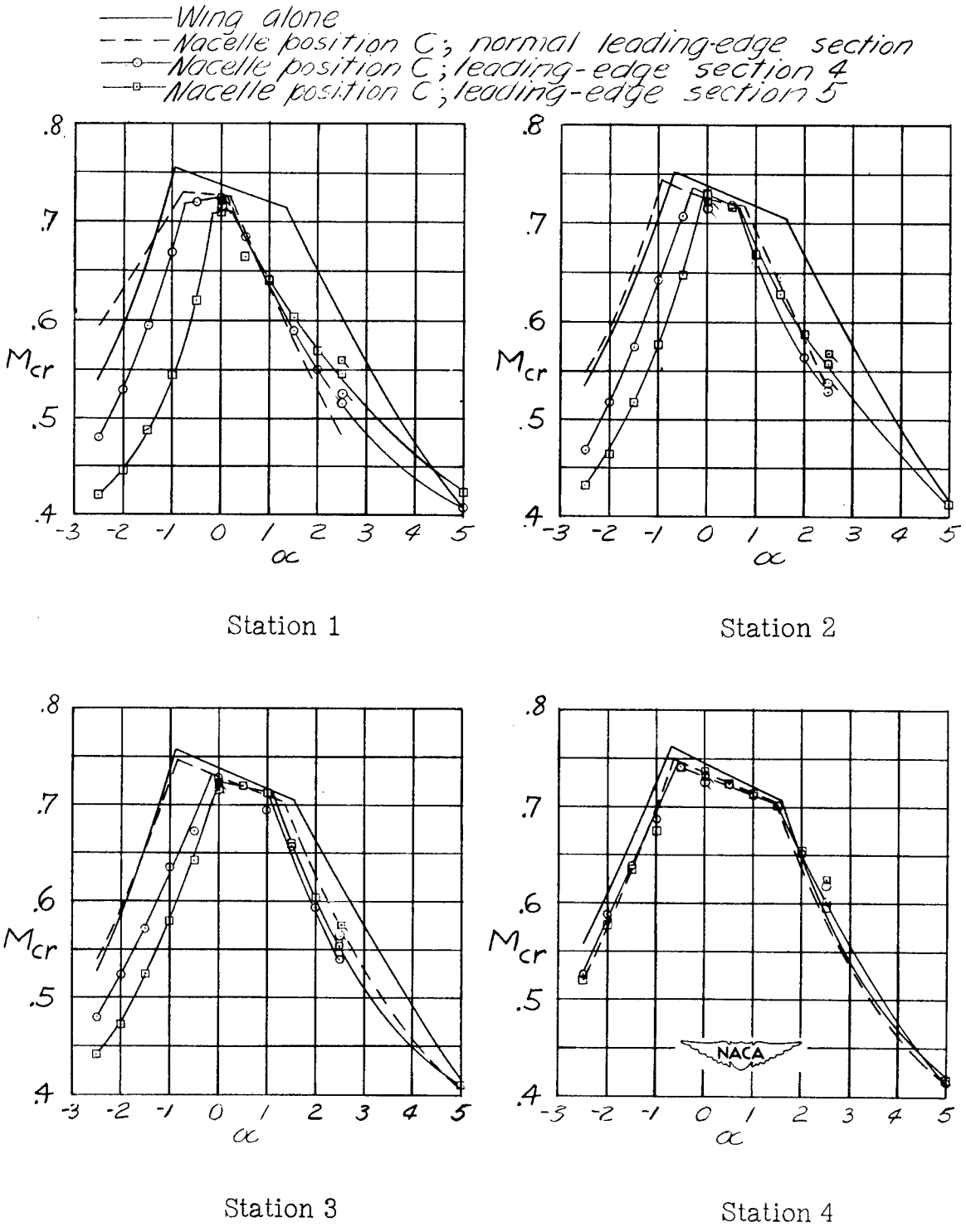


(b) Leading-edge sections 4 and 5.

Figure 45.- Continued.

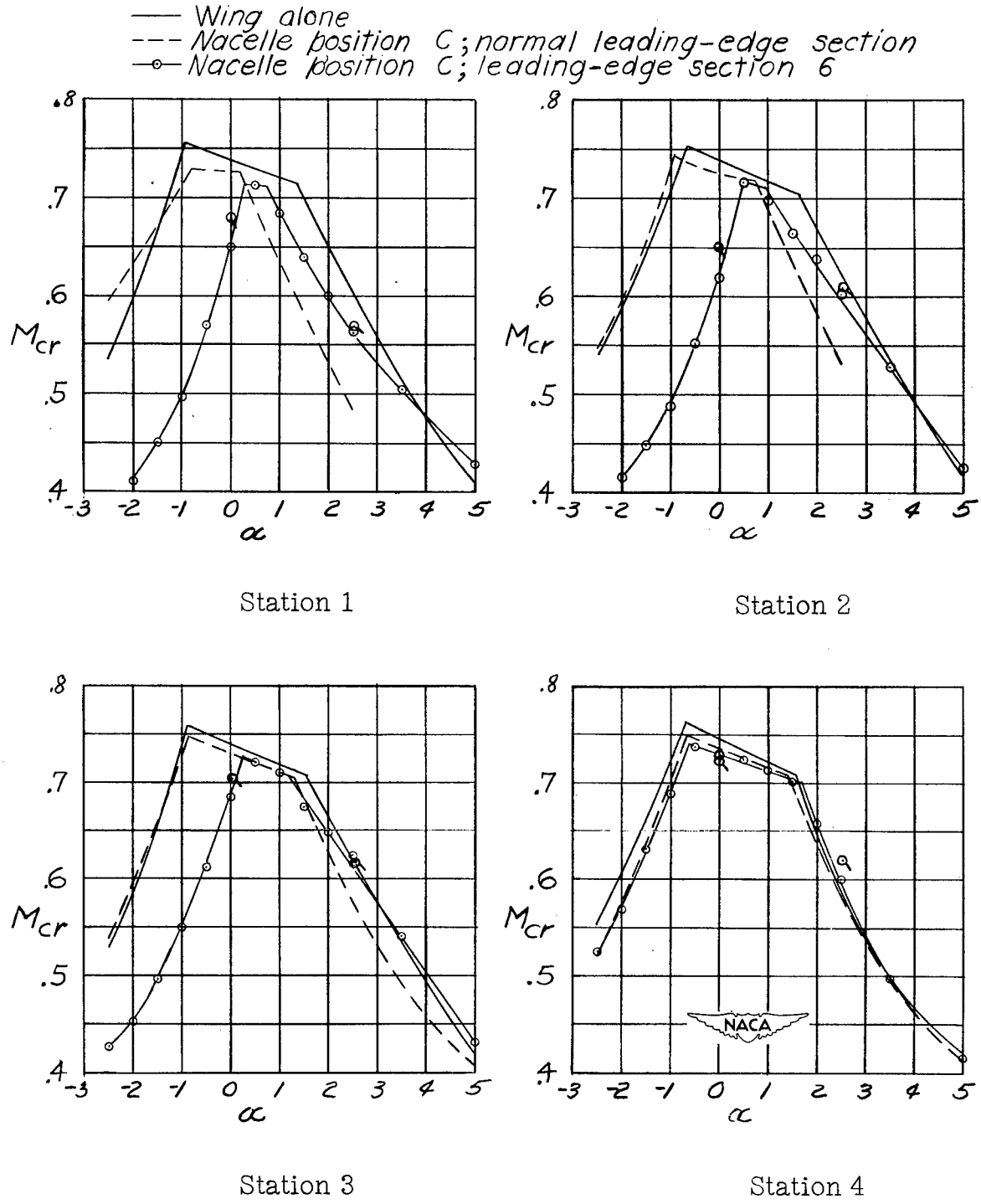


(c) Leading-edge section 6.

Figure 45.- Concluded.

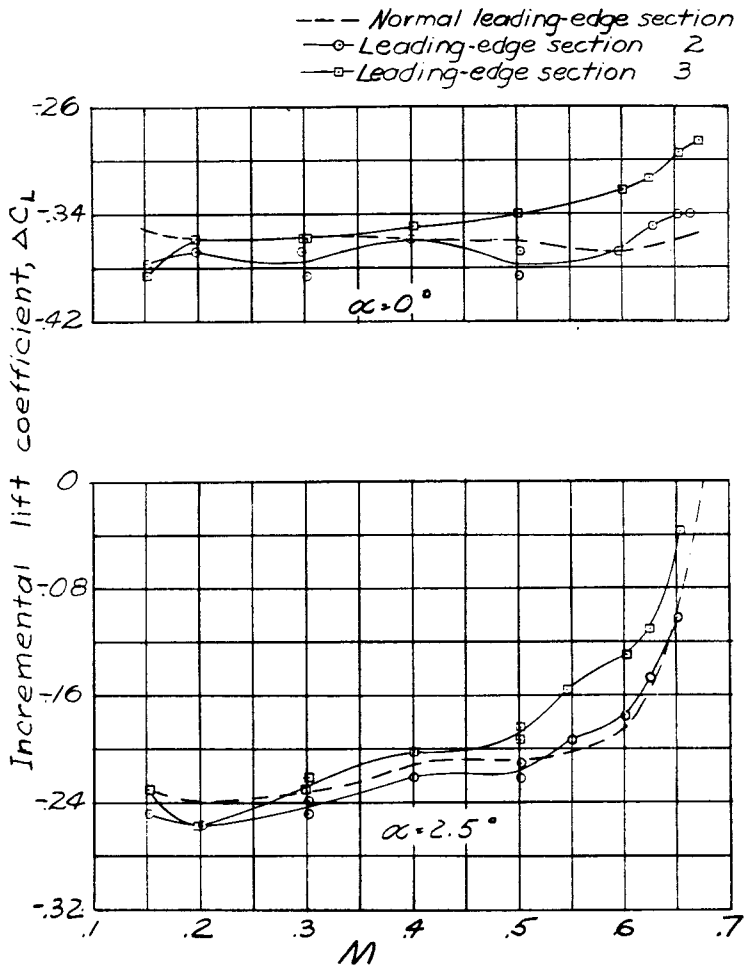


(a) Lift.

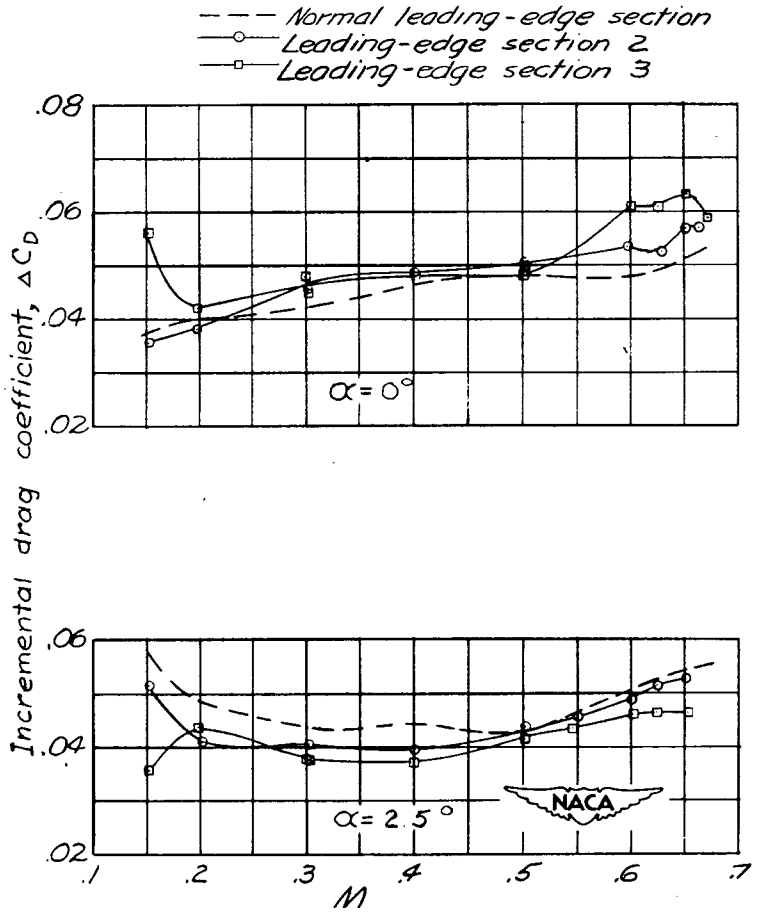


(b) Drag.

Figure 46.- Comparison of nacelle incremental lift and incremental drag characteristics for leading-edge sections 2 and 3 with those for the normal leading edge, nacelle in position C.

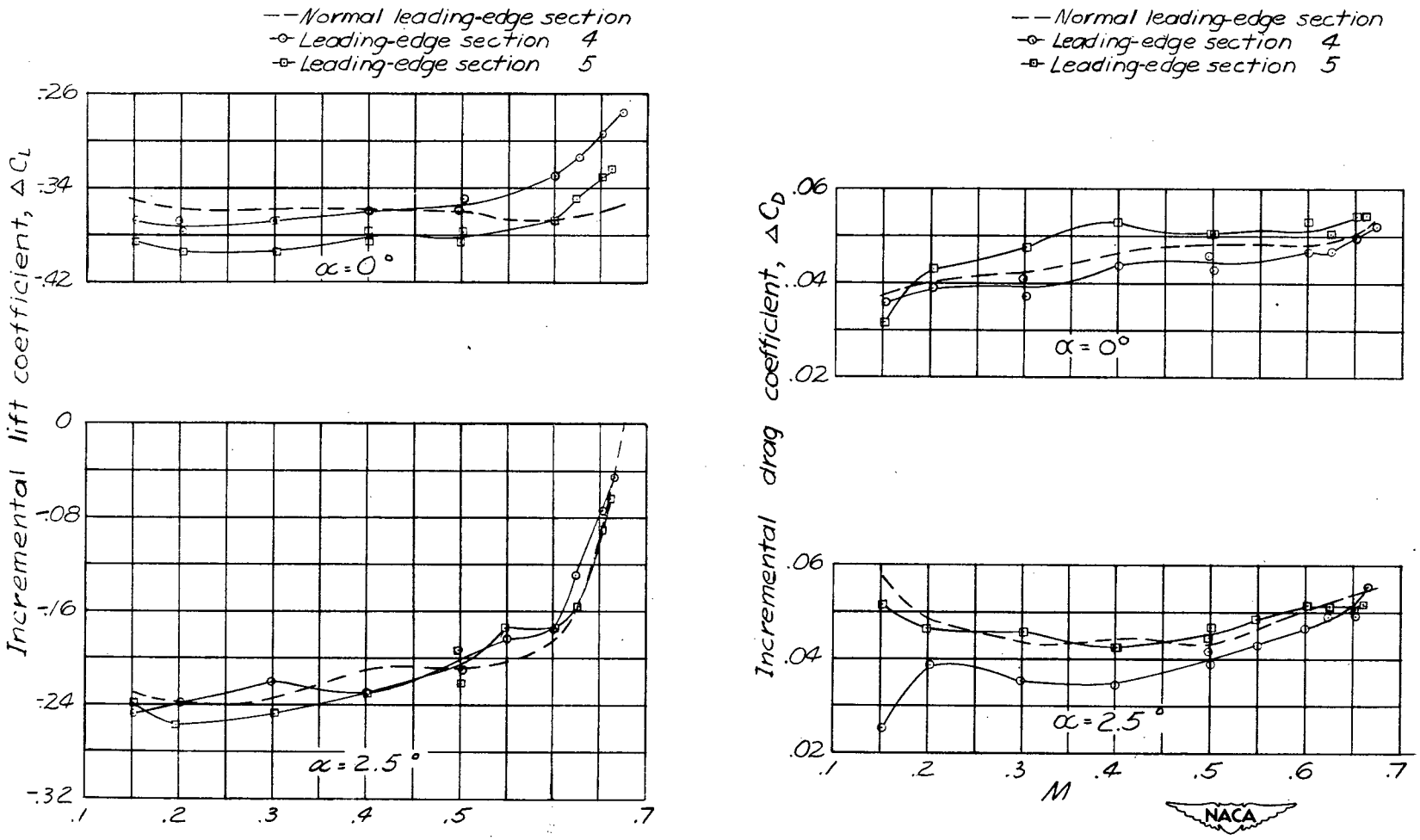


(a) Lift.

(b) Drag.

Figure 47.- Comparison of nacelle incremental lift and incremental drag characteristics for leading-edge sections 4 and 5 with those for the normal leading edge, nacelle in position C.

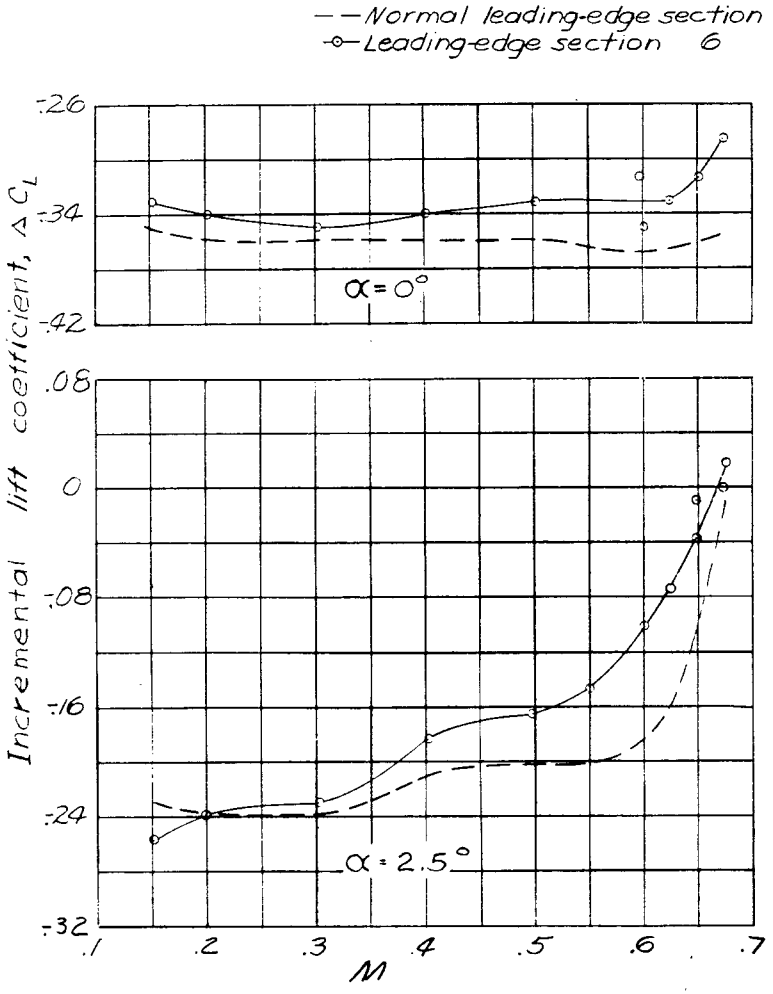


(a) Lift.

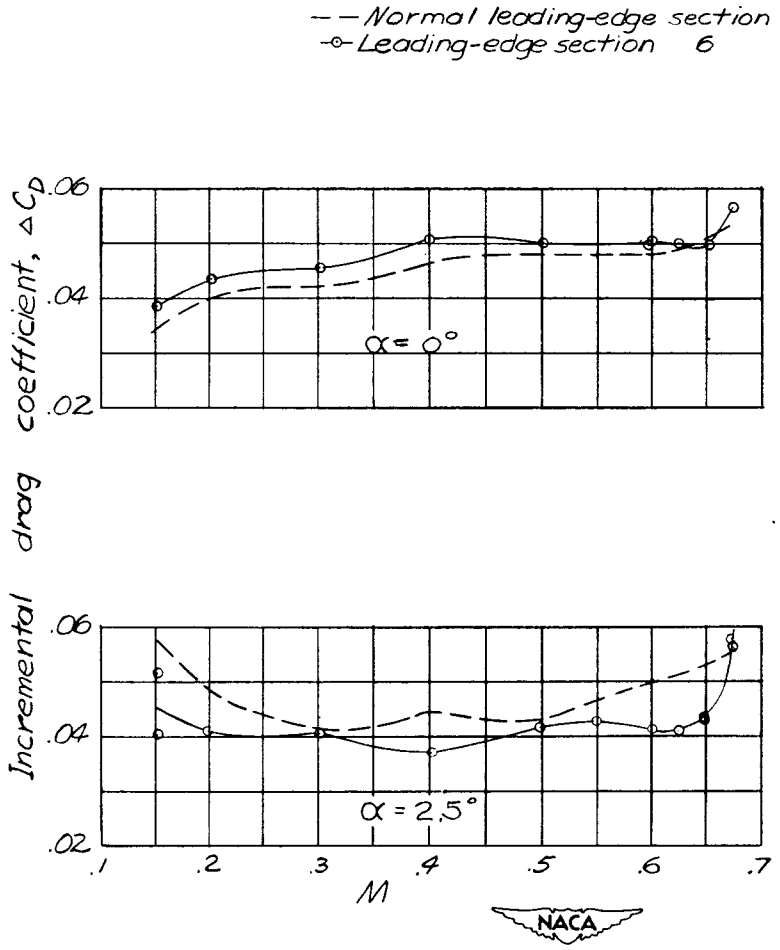


(b) Drag.

Figure 48.- Comparison of nacelle incremental lift and incremental drag characteristics for leading-edge section with those for the normal leading edge, nacelle in position C.

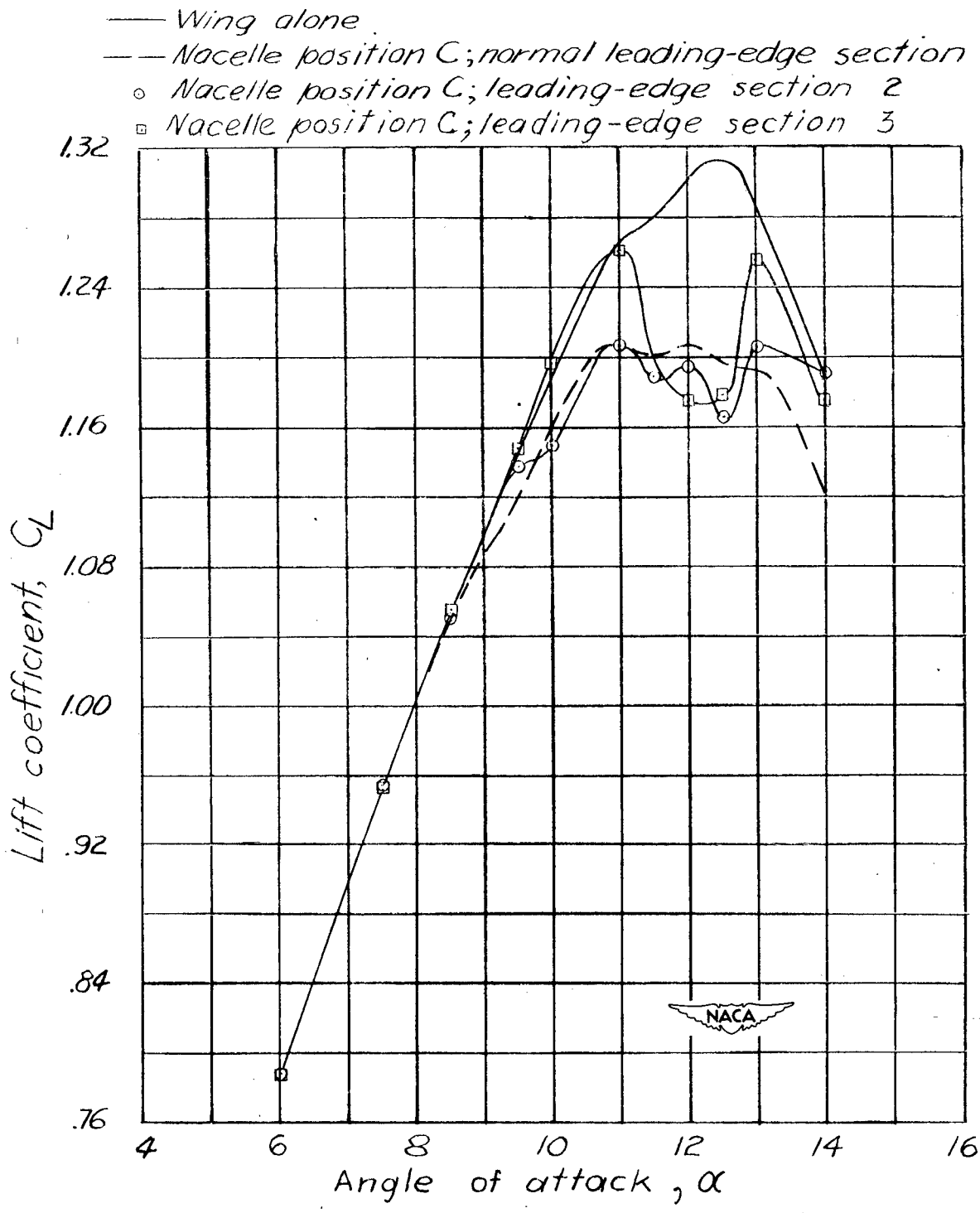


(a) Leading-edge sections 2 and 3.

Figure 49.- Variation of lift coefficient with angle of attack for several wing leading-edge sections. M = 0.2. (Second series of tests.)

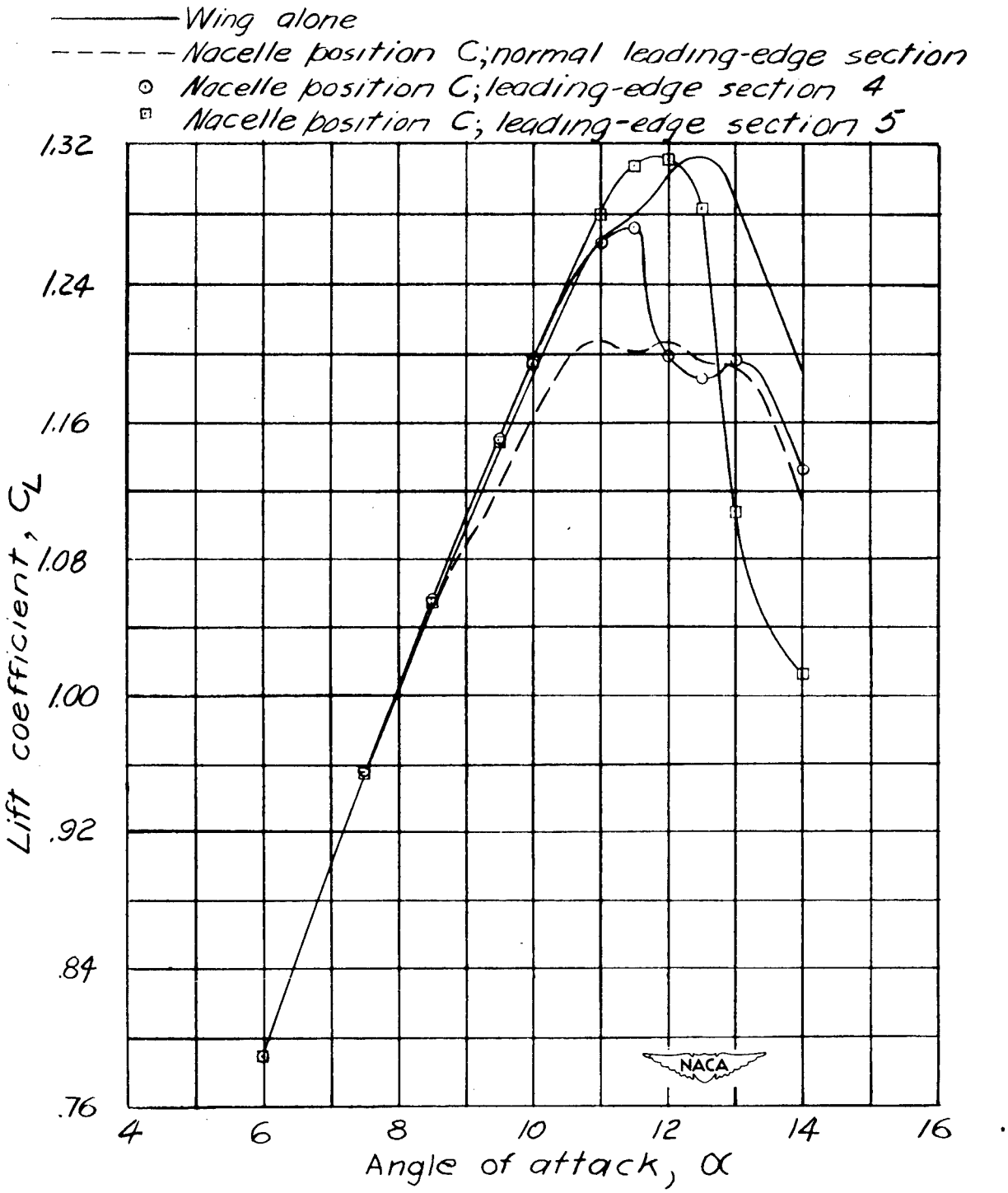


(b) Leading-edge sections 4 and 5.

Figure 49.- Continued.

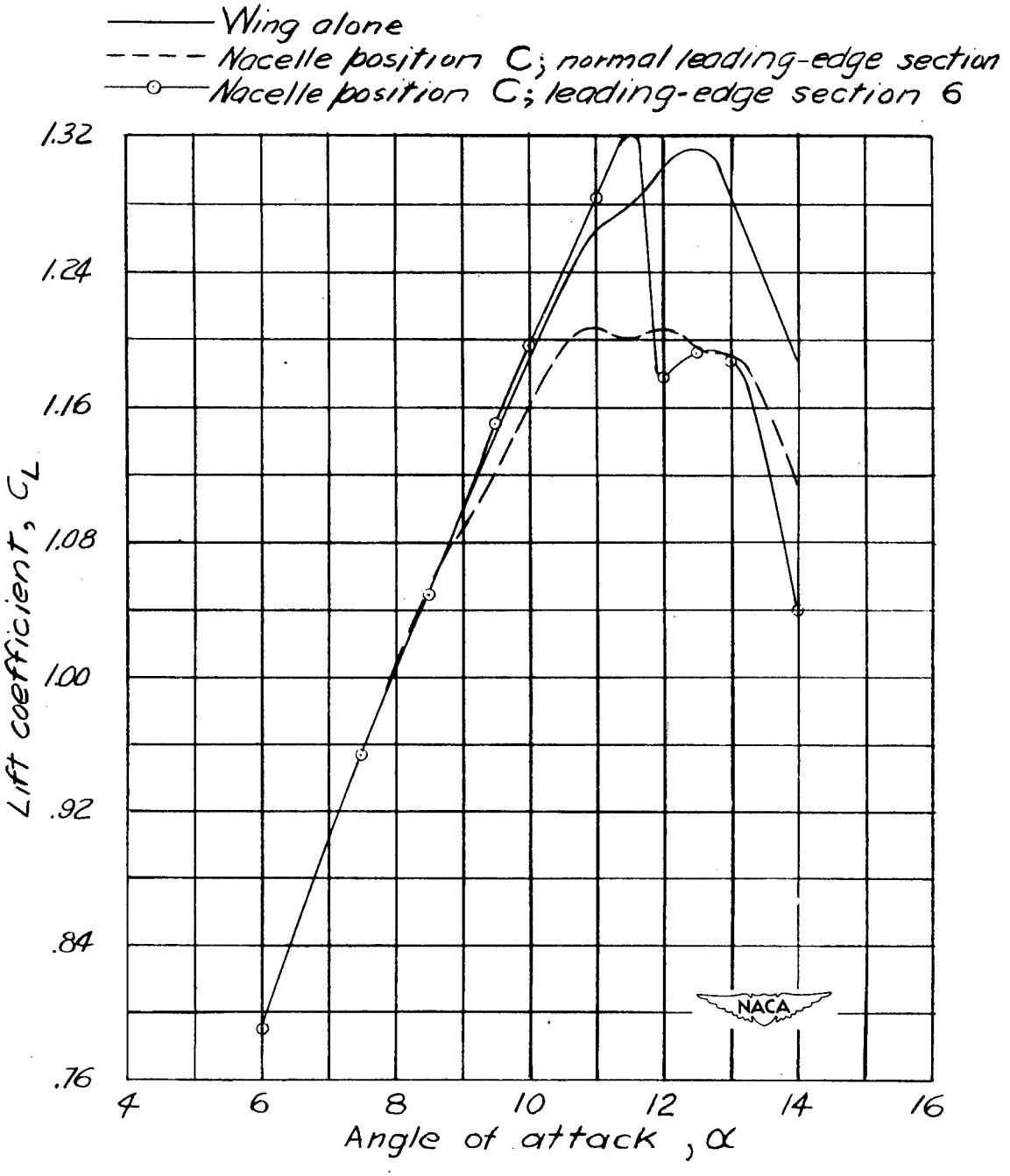


(c) Leading-edge section 6.

Figure 49.- Concluded.